Modelling and Testing the E ects of Space Radiation on Space-borne Electronic Components

by

Holly Snell

A dissertation submitted in partial fulfillment for the degree of
Master of Philosophy in Space Studies

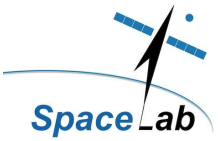

SL17-02M

December 2017

Declaration of Authorship

I, HOLLY SNELL, declare that this dissertation titled, 'MODELLING AND TESTING THE EFFECTS OF SPACE RADIATION ON SPACE-BORNE ELECTRONIC COMPONENTS' and the work presented in it are my own. I know the meaning of plagiarism and declare that all the work in the document, save for that which is properly acknowledged, is my own. This dissertation has been submitted to the Turnitin module (or equivalent similarity and originality checking software) and I confirm that my supervisor has seen my report and any concerns revealed by such have been resolved with my supervisor. I confirm that:

- This work was done wholly while in candidature for a research degree at this University.
- Where I have consulted the published work of others, this is always clearly attributed.
- Where I have quoted from the work of others, the source is always given. With the exception of such quotations, this thesis is entirely my own work.
- I have acknowledged all main sources of help.

Signed: Signed by candidate

Date: October 2017

"It's human nature to stretch, to go, to see, to understand. Exploration is not a choice really; it's an imperative"

Michael Collins

Modelling and Testing the Effects of Space Radiation on Space-borne Electronic Components

by Holly Snell

SpaceLab, Department of Electrical Engineering

Abstract

Outer space is a hazardous environment for satellites as they are continuously exposed to harsh space radiation in the form of cosmic rays and high-energy electrically charged particles (protons, electrons and alpha particles). Mission-critical electronic components are especially susceptible to space radiation as high-velocity charged particle impacts on molecular-sized circuitry can cause significant device upsets or permanent damage, compromising a satellite's functional integrity. In order to mitigate this radiation hazard, electronic components are carefully selected and tested prior to deployment. Part of this process involves consulting a space radiation model in order to be able to estimate the type of radiation environment the electronics will be exposed to. There are many different environmental models to choose from and the output from the models will influence whether a certain device will be selected or not. Due to this, the model selection process should be very well understood and all parameters carefully chosen. This project aims to describe the radiation environment in low Earth orbit, and to provide guidelines for using the space radiation models found on the Space ENVironment Information System (SPENVIS). By going through the modelling process in detail, we have found that the trapped radiation models are completely independent of the date specified when describing the orbit of interest. We found that all long-term solar proton models (except King) assume a zero flux for solar minimum dates. The accuracy of the model output for a specific orbit depends on the duration of the model's time span. For instance, we found that for certain low Earth orbits, the accuracy of the model output could be easily improved by increasing the number of days in the orbit generator from one to three. For the low Earth orbits we selected to analyse, we found that a one-year mission delay at any point on the solar cycle will not have great enough an effect on the output to warrant a re-calculation. It is important to consider both trapped and non-trapped radiation when calculating an upset rate and, lastly, the upset rate calculation could be altered by a factor of 1000 simply by selecting different models for the exact same device and orbit. We conclude this study with some guidelines for the use of SPENVIS for radiation modelling during mission planning.

Acknowledgements

I would firstly like to thank the University of Cape Town, and specifically the NASSP programme, for giving me the opportunity and funding to conduct this research. Secondly, of course, my supervisors, Prof. Peter Martinez and Mr Arno Barnard, for being willing to assist in any way they could. Professor Peter Martinez meticulously read through the first draft of my thesis and provided many helpful comments and suggestions. Mr Arno Barnard dedicated hours of his afternoons to assisting me whenever I ran into difficulties, while still allowing me to figure the important things out on my own. I would also like to thank Dr Ed Elson for teaching me phython and for being there to assist with my coding difficulties.

A huge thanks goes out to all the NASSP lecturers, especially Prof Pierre Cilliers and Prof Manfred Hellberg, for lighting the passion within me for space science right from the beginning of my Master's degree. At this stage I would also like to thank the excellent lecturers at the Rhodes University Physics Department for being so passionate about physics and for leading me to be too.

The biggest thanks goes out to my mother and father for their unwavering support of me throughout my whole life and especially through my studies. Both of you are such inspirations to me, and it is thanks to you that I am so driven and strive to do well. Lastly, to all my friends in Cape Town for being so supportive over these past two years. For always encouraging me to work hard when I need to and for being interested in my studies even though you have no idea what I am talking about most of the time!

Contents

List of Figures

List of Tables

Abbreviations

ASIC	**A**pplication **S**pecific **I**ntegrated **C**ircuit
BJT	**B**ipolar **J**unction **T**ransistor
CME	**C**oronal **M**ass **E**jection
CMOS	**C**omplementary **M**etal-**O**xide-**S**emiconductor
COTS	**C**ommercial **O**ff-**T**he-**S**helf
CREME	**C**osmic **R**ay **E**ffects on **M**icro**E**lectronics
CRRES	**C**ombined **R**elease and **R**adiation **E**ffects **S**atellite
DRAM	**D**ynamic **R**andom **A**ccess **M**emory
DUT	**D**evice **U**nder **T**est
ESA	**E**uropean **S**pace **A**gency
FPGA	**F**ield **P**rogrammable **G**ate **A**rray
GCR	**G**alactic **C**osmic **R**ays
IC	**I**ntegrated **C**ircuit
IGE	**I**nternational **G**eostationary **E**lectron
IRPP	**I**ntegral **R**ectangular **P**arallele**P**iped
ISS	**I**nternational **S**pace **S**tation
LABS	**L**aboratory for **A**ccelerator **B**ased **S**cience
LEO	**L**ow **E**arth **O**rbit
LET	**L**inear **E**nergy **T**ransfer
MOSFET	**M**etal **O**xide **S**emiconductor **F**ield-**E**ffect **T**ransistor
NASA	**N**ational **A**eronautics and **S**pace **A**dministration
ONERA	**O**ffice **N**ational d'**E**tudes et **R**echerches **A**érospatiales
POLE	**P**article **O**NERA-**L**ANL **E**nvironment
PWM	**P**ulse **W**idth **M**odulated
RPP	**R**ectangular **P**arallele**P**iped

SAA	**S**outh **A**tlantic **A**nomaly
SAC	**S**pace **A**dvisory **C**ompany
SCS	**S**pace **C**ommercial **S**ervices
SDRAM	**S**ynchronous **D**ynamic **R**andom **A**ccess **M**emory
SEE	**S**ingle **E**vent **E**ffect
SEL	**S**ingle **E**vent **L**atchup
SEU	**S**ingle **E**vent **U**pset
SMPS	**S**witched-**M**ode **P**ower **S**upply
SOHO	**SO**lar and **H**eliospheric **O**bservatory
SPENVIS	**SP**ace **ENV**ironment **I**nformation **S**ystem
SRAM	**S**tatic **R**andom **A**ccess **M**emory
TID	**T**otal **I**onising **D**ose
TMR	**T**riple **M**odular **R**edundancy

Physical Constants

Speed of Light	c	=	$2.997\ 924\ 58 \times 10^{8}$ m.s^{-2} (exact)
Elementary Charge	e	=	$1.60217662 \times 10^{-19}$ C
Gravitational Constant	G	=	6.67408×10^{-11} m^{3} kg^{-1} s^{-2}

Symbols

m	mass	kg
v	velocity	$\mathrm{m.s^{-1}}$
q	charge	coulomb (C)
B	magnetic field strength	tesla (T)
E	electric field	newtons per coulomb ($\mathrm{N.C^{-1}}$)
ω	angular frequency	$\mathrm{rad.s^{-1}}$
σ	Cross-section	$\mathrm{cm^{-2}\ device^{-1}}$

Chapter 1

Introduction

For 60 years, man-made satellites have been orbiting our planet, performing various important functions and mankind has become increasingly reliant on the services they provide. Navigation, defence, Earth observation and space weather monitoring systems and telecommunications would not be the possible without satellites. Over time, these satellites have evolved to meet our changing needs, becoming more and more complex with every new design. The electronics on-board these satellites therefore have been upgraded every few years so that they are able to execute the increasingly demanding tasks we require of them. Unfortunately, a large number of the important electronic components that are used contain sensitive semiconductors, which are particularly susceptible to radiation damage.

Space is generally seen as a desolate and empty region, and one can easily imagine that a satellite orbiting Earth would have a fairly solitary and serene life. However, this is in fact not the case. Many satellites travel through regions that are filled with high-energy particles that come from various sources, providing a large amount of hazardous radiation. It is therefore very important for the satellite designing and testing process to include an element of radiation hardness testing, in order to make sure that the electronics on-board can handle the radiation environment it will be exposed to. There are three main steps that need to be considered when one performs a radiation hardness test. The space environment where the device will be flying needs to be well understood and characterised. The way that the device responds to particles of different energies needs to be known or tested. Lastly, one needs to be able to correlate the information

gathered from the device tests with what can be expected in space. This will help us to be able to understand what we can expect once the satellite is in orbit, and we can then make conclusions as to whether the performance of the selected electronic components will meet the requirements of the client or not.

In order to fully understand the space environment wherein the satellite will be flying, one needs to consult space environment models. These are resources that use data that has been collected by satellites in orbit in order to attempt to predict the future behaviour of the space environment. However, there are many different input parameters that will affect the outputs of these models, as well as various models to choose from, all of which will modify the conclusion that one can draw from the radiation tests, and can therefore change whether one concludes that a device is safe for use in space or not. A useful platform to be able to gather information from these different models is an online platform called the Space Environment Information System (SPENVIS). It is available at the URL *http:// www.spenvis.oma.be/* and can be accessed by anyone who registers for a free account. Although there are comprehensive help facilities on the SPENVIS website that provides information on the background and usage of the models, there is no documentation to aid a user as to how to interpret the results. Due to this, a spacecraft engineer would not know which models may be over-estimating or underestimating the radiation environment that a particular spacecraft will experience.

The terrestrial testing procedure and the upset rate calculation are also areas wherein errors could be made if one does not fully understand the processes involved. There is an upset rate calculator on the SPENVIS website which can be used to get an idea of the performance of a device in a particular radiation environment. Using this upset rate calculator requires one to obtain parameters from a terrestrial laboratory test and combine this with model outputs.

This project aims to provide a description and evaluation of the environmental modelling process that is adopted when one conducts radiation hardness assurance tests for electronic components in order to obtain an accurate estimation of the expected error rates when those components are operated in space. Different environmental models and parameters will be compared at each step of the process, and the discrepancies noted. The effect of these discrepancies on the error (or upset) rate will be discussed, as well as a discussion on the accuracy of these available models and therefore the results obtained

when using them. An attempt to identify which models and parameters are the most important for specific missions will be made in order to assist the future testing and evaluation processes of electric components for use in space. The process for the upset rate calculation will also be examined in detail, and areas where inaccuracies could arise will be discussed. This is done in order to attempt to demonstrate how certain parameters could alter the upset rate by a large amount, thereby leading to a significantly different upset rate calculation result. This could potentially make the difference between a device being selected for flight or not, and so it is a very important aspect to consider.

Results from previous papers were consulted where electronic components were tested in a radiation environment. Using this data, as well as the space environment models, we are able to comment on the modelling and testing process in order to demonstrate, quantitatively, how dramatic the differences between model outputs can be for the upset rate calculation. Finally, we provide a set of guidelines on the use of SPENVIS to assist a spacecraft engineer in selecting a model, understanding the model output and interpreting the results.

This thesis is structured such that Part I, containing Chapters 2, 3 and 4 are explanatory chapters that describe, in detail, the space environment, its effect on electronic components as well as the ground testing procedure. Part II contains Chapters 5 and 6, which describe the experimental procedure that was adopted and contain a detailed account of how the space environmental models are used. Chapter 6 describes the method of combining the terrestrial test data with model outputs in order to obtain an upset rate. In Part III we have Chapters 7, 8 and 9. Chapter 7 provides the results that we obtained from the modelling process and offers an explanation of what these results imply. Chapter 8 provides the results from upset rate calculations and a discussion on the differences obtained for various situations. Chapter 9 comprises the Conclusions and Recommendations. A comment on the discrepancies observed between the models and how this will affect the upset rate calculations is given. Chapter 9 also provides a set of guidelines for the specific aspects we think a SPENVIS user should take note of when using the platform. The Appendix contains the code that was used in the discussion in Chapter 5, as well as the code for extracting the data from a SPENVIS .txt file.

Part I

The Space Environment and its Effects on Electronics

Chapter 2

The Space Environment

There are many different types of radiation which have various origins in space. They can be divided into two main categories of radiation: trapped, and non-trapped particles. The particles, their energies and the altitudes at which the radiation is the most severe will all depend on whether the radiation is trapped or non-trapped.

2.1 Trapped Radiation

Trapped particles are those confined to the Earth's magnetic field lines. Particles from the solar wind enter the magnetosphere and become trapped on the field lines. These exist within the plasmasphere (a region of our atmosphere which starts at an altitude of approximately 1000km) and are the result of charged particles circling around the Earth's magnetic field lines, and bouncing back and forth between the poles. The circling (or gyration) is a direct result of the presence of a magnetic field. The motion can be represented by Equation 2.1 (Chen 2012), where m represents the mass, $\mathbf{v}$ the velocity, q the charge and $\mathbf{B}$ the magnetic field.

$$m\frac{d\mathbf{v}}{dt} = q\mathbf{v} \times \mathbf{B} \tag{2.1}$$

This gyration occurs at a frequency which is unique to a specific type of particle. This is called the cyclotron frequency, ω_c, and can be calculated using Equation 2.2 (Chen 2012).

$$\omega_c = \frac{|q|B}{m} \tag{2.2}$$

In addition to this circular motion, the particle will move **along** the magnetic field line. This is a straightforward acceleration along **B**, and can be seen in Equation 2.3 (Chen 2012). This equation comes from looking at the z component of 2.4 (Chen 2012), where we have included the presence of an electric field, E, and assumed B to be in the z direction.

$$m\frac{dv_z}{dt} = qE_z \tag{2.3}$$

$$m\frac{d\mathbf{v}}{dt} = q(\mathbf{E} + \mathbf{v} \times \mathbf{B}) \tag{2.4}$$

The bouncing back and forth between poles can be explained by considering a magnetic field wherein the strength of the magnetic field increases in the direction parallel to the field lines. The Earth's magnetic field becomes stronger toward the poles and is therefore similar to a dipole field. A "magnetic mirror" is set up as a result of the converging field lines, and this causes the particles to bounce between the poles.

As seen in Figure 2.1 (Hutchinson 2001), a particle will experience a strengthening field as it travels along the field line. As it enters a stronger field, the velocity along **B** will decrease. Eventually it will encounter a point where the field is so strong that the particle will lose all of its parallel velocity, and a turning point will be reached. Here the particle changes direction and is reflected back along the same magnetic field line (i.e. a mirror).

The particles will also experience a drift around the Earth, the direction of which depends on the charge of the particle. The total motion of an individual particle can be seen in Figure 2.2.

These particle motions all combine together to produce something called a "drift shell". These are regions of trapped radiation that exist around the Earth in a toroidal shape, forming the Van Allen radiation belts.

Electrons, protons and other low-energy heavy ions all exist in this region and are all bouncing back and forth between the poles. We are, however, more interested in the effects of the protons, as they give rise to something called Single Event Effects (SEE) in the electronics, which will be discussed in detail in Chapter 3. Most of the protons in this region have energies exceeding 10 MeV (Stassinopoulos & Raymond 1988), and can be as energetic as 10^3 MeV.

2.1.1 Trapped Protons

For the purpose of the present investigation, we are primarily interested in satellites that will fly within a specific altitude range called Low-Earth Obit (LEO). The majority of all

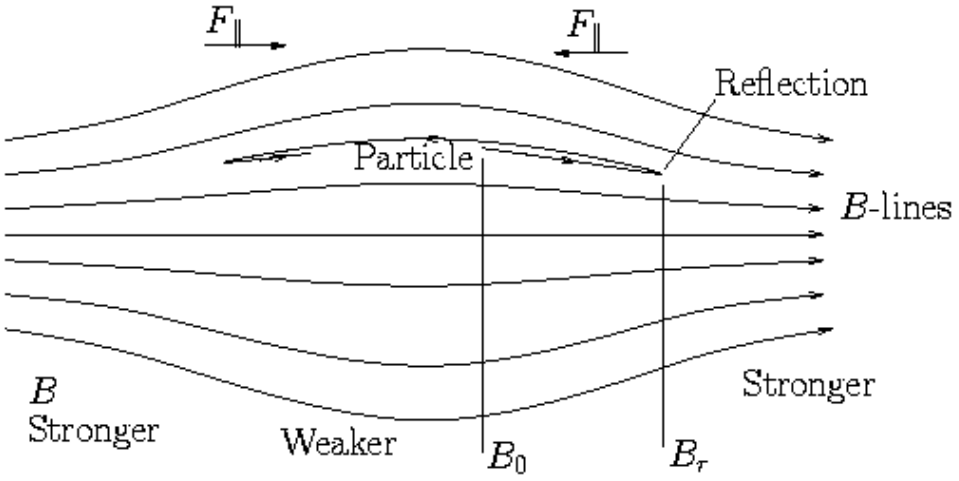

FIGURE 2.1: Magnetic mirror - (Hutchinson 2001).

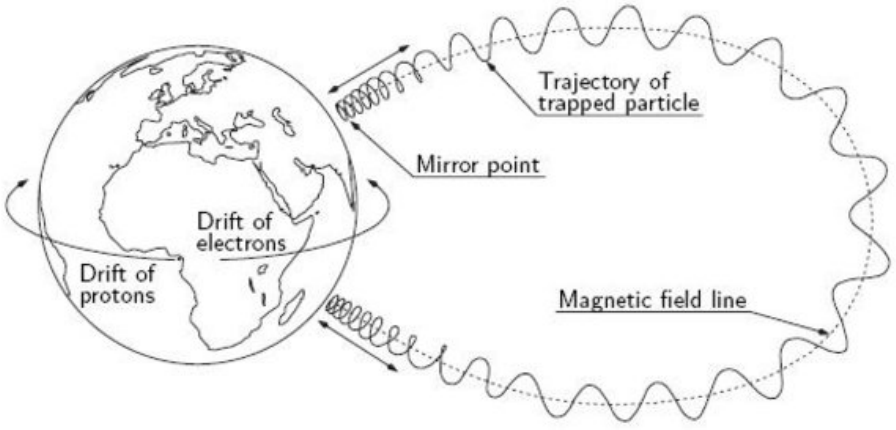

FIGURE 2.2: Motion of a trapped particle on one of the Earth's magnetic field lines - (European Space Agency (ESA) 2014).

satellites that have been launched have been to LEO, as well as all human space flights (with the Apollo lunar program being the only exception). The characteristic altitudes of the LEO orbital regime are between 160km and 2000km above the Earth's surface, and are therefore mostly protected from cosmic rays by the Earth's magnetic field.

The Van Allen belts seen in Figure 2.3 (Zell 2015) are regions of intense trapped particle radiation surrounding the Earth discovered by James A. Van Allen using the Explorer 1 satellite in 1958 (Allen 1961). The radiation belts are mostly at altitudes higher than 600km above the Earth's surface, so satellites in LEO are mostly safe from this trapped radiation. These radiation belts are split into two regions: a stable inner belt, also known as the "hard" belt, consisting of high energy protons, and an outer belt (the "soft" belt) consisting of low energy electrons.These belts are not static; particles within them are constantly lost to the atmosphere, and particles from the sun and from cosmic rays replenish these losses.

The largest amount of radiation that a satellite in LEO experiences comes from passing through a region called the South Atlantic Anomaly (SAA). This is a region where the Van Allen belts dip to their lowest altitude (around 200 km). Due to this, a satellite in LEO will now pass through a portion of the inner radiation belt.

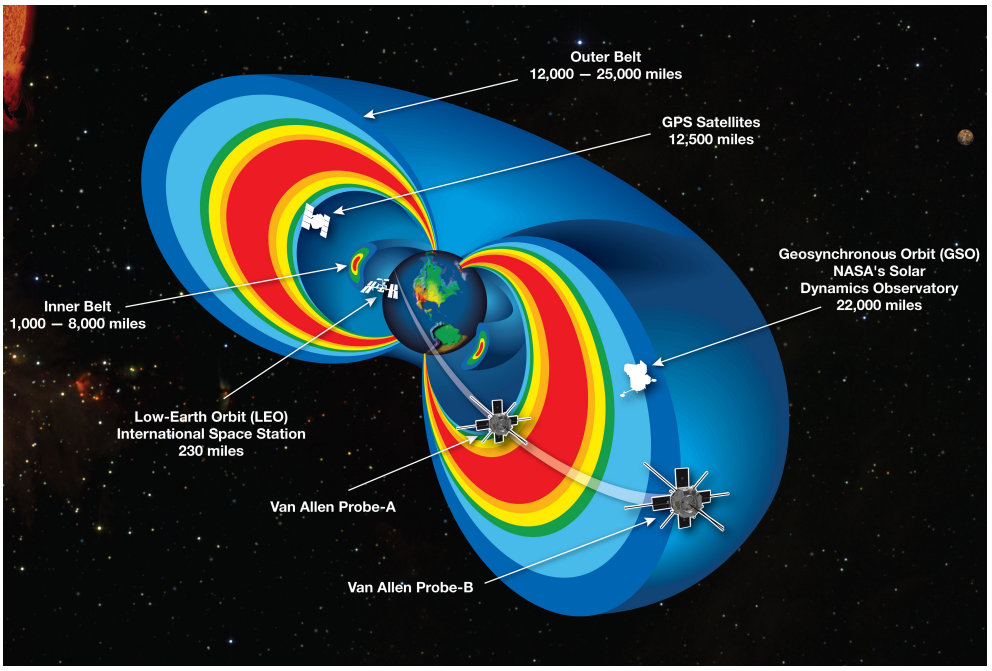

FIGURE 2.3: The Van Allen belts - (Zell 2015).

This region will therefore add to the amount of radiation the satellite is exposed to, in the form of trapped particles. This zone expands over most of the central area of South America, and extends all the way across the South Atlantic ocean, towards Southern Africa. It exists because the Earth's magnetic field is the weakest in this region. As can be seen in Figure 2.4 (European Space Agency (ESA) 2012), the region where the magnetic field is the weakest (near Brazil) corresponds to the area where the majority of radiation damage occurs. In the image, the white spots are the geographical locations where satellites in LEO have experienced single event effects due to radiation.

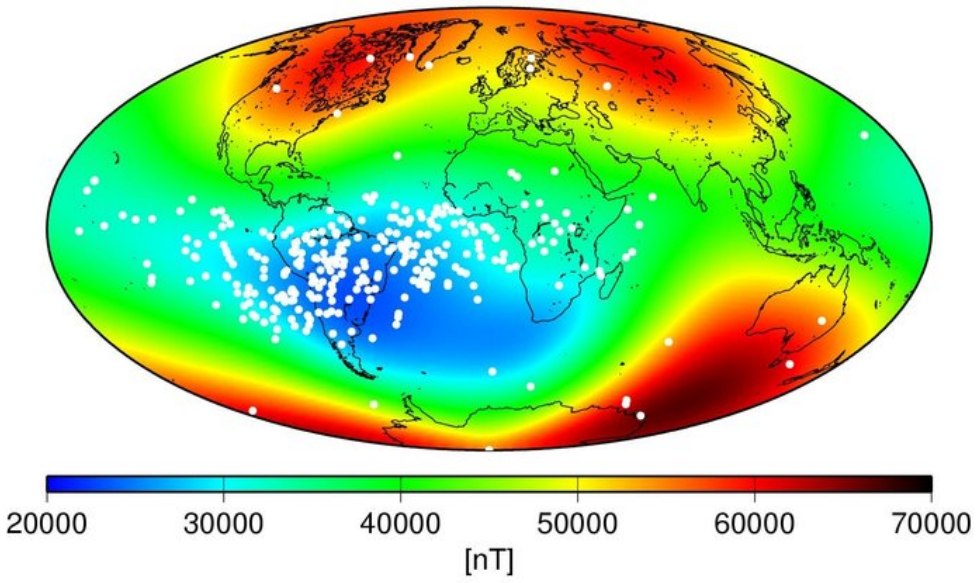

FIGURE 2.4: Positions at which a satellite (TOPEX/Poseidon) experienced single event effects due to the South Atlantic Anomaly - (European Space Agency (ESA) 2012).

When assessing long-term exposure to trapped radiation, it is important to take into consideration the 11-year solar activity cycle. The sun spends approximately 7 years of this cycle in solar maximum (Petersen 2011). This is a period in which the Sun's magnetic field forms many regions of high magnetic intensity, called sunspots. These sunspots can be seen on the surface of the sun as dark spots. The number of sunspots can therefore be used to predict solar activity as the two are directly related. Observing and monitoring the solar cycle allows one to be able to predict the years when the sun will be more active and therefore when there will be a higher probability of solar flares, coronal mass ejections and a strong solar wind. Figure 2.5 shows the variation of solar activity during the course of three consecutive solar cycles.

During an active phase, the Earth's neutral atmosphere expands and thus causes the density of neutral particles at specific altitudes to increase (Stassinopoulos & Raymond

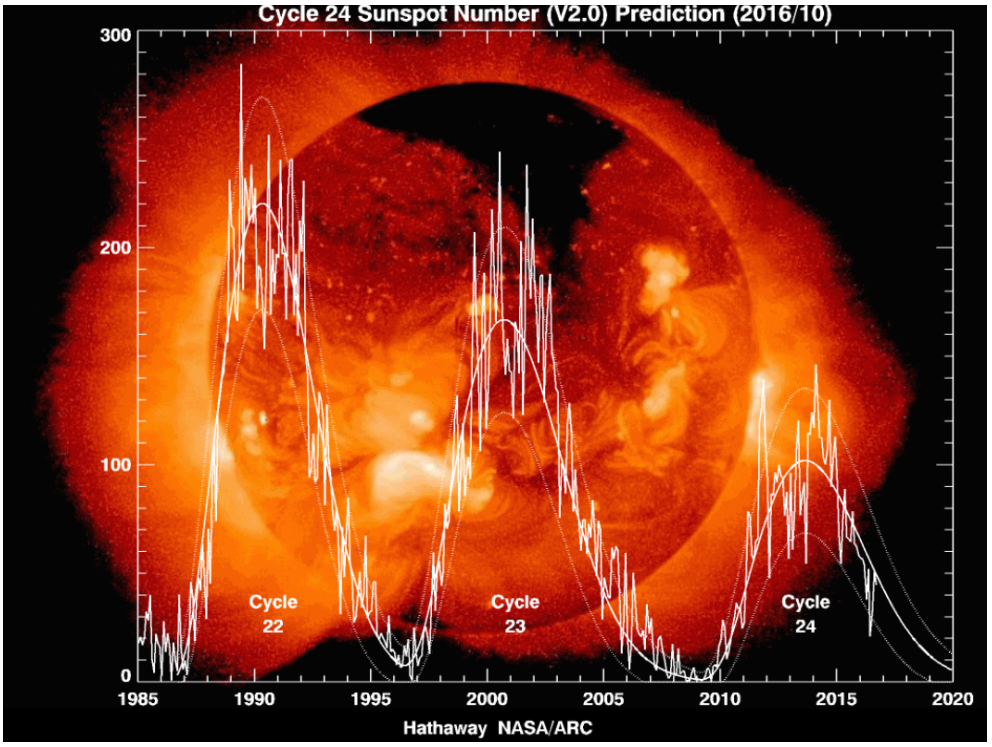

FIGURE 2.5: Solar Cycles 22, 23 and 24 - (Hathaway 2016).

1988). As the neutral constituents move further upward, they interact with the radiation belts and tend to cause a decrease in the number of charged particles, and therefore a decrease in the amount of trapped particle radiation. The opposite is observed during solar minimum, resulting in a larger amount of trapped particle radiation. This effect is more strongly seen at lower altitudes, and so it is certainly something that one needs to consider when planning and designing LEO missions.

2.1.2 Trapped Electrons

Both the inner and outer regions of the Van Allen belts contain trapped electrons. The electrons in the outer belt are more energetic than those in the inner belt, with energies reaching up to 10 MeV (the inner belt only has electrons with energies of hundreds of keV). The inner belt is usually located at altitudes of 1000 - 6000km, and outer belt extends from about 13 000 to 60 000 km in altitude. Between these two regions is an area of low electron density called the slot region. The density here can however increase by several orders of magnitude during a magnetic storm (Stassinopoulos & Raymond 1988).

2.2 Non-Trapped Radiation

Non-trapped and transiting radiation is caused by either solar cosmic rays or galactic cosmic rays. These particles come from external sources, and are not confined to the magnetic field lines of the Earth. Cosmic rays and coronal mass ejections consist of protons and some other heavy ions. The Earth's magnetic field protects most satellites from this radiation. The magnetic fields usually do not allow the radiation to penetrate to the lower altitudes.

This phenomenon can be explained using the "Frozen-in Flux Theorem", which states that particles on a particular magnetic field line will move with that field line, and will therefore not be able to penetrate another system of magnetic field lines (unless magnetic recombination occurs). Due to this, satellites that are at altitudes lower than the radiation belts will usually be safe from this type of radiation, and so these non-trapped particles will not be the the main focus of this project. However, this process is not perfect, and so there is a possibility that non-trapped radiation may penetrate through, and therefore increase the amount of radiation the satellite is exposed to.

A particle from outside the terrestrial magnetosphere will need to cross the Earth's magnetic field lines to reach a certain altitude. A particle of higher energy will be able to penetrate further than one of a lower energy due to the fact that it can cross more magnetic field lines. A particle's penetrating power is determined by its magnetic rigidity (momentum divided by charge) (SPENVIS 2011*b*). Due to this, it is only the highly energetic particles that will reach lower altitudes. A quantity called the geomagnetic cutoff determines (at a specific position in the magnetosphere) the minimum magnetic rigidity that a particle needs to reach that altitude. During magnetic storms however, this value decreases, allowing more particles of lower energies to enter too (SPENVIS 2011*b*).

2.2.1 Solar Particles

Protons, alpha particles, heavy ions and electrons are all hurled towards Earth from the sun's corona in the form of a solar wind. The wind is always present, but can vary dramatically in density, temperature and speed. Strong winds are the result of

active regions on the sun called sunspots. These are the result of the kinetic dynamo mechanism that twists the magnetic field lines of the sun. A detailed account of the dynamo mechanism, as well as the production of sunspots is given by Thomas E. Cravens (Cravens 2004) (Chapter 5 of “Physics of Solar System Plasmas"). The number of sunspots increases with the solar cycle, being at a maximum with solar maximum. Coronal Mass Ejections (CMEs) are the result of a large eruption of plasma that pushes and accelerates particles outward from the sun. This process releases extremely large amounts of energy and pushes particles away at a speed called the Alfvén Speed (Cravens 2004). This results in particles streaming toward Earth from the sun at much higher energies than usual. An image of a CME taken by the SOHO (Solar and Heliospheric Observatory) satellite can be seen in Figure 2.6 (Space Weather Prediction Center 2000).

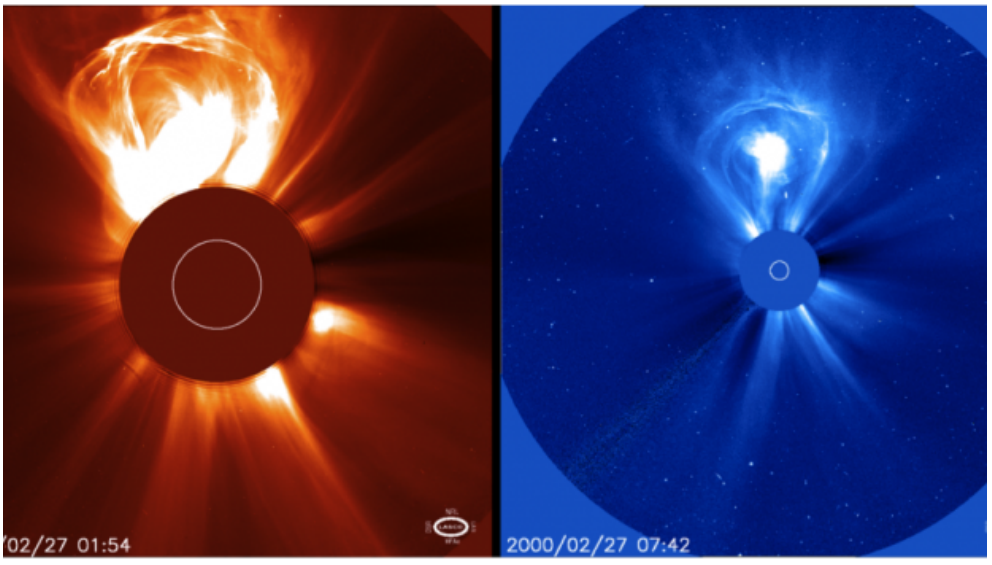

FIGURE 2.6: Two images of a CME captured by the SOHO satellite - (Space Weather Prediction Center 2000).

The particles emitted from this burst will arrive at Earth at different times, depending on their energies. The most energetic particles will arrive within 10-30 minutes (travelling at relativistic speeds), while others could take up to 2 days to arrive. If the particles are energetic enough, they could travel straight past the Earth’s magnetic field lines, and penetrate through to altitudes where satellites in LEO are orbiting. As these particles have much higher energies than the trapped protons (up to several hundred MeV), they can cause much more damage than the trapped radiation.

2.2.2 Galactic Cosmic Rays

Galactic cosmic rays (GCR) originate outside our solar system entirely. These are high-energy ions (around 1 GeV) that have been accelerated to nearly the speed of light. The Earth is constantly being bombarded with this radiation from the whole Milky Way galaxy, and so it can be considered as roughly omnidirectional. These cosmic rays are most likely formed by supernova events, and contain a wide range of positively charged heavy ions. The composition is around 85% protons 14% alpha particles, and the remaining 1% is made up of heavy ions (Stassinopoulos & Raymond 1988).

Near solar maximum, the solar wind is much stronger than at solar minimum, and this actually acts to shield the Earth from the GCR. It is therefore around solar minimum that one needs to worry about these highly energetic particles travelling through the Earth's magnetic field and hitting satellites (Petersen 2011). The Earth's magnetic field is also only efficient at deflecting the GCR away near the equator. At the polar regions (high magnetic latitudes, there is a lot less shielding from the magnetic field and so satellites and even aircraft are highly vulnerable when passing through these regions.

2.3 Modelling the Environment

It is important to be able to predict accurately the amount of radiation that a satellite will be exposed to during its lifetime. For this purpose, we require an accurate model that will be able to quantitatively represent the amount of radiation we can expect for a specific mission. The model chosen should be specific to orbital altitude, orbital type, mission lifetime and stage of the solar cycle.

It is very important for the model output to be dependant on the orbit parameters, as a change in altitude or position of the satellite could greatly affect the amount of exposure to the SAA and therefore the Van Allen belts. The model should also take into account the solar cycle, as the amount and type of radiation (both trapped and solar protons) greatly varies with solar activity, and therefore solar cycle.

We need to be able to perform tests that will correctly represent the kind of conditions that are present in space and therefore we need to attempt to replicate those conditions here on Earth by using a particle accelerator. In order to be able to relate our terrestrial

experiments with what might be expected in the space environment, we need to combine test results with accurate models. We therefore relate parameters obtained for a specific electronic device (from a radiation test) to the space environment (predicted by the models), and in doing so we obtain information on how it may operate in space.

2.3.1 Trapped Radiation Models

There are several widely used models for the trapped radiation environment. These include NASA's AP-8 (proton) and AE-8 (electron) model, the Air Force Research Laboratory's CRRESPRO and CRRESELE, ESA's SAMPEX/PET low-altitude proton model and the ONERA/DESP electron models.

- **AP-8 and AE-8**

  The NASA models are static proton (AP-8) and electron (AE-8) models, which include the effects of the solar cycle. This is however the only variation that these models take into account. The data is based on knowledge gained from over 24 satellite missions from July 1958 to June 1970 (Vette 1991). The maps include the fluxes of protons from 0.1 - 400 MeV and electrons from 0.04 to 7 MeV (Vette 1991). The fact that the satellite data runs from the late 1950s to 1970 means that the model covers more than one full solar cycle, and therefore has data for both solar maximum, and solar minimum.

  A graphical representation of an output from the AP-8 model can be seen in Figure 2.7. The distances are expressed in Earth radii, and the semi-circle represents the surface of the Earth (SPENVIS 2010*b*).

- **CRRESPRO and CRRESELE**

  The Combined Release and Radiation Effects Satellite (CRRES) mission did however demonstrate that the static environment does not fully describe the actual radiation environment, as it is much more variable and dynamic than what the AP-8 and AE-8 models describe. Unfortunately, there is no global, dynamic, trapped radiation belt model that can fully describe the environment yet.

  CRRESPRO and CRRESELE are two Air Force Research Laboratory models included in SPENVIS. CRRESPRO is a model that predicts proton omnidirectional fluence from 1 - 100 MeV per year. It uses data collected on-board the CRRE satellite for just over a year from 1990-1991 (Meffert & Gussenhoven 1994). That year was a solar maximum year, and so the data collected pertains to solar maximum. It offers a “quiet" model, and an “active" model, as there was a geomagnetic storm during its flight (which occurred in late March, 1991) (Meffert & Gussenhoven 1994). During the storm, there were major discrepancies between the CRRES model and the NASA model. This can be seen in Figures 2.8 and 2.9, which are plots of the two fluxes obtained from SPENVIS for a mission segment of 0.25 years starting on the 26th of March, 1990.

  CRRESELE is the trapped electron component of the model. It can be use to calculate omnidirectional fluences for electrons between 0.5 and 6.60 MeV (Brautigam

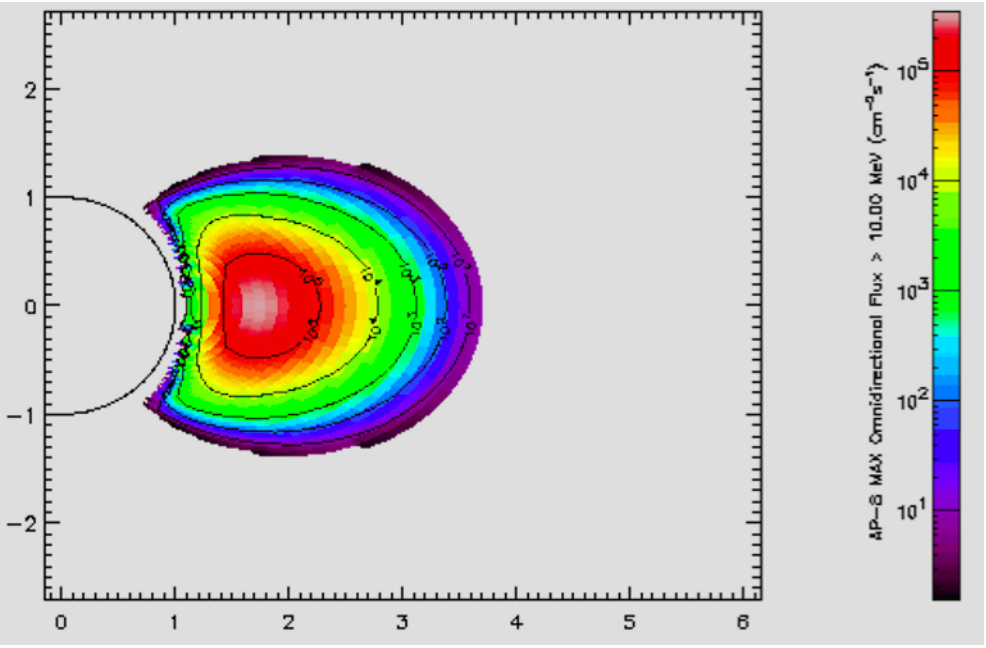

FIGURE 2.7: Output from NASA’s AP-8 model - (SPENVIS 2010*b*).

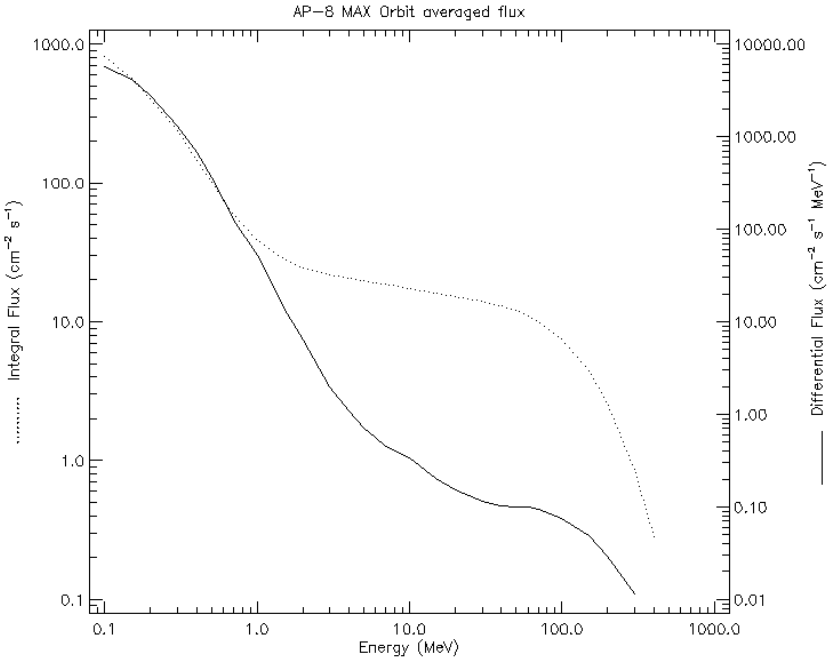

FIGURE 2.8: Output from NASA's AP-8 Model during the March 1990 Geomagnetic storm.

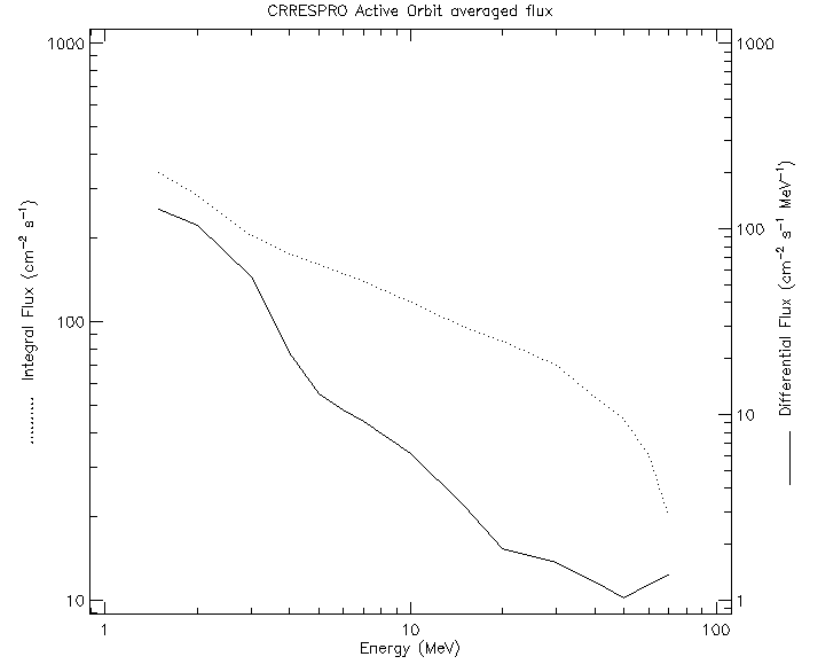

FIGURE 2.9: Output from CRRESPRO during the March 1990 Geomagnetic storm.

& Bell 1995). The data used in producing the model is also from the CRRE satellite. The preliminary model (Brautigam et al. 1992) was updated in 1995, but only in the outer belt. It is therefore not fully reliable at the lower altitudes, and caution should be exercised when attempting to use this model for the inner electron belt (Brautigam & Bell 1995).

- **SAMPEX/PET**

  SAMPEX/PET is a trapped proton model for altitudes below 600km. The data was obtained from the SAMPEX satellite, which flew during solar minimum, and so this model only represents those conditions. This is also a directional model. In order to make it omnidirectional, the fluxes are multiplied by 4 π in the SPENVIS Radiation Effects package (SPENVIS 2010*b*). SAMPEX/PET is a static model, but a new update is under development, where 8 years of data and solar cycle variation are being implemented into the model, making it a dynamic one which will more fully describe how the trapped proton population varies (SPENVIS 2010*b*).

- **ONERA**

  ONERA (Office National d'Etudes et Recherches Aérospatiales), the French national aerospace research centre, developed models for the trapped electron environment. These models are POLE V1 and V2 (Particle ONERA-LANL Environment) and IGE-2006 (International Geostationary Electron model).

  The statistical model IGE-2006 uses data collected over 2 solar cycles from satellites in geostationary orbit (SPENVIS 2010*b*). A comparison of IGE-2006 with AE-8 can be seen in Figure 2.10 from (SPENVIS 2010*b*).

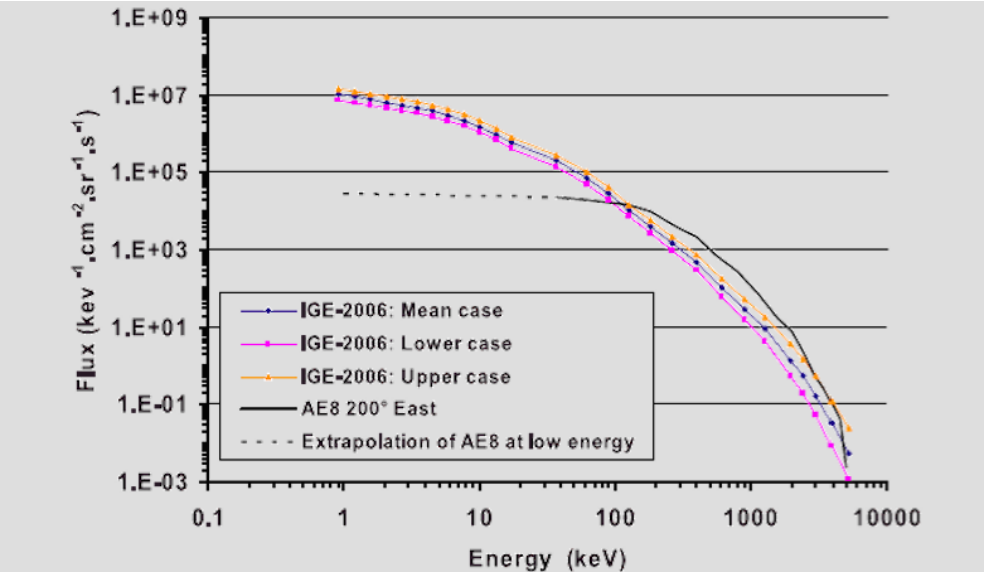

FIGURE 2.10: Comparison of IGE-2006 with AE8 for an 11 year mission - (SPENVIS 2010*b*).

2.3.2 Non-trapped Radiation Models

There are also various non-trapped radiation models to choose from. The solar proton models are King, JPL, the Rosenqvist et al. (2005, 2007) model and the ESP model.

- **King**

  The King model (King 1974) is based on data that was collected by 3 satellites, IMP 4, 5 and 6. These collected data from 1966 - 1972, which was the active phase of solar cycle 20 (King chose to ignore solar cycle 19 (SPENVIS 2010*b*)). Within the King database, there are 25 individual solar proton events, most of which are *ordinary* events, and one being an *anomalously large* (AL) event. This

event occurred in August 1972 and accounted for about 70% of the total fluence for protons greater than 10 Mev (SPENVIS 2010*b*).

- **JPL**

  The first version of the JPL model (JPL-85) uses data that starts in 1956 and covers 3 solar cycles. Feynman and his colleagues (Feynman et al. 1993*a*) disagreed with King on a number of things (omitting solar cycle 19, separating events into ordinary and anomalously large, the low number of events during cycle 19, etc.), which led them to the first version of the JPL model (J. Feynman 1990). JPL-85 was later replaced with JPL-91, whose data consists of a nearly continuous record of daily average fluxes. These fluxes are above 1, 4, 10, 30 and 60 MeV (Feynman et al. 1993*b*).

  JPL-85 did not form a uniform data set, due to the fact that there was only one major event that occurred during the data collection period. In the period from 1957-1963 there were 3 or 4 major events, and 4 or 5 between 1989 and 1991 (SPENVIS 2010*b*). Therefore, JPL-91 is a better representation than the previous JPL model .

- **Rosenqvist et al.**

  JPL-91 does however underestimate the fluence, and so the parameters used in that model (μ, σ and w) have been updated (Rosenqvist et al. 2005). These new parameters can be found in the Rosenqvist et al. models. SPENVIS therefore uses these parameters for >10 MeV and >30 MeV, while keeping the original values from JPL-91 for >1 MeV, >4 MeV and >60 MeV (SPENVIS 2010*b*).

- **ESP**

  Both the King and JPL models have incomplete data sets however. Due to this, they are only effective at predicting long-term fluences. High-quality space data is available for 3 full solar cycles, yet neither King nor JPL include all 3 (Xapsos, Barth, Stassinopoulos, Burke & Gee 1999). The ESP model aims to solve some of these issues, by reassessing the solar event fluence models using a process based on maximum entropy theory (Xapsos, Barth, Stassinopoulos, Burke & Gee 1999). The ESP model also uses data from all 3 of the solar cycles (cycles 20, 21 and 22).

2.3.3 Radiation Effects Models

Models exist that estimate the radiation effects on electronics. A few of these models are the SHIELDOSE and SHIELDOSE-2 (for Total Ionising Dose (TID)) and CREME-86 code (for Single Event Upset (SEU) rates) and Xaspos et al.

- **SHIELDOSE**

  SHIELDOSE is a computer code that calculates the absorbed dose as a function of various thicknesses of aluminium shielding. It uses data from experiments where the depth-dose was calculated for an isotropic broad-beam fluence on uniform aluminium media (SPENVIS 2011*a*). It outputs values for proton and electron dose absorbed in small volumes of aluminium. SHIELDOSE contains data for a semi-infinite plane medium (from one side only), a finite plane slab (from one side only) and a solid sphere (from all directions) (SPENVIS 2011*a*). SHEILDOSE-2 (released in 1994) differs from SHIELDOSE (released in 1980), in that the newer model contains new cross sections and new detector materials (SPENVIS 2011*a*).

- **CREME**

  Cosmic Ray Effects on MicroElectronics (CREME) can be used to calculate the estimated SEU rates in the radiation environment. This model was developed by the Naval Research Laboratory, and transforms the energy spectra to Linear Energy Transfer (LET) spectra, as well as calculating the SEU rates (SPENVIS 2011*b*). SEU rates are calculated by determining how much charge is collected within the device, and determining whether this is large enough to cause an upset. This upset mechanism is discussed further in Chapter 3. The CREME models contain data that was collected during the period of 19-27 October 1989, when very large solar proton events occurred.

- **Xaspos et al.(2003)**

  Xaspos et al. (Xapsos, Summers, Barth, Stassinopoulos & Burke 1999) is a probabilistic model which uses the same data set as CREME (i.e. the events of the 19th, 22nd and 24th of October 1989). Due to the fact that there is not a lot of data for solar proton events (only 3 events over the span of 33 years (Xapsos, Summers, Barth, Stassinopoulos & Burke 1999) (NOAA 1994)) it is difficult to describe the energy spectra of the solar protons.

  The Xaspos et al. model uses the maximum entropy method to determine a probability distribution that a large solar event would occur. The maximum entropy method is a way of calculating the probability distribution of an incomplete data set, by selecting the distribution with the largest entropy.

2.3.4 The SPENVIS platform

In order to make the modelling process easier and more user-friendly, the European Space Agency (ESA) combined many of the space environment models into one platform, called SPENVIS (SPace ENVironment Information System). This platform has been widely used for many years as an accurate source for models of the hazardous space environment (Benton & Benton 2001), (Heynderickx et al. 2004). The web-interface gives the user access to the space environmental models and their output, without having to write or interpret any code. The output from the models can be easily plotted using SPENVIS, or can be downloaded as a .txt file. This allows the user to jump between radiation models with relative ease, therefore providing a tool for an easy comparison of models.

FIGURE 2.11: SPENVIS home page at *https://www.spenvis.oma.be/intro.php*

Extensive help and background information on the models can be found on the SPENVIS website, which allows a user with very little knowledge of the space environment and no model experience to generate and gather results. SPENVIS also uses an ESA-developed orbit generator which will tailor all the output values from a given model to the specific

orbit of interest. This takes into account the number of times that the satellite will pass through the SAA or over the poles (for trapped radiation), or the exposure time for solar protons. The exposure time is the period of time in which the satellite will be on the sun-side of the Earth, and therefore will be vulnerable to solar protons. The orbit is specified at the beginning of the modelling process, and so the user does not need to re-specify the orbit parameters every time a new model is consulted.

However, because of the user-friendliness of the platform, many of its users do indeed have very little understanding the space environment as well as the specifics of the models within the platform. Using SPENVIS without fully understanding the space environment and the models thereof may lead to a misinterpretation of the results. A detailed account of how SPENVIS is used is given in Chapter 5 and the effects of altering certain input parameters is discussed in Chapter 7.

Chapter 3

Effects on Electronics

3.1 Semiconductor Electronics and Charge Deposition

All semiconductor devices, such as transistors, are susceptible to radiation effects and potentially even permanent damage. This makes any circuit or device that contains transistors vulnerable to radiation. Whether the transistor is a Bipolar Junction Transistor (BJT) or a Metal Oxide Semiconductor Field-Effect Transistor (MOSFET) will lead to different effects when a particle travels through the component. The main difference between these two, is how the current travels through the component. As can be seen in Figure 3.1 (Hitek 2016), in a BJT the current needs to travel through the base itself in order to get from the collector to the emitter. However, in a MOSFET, the current doesn't travel through the gate directly, but instead the gate acts as a throttle to control the flow between the drain and source.

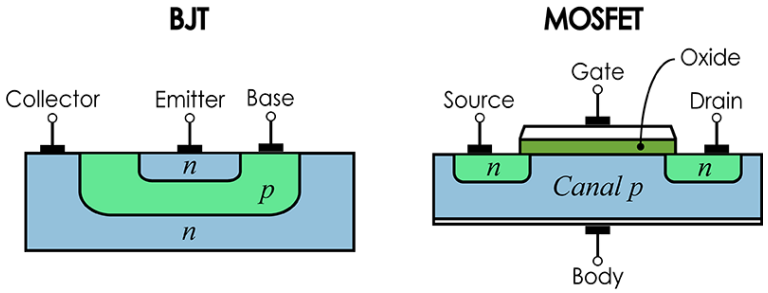

FIGURE 3.1: Illustration of the difference between a BJT and a MOSFET- (Hitek 2016).

As a charged particle travels through matter, it will deposit some of its energy within that matter. At some specific point after travelling a certain distance it will come to

rest. As the energy loss of charged particles is inversely proportional to the square of their velocity, most of the energy loss occurs just before the particles come to a stop. Each material has a certain characteristic depth of penetration for incoming particles of a given energy. This point is called the *Bragg Peak* on the Bragg curve, and it represents the maximum amount of energy deposited as a function of path length (see Figure 3.2 (Scripps 2016)).

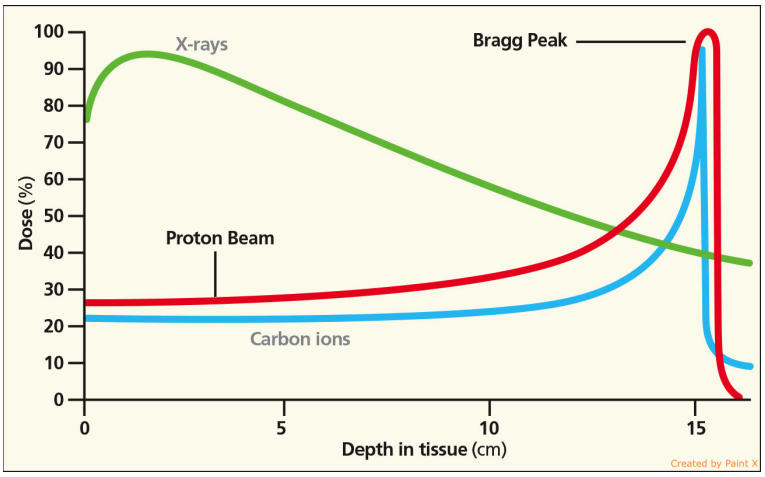

FIGURE 3.2: A Bragg Plot of X-rays, protons and carbon ions within human tissue- (Scripps 2016).

For direct ionisation, if the Bragg peak falls within a sensitive region of the device, it will deposit charge there. A particle of low energy will deposit its charge in a shorter path length than one of higher energy. This means that only particles with a very specific energy will deposit their charge within the device, causing direct ionisation. Most of the particles in the space environment are of such high energies that the Bragg peak falls outside the device, and so the particle itself will not deposit enough energy within the device to cause a problem.

For the case of indirect ionisation, however, a charged particle can interact with other atoms and cause secondary particles to be produced. A secondary particle may have a Bragg peak that falls within the dimensions of the device. Alpha particles are often observed as secondary particles. These are produced inside the component, and deposit most of their energy within a very small distance, so these will deposit a large amount of charge within the semiconductor device. Different effects will occur when this charge is deposited within different areas of the device, so one needs to consider all the different effects that could occur.

3.2 Total Dose

The first type of radiation effects that were observed to cause failure of space electronics were ionisation (or total dose) effects (Pease et al. 1988). These are long-term, cumulative effects that will slowly degrade the performance of a device over time.

Electron-hole pairs are created when radiation passes through a semiconductor device. This happens when a charged particle travels through the neutral SiO_2 layer of the device. The electrons, being more mobile than the holes, are swept out and leave an abundance of holes behind (Maurer et al. 2008). These holes are then transported to an interface within the semiconductor device and become trapped there. Crystalline flaws that are present within the oxides will trap the holes as they pass by, leading to the layer no longer being neutral.

The rate at which the holes move depends on the magnitude of the electric field they are exposed to. The time taken to travel ranges from microseconds in a strong electric field, to hours in a much weaker field (Pease et al. 1988). These trapped holes cause a negative shift in the threshold voltage of the device, by changing the amount of throttling of the gate. This is due to an electric field now being present in the usually neutral SiO_2 layer. In n-channel devices, if enough holes are trapped, the shift can be so large as to decrease the threshold voltage so much that a transistor that is normally “off" could be turned “on" at zero volts (Pease et al. 1988). This shift in the threshold voltage may also cause the supply current to increase, and slow down the device. This is because the output drive, power consumption and speed are all related to the threshold voltage (Maurer et al. 2008).

In a MOSFET device, total dose will change the threshold voltage of the device. This could lead to a device being permanently off or permanently on (depending on whether it is a positive/negative charge deposition, and whether the device is an n-channel or p-channel device). In a BJT, the charge deposited could create a local electric field within the device, modifying the p-n junction. This will change the gain of the device, which in turn will modify the way the circuit operates. This is due to the fact that the amount of amplification will be modified, which could lead to a saturated output.

Total Ionizing Dose (TID) can be defined as the long-term ionising damage to a semiconductor device that occurs when it is exposed to high energy particles (Wirthlin et al.

2003). TID can be reduced by using aluminium shielding, however, protons with energies of 10-100 MeV can easily penetrate a few mm of the shielding. These energies are highly abundant in the Van Allen Belts, and so aluminium shielding does not provide a lot of protection for satellites in LEO that will pass through the SAA.

3.3 Displacement Damage

Particles such as protons, neutrons and electrons that strike the device will deform and impair the structure of the lattice. This effect is known as displacement damage. It deforms the crystalline structure and will therefore alter the electrical properties of the material. It differs from the other types of radiation damage we are discussing, as it is not actually an ionising effect, but instead it is the result of a ballistic collision. Figure 3.3

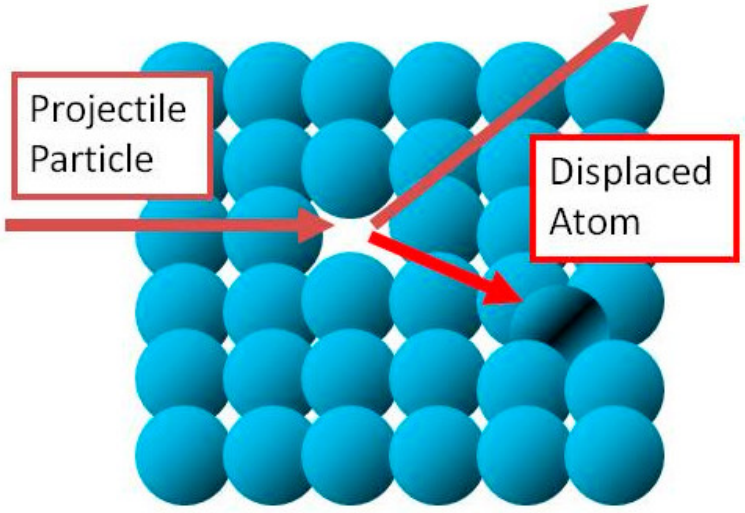

FIGURE 3.3: Diagram to show the principle of displacement damage - (Group 2015).

Displacement damage also causes the lifetime of the minority charge carriers in the transistors to be reduced. In n-type transistors, these are the holes and in p type, these are the electrons. Their lifetime is defined as the amount of time (on average) that it will take for that carrier to recombine with a carrier of opposite charge. If this lifetime is reduced, it means that over a certain period of time, there will be fewer charge carriers than usual.

Due to the fact that the damage to the structure cannot be repaired, displacement damage is a cumulative effect which will degrade the lattice over time. Bipolar transistors

and solar cells, particle detectors and light sensors are particularly susceptible to this type of radiation damage. These devices collect charge in order to give a measurement. If the charge capturing capability changes, then the calibration will be off, leading to incorrectly calibrated measurements being taken.

3.4 Single Particle Effects and Transients

Ionisation caused by the passage of a *single* particle through a sensitive region in a semiconductor device could result in a failure, thereby causing a single event effect. A particle travelling through a semiconductor would collide with atoms within the semiconductor, releasing charged particles that leave an ionisation track. The amount of charge per unit length of the track is called the linear energy transfer (LET). LET is measured in pC/μm or MeV/mg/cm^2 and is dependant on the particle type and energy (Pease et al. 1988). It is normalised by the density of the target material, so it can be quoted roughly independently of the target material (Dodd & Massengill 2003). The amount of energy that a particle can deposit within a device will depend on where the Bragg Peak (Figure 3.2) is located for the materials comprising that device. If it is located within the device, it will have a very large LET, depositing lots of energy (usually only for low-energy particles). We can define a threshold LET as the minimum energy required to produce a single event effect (SEE). This threshold LET is decreasing as electronics become smaller and more compact, and so the chance of SEEs occurring is actually increasing(Nwosa 2011).

One also needs to consider the possibility of indirect radiation causing an upset. This occurs when a high energy particle (such as a proton or a neutron) undergoes an inelastic collision with another particle or target nucleus within the device. These collisions may result in much heavier particles being produced, which would then deposit a larger amount of charge (due to their Bragg peaks being within the material) and therefore LET (Dodd & Massengill 2003). A graphical representation of the ionisation track can be seen in Figure 3.4 (Sawant 2012). Voltage and current transients can occur if the ionisation track occurs at the depletion region of an N-P junction (Sawant 2012) (a region where there are usually no mobile charge carriers).

These transients are a problem because they can potentially cause a logic flip, or even a short circuit within the device. This could lead to temporary service blackout, loss of data that has been stored, impaired operation and even complete failure of the satellite in extreme cases. Power supplies, logic devices, memories and detectors are all vulnerable to SEE, so it is very important for one to consider this when designing and testing satellite electronics.

3.4.1 Single Event Latchup

All Complementary Metal-Oxide-Semiconductor (CMOS) devices are susceptible to Single Event Latchups (SEL). A latchup is the effect that occurs when a parasitic p-n-p-n structure of bulk CMOS is triggered into regenerative forward bias. If a low-resistance path is created between the gate and collector, gate and emitter or even the power and ground rail a latchup could occur. The path comes about as a result of a charged particle traversing through the device, depositing charge via LET, and causing a current to flow. This low-resistance path (short circuit) develops between the higher power supply rail and the ground rail, and continues to exist even after the event has occurred (Sexton 2003), due to the fact that the current flowing through the path actually maintains the path itself. Latchup is particularly likely when a heavy ion passes through the device, as it will have a high enough LET to cause the path to be formed.

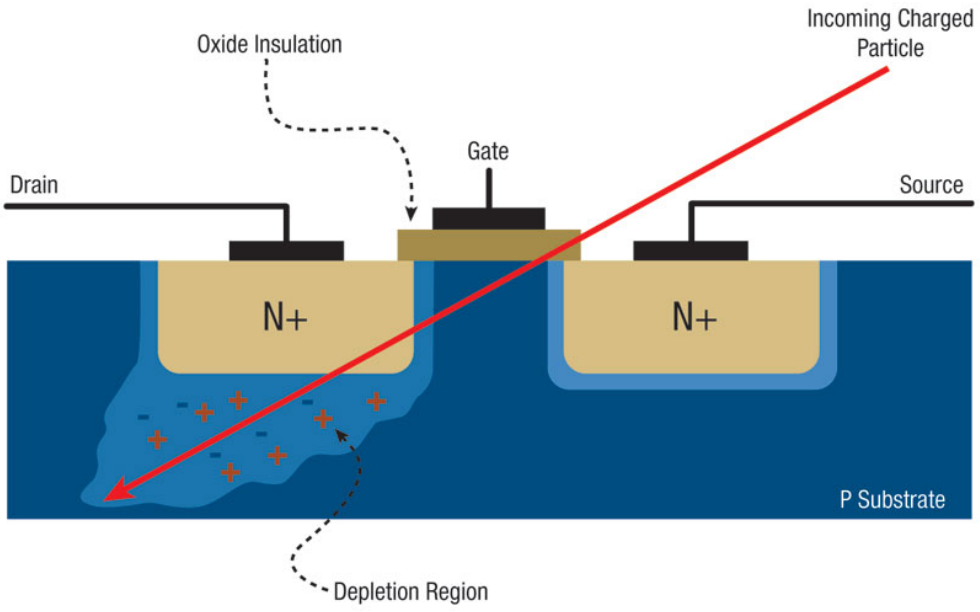

FIGURE 3.4: Ionisation track caused by a single particle - (Sawant 2012).

Large runaway currents can flow along these low-resistance paths. The increased current causes more heat to build up and can cause wires to fuse open and silicon regions to melt. The current will continue to flow until power is removed from that part of the circuit, or until the device fails completely (Sexton 2003). The latchup can be released either by lowering the voltage (lowering the gain of the transistor) (Swift 2014) or by turning the device off. One needs to ensure that the device is powered down soon after latch-up occurs in order to avoid permanent damage. This can be done using a watchdog that will cause a power-down if it senses a latch.

3.4.2 Single Event Upsets

Single event upsets are characterised by bit-flip errors. An ionising particle may produce electron-hole pairs within a semiconductor device as it travels through it by charge deposition. This will lead to a single event upset (SEU) if the charge accumulated is large enough to cause a change in state (SPENVIS 2011*b*). An event will therefore only occur if the charge is equal to a certain threshold value, called the critical charge of the device (Pease et al. 1988). The regions which are most sensitive to SEU are reverse-biased p/n junctions (Dodd & Massengill 2003). This is due to the fact that triggering of a gate will cause the device's state to flip. Even after the transient goes away (i.e. the charge gets depleted), the device stays in the flipped state.

SEUs are known as "soft errors" due to the fact that they do not cause permanent damage to the circuit. They are also equally likely to occur at any time within the mission lifetime. This means that once an SEU is corrected it can reoccur again in the same location or at a completely different location. Although SEUs are not as fatal as latchups, they do occur much more often. The consequences of SEU will have varying harshness on the system, depending on where they occur. Upsets within stored or collected data are less severe than upsets that could result in processing errors (Caffrey et al. 2002). For example, if an error occurs within a register, it could cause the whole integrated circuit (IC) to stop working.

Due to the non-permanent nature of these errors, they can be corrected by re-writing the original code onto the device (i.e. the code stored in the configuration memory). Configuration memory is used to specify the hardware layout of the FPGA. If an upset

occurs here, it is a lot more serious, as it could change the design of the FPGA and therefore change the operation of the circuit.

In Dynamic Random Access Memory (DRAM), any error (i.e. change in state) of the stored information will remain until corrected by external circuitry (Dodd & Massengill 2003). With this type of memory, the vulnerability is also not constant with time, but is related to the clocking of the cell (Dodd & Massengill 2003). In Static Random Access Memory (SRAM), active feedback is present. A particle travelling through the device can result in an induced current in a transistor. The feedback mechanism attempts to balance out this current. Due to this, a voltage drop in the drain of the transistor occurs. In SRAM, this is the signal for a “write" command, and so an error can occur where the wrong memory state is fixed onto that memory cell (Dodd & Massengill 2003).

These effects cannot be reduced using shielding. The mitigation techniques that have been shown to be the most effective are Triple Modular Redundancy (TMR) and scrubbing.

3.5 Important Circuits to Consider

As the demand for performance and capability of satellites is ever rising, the strain on the electronics on board is increasing too. This means that the general trend is toward more powerful electronics that can handle more tasks more quickly. It is therefore important to perform radiation hardness assurance tests on certain devices which would be useful to have on future satellites.

A Field Programmable Gate Array (FPGA) is a semiconductor device that contains a matrix of logic blocks and programmable interconnects (Xilinx 2011). It is used to implement a combinational logic circuit in order to perform Boolean algebra. FPGAs differ from Application Specific Integrated Circuits (ASICs) because they are able to be programmed after manufacture, whereas ASICs are task-specific due to the fact that they are manufactured for one function. In other words, FPGAs allow one to program the actual hardware of the circuit, as opposed to only being able to write software to run on an existing processor circuit. FPGAs are becoming more popular in space-related applications, as they are re-programmable, and have the unique ability to be configured after the spacecraft has been launched (E. Johnson & Caffrey 2002). Due

to this, changes in the hardware of the device after launch, as well as multiple missions become a possibility. FPGAs are however sensitive to radiation effects.

Another important device on-board a satellite is flash memory. Flash differs from Random Access Memory (RAM) in that it retains all data written to it, even after a shutdown or a reset. This is useful as the satellite may need to do a total reset while in space, or it may unexpectedly shutdown and need to be rebooted. This would lead to data loss if the data were not stored in flash memory.

Of course, power needs to be supplied to all the other circuits and devices, so it is also very important to consider a Switched-Mode Power Supply (SMPS). This is a device that is able to regulate the amount of voltage at a specific point. One needs to ensure that the correct voltage is present for a device to operate properly. The SMPS uses switching transistors and feedback to generate a Pulse-Width Modulated (PWM) waveform which will change form in order to ensure the correct amount of voltage is supplied.

The general trend with many satellite manufacturers nowadays is towards using Commercial Off-The-Shelf (COTS) components. These are more susceptible to space weather effects than space-grade components, but are much more affordable, and therefore easily accessible to smaller businesses and academic institutions. Due to the fact that these are not space-grade components, one is required to perform radiation tests prior to launching, in order to ensure the reliability of the components and therefore the operation of the satellite.

Chapter 4

Terrestrial Tests and Calculating the Upset Rate

4.1 Terrestrial Testing

In order to be able to estimate how many upsets one would expect for a certain component as a function of time (upset rate), we need to understand how the electronic device behaves under certain conditions. Due to this, we need to perform ground-based laboratory tests on the different components before the satellite is put into orbit. These ground tests help the engineers to make a decision about whether the device is fit for use in space or not.

There are two types of radiation ground testing that are important for this project. The first is a total dose test, where the Device Under Test (DUT) is irradiated with radiation for a period of time in order to test the total amount of radiation it can withstand over its lifetime.

The second type of radiation test is a single event test, which is performed in order to obtain a cross-section curve that represents the DUT. These are carried out in a different manner to the TID test, as the upsets or errors are time-independent and can therefore occur at any stage of the test. The cross-section curve that one obtains from the radiation test is a curve that represents the sensitivity of the device to particles of different energies. An example of such a curve can be seen in Figure 4.1 from a study by D. Shougang, Y. Suge, L. Hongxia, F. Long and Z. Hongchao (Shougang et al. 2015).

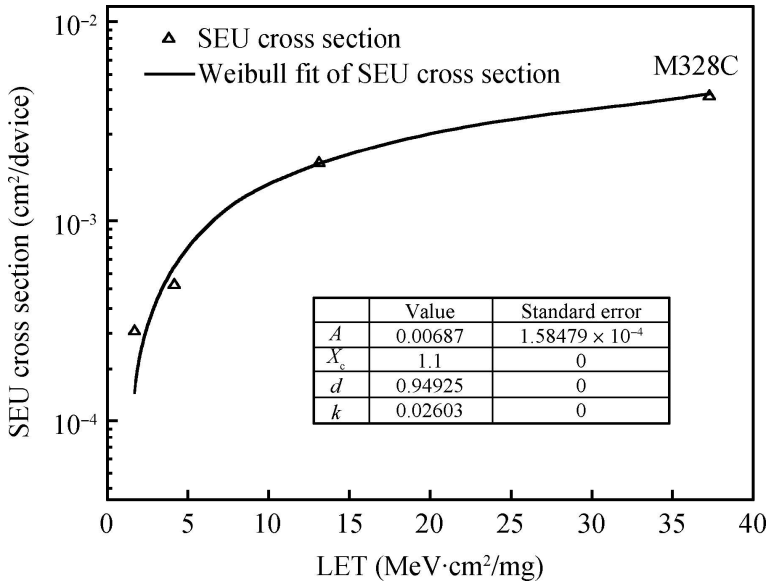

FIGURE 4.1: A cross-section curve for a SRAM device as determined by Shougang et al.- (Shougang et al. 2015).

The concept of an upset cross-section curve can be understood if one thinks of the device turning on when a certain amount of charge (critical charge) gets deposited within that device (Petersen 2011). The charge deposited is the LET from the particle, and so we can think of the device turning on when the LET is above a certain threshold value. One would therefore expect the upset curve to look like a step-function, being zero up until a certain LET value is reached. The process is a bit more complicated than that, which is why real cross-section curves are not step-functions. This is due to the fact that not every device on an electronic circuit board has the same sensitivity to upsets. While the LET is determined by how much energy the particle deposits into the device along its path, the critical charge that is needed to cause an upset is determined by the sensitivity of a particular component. The rectangular parallelopiped model (RPP model) assumes that the critical node (the place in which the charge is collected) is surrounded by a sensitive volume (SPENVIS 2010*a*). This sensitive volume is assumed to be described by a parallelopiped shape, which means that each face of the 3D structure is a parallelogram. It is also important to note that not only does the trail of the particle deposit charge into the device, but it also leads to an alteration of the electric field within the device, which enhances the charge collection process, leading to a funnelling effect (SPENVIS 2010*a*).

Laboratory tests are performed in order to produce this cross-section curve. The curve is produced by irradiating the Device Under Test (DUT) and counting the number of

errors that occur during the test. The cross-section for a proton or heavy ion test can be thought of being similar to the concept of a cross-section in nuclear physics (Petersen 2011). Each circuit that gets tested will have its own sensitive volume, and all the devices within the circuit each have a particular device sensitivity. These are what determine the number of upsets that occur in a proton test. The cross section per chip can be defined as the number of upsets observed per unit of fluence (Equation 4.1). The fluence, F, has units of particles/cm^2 and the cross section, σ, will therefore have units of cm^2. One can also calculate the cross-section per bit of the chip, by dividing Equation 4.1 by the number of bits (M), to get Equation 4.2 (Petersen 2011). The flux of the beam is defined as the rate at which the particles strike a unit of surface area (units of particles.cm^{-2}s^{-1}). By integrating the flux over time, we get a value called the fluence (F in Equations 4.1 and 4.2) (Petersen 2011).

$$\sigma = \frac{N}{F} \tag{4.1}$$

$$\sigma_M = \frac{N}{FM} \tag{4.2}$$

4.1.1 Specifics of a Terrestrial Test Set-up

Terrestrial tests for SEE are performed using particle accelerators. The beam from the accelerator is used to characterise the sensitivity of the device for particles of specific energies. From looking at a cross-section curve, one can see that more than one energy needs to be tested in order to be able to produce the curve. Many accelerators have the capability to alter the energy of the particles, however this is a very lengthy process and could take many hours for the facility to alter the energy. Due to this, many test set-ups are designed to use a beam of a specific energy supplied by the facility, and then the beam is degraded to different lower energies using perspex. For example, a 200 MeV proton beam can be degraded to 70 MeV (Wieszczycka & Scharf 2001) and an electron beam of 6 MeV can be degraded to 3.9 MeV by using just 6mm of perspex (Hensley et al. 2014). Therefore, by using different thicknesses of perspex, one can test the devices at energies lower than the beam energy. It is however important to note that the exact energy of the beam after degradation must be well known. This can be done either by

testing the beam once it has passed through the perspex, or by calculating the amount of degradation based on the thickness of the perspex.

The DUT should be placed within the beam diameter, while all test circuitry should be well outside the beam diameter (at least twice the diameter of the beam (Schwank et al. 2013)). This is to ensure that the test circuitry will not be susceptible to total-dose degradation. This can be done by using apertures to decrease the diameter of the beam. For proton tests, one does not require the DUT to be within a vacuum chamber. This allows for multiple circuit boards to be tested without having to shut off the beam, as a mechanical rig can be used to position the different circuits in front of the beam.

The beam itself needs to be well characterised. The beam shape, diameter, energy and current should all be known before the test starts. The beam flux should also be close to a flat spectrum over the area to be irradiated, and should not vary by more than 20% across the DUT (Schwank et al. 2013). A Faraday cup is usually used in accelerator facilities to stop the beam and also to measure the beam current. A reading of the current should be taken just before and just after the experiment to see if the current has changed in any way during the experiment.

Once the test is running, the beam is incident on the DUT and the number of errors obtained can be counted. Software can read in a stream of data from the DUT and this can be compared with the original data in order to see if there are any errors. The errors are usually corrected, and so if one counts the number of times that errors are corrected, this yields a count of the number of errors that have occurred. The statistical uncertainty can be calculated as approximately $\frac{1}{\sqrt{N}}$ where N is the number of particles (Schwank et al. 2013). The greater the number of particles we expose the device to, the smaller the uncertainty. However, one needs to ensure that the number of particles the DUT is exposed to is well below the total dose conditions (less than 80%) (Schwank et al. 2013).

4.2 Terrestrial Tests in South Africa

FIGURE 4.2: iThemba LABS facility- (iThembaLABS 2017).

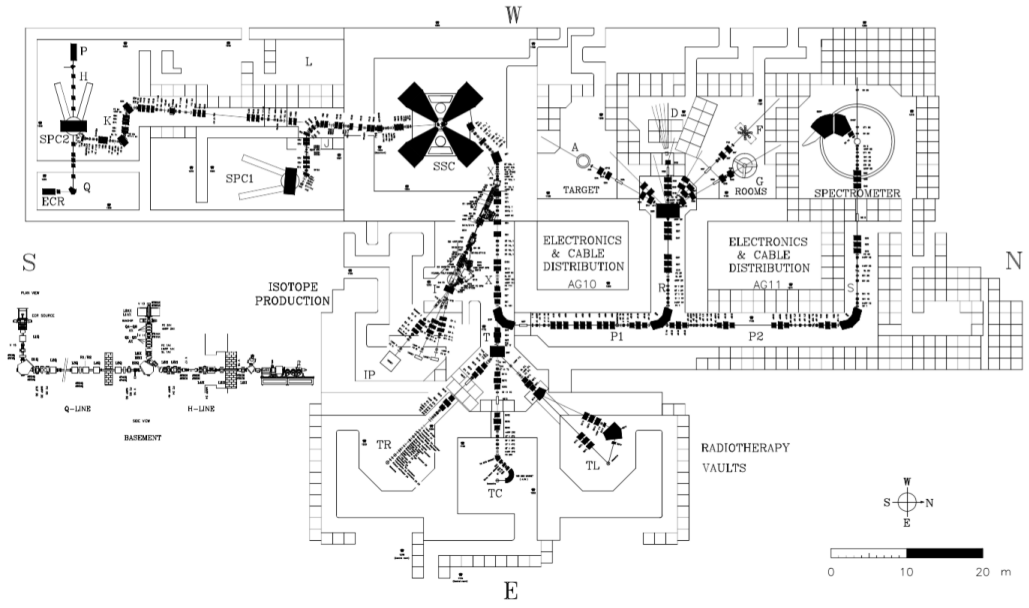

FIGURE 4.3: iThemba LABS floor layout - (iThembaLABS 2017).

In South Africa, the iThemba Laboratory for Accelerator-Based Science (LABS) facility in the Western Cape can be used for carrying out the laboratory tests described above.

At this facility, there are a number of sub-atomic particle accelerators which can accelerate protons up to 200 MeV (iThembaLABS 2017). This beam is used for many different applications, including neutron therapy, proton therapy, radio nuclide production and nuclear physics experiments. The beam that is used on Tuesdays to Thursdays is a proton beam of 66 MeV. Mondays and Fridays the beam is set to 200 MeV for proton therapy, and on the weekends the beam energy may be set to either 66 or 200 MeV for the nuclear physics experiments (iThembaLABS 2017). The majority of the time the beam is set to 66 MeV, and so it is likely that if one were to be given a slot to perform a radiation hardness test, this is the beam that the tests would be performed with. It is possible to obtain a cross-section curve for single event upsets using this energy, and degrading the beam using perspex. However, testing for latchups would require the 200 MeV beam.

Therefore the radiation hardness tests that are likely to be performed in South Africa at the iThemba LABS facility are single event upset tests using the 66 MeV proton beam. Due to this, this project will focus mainly on the proton-rich radiation environment, proton models and single event upset cross section curves that are obtained using proton beams. It is also possible to perform latchup tests using the 200 MeV beam, but obtaining beam time would be more difficult.

4.3 Obtaining an Upset Cross-section Curve

Once the tests have been performed and the number of errors counted for an array of different beam energies, a cross-section curve can be produced. The number of events counted for each energy can be converted to a cross section value by using Equation 4.1 and then plotted against either the energy of the protons in the beam, or the LET. For proton tests it makes more sense to plot the SEU cross-section against proton energy and not LET, as nuclear interactions are involved. Many papers and experiments still choose to quote LET, however. The cross-section shape usually follows an integral Weibull shape or a lognormal curve. It is best to have at least 4 different energies, and therefore 4 data points, to be able to accurately define the curve shape (Petersen 2011). The Weibull equation can be seen in Equation 4.3. If it is impossible to obtain many data points due to limitations in the testing procedure, one can use the Bendel 1-parameter equation (Equation 4.4) or the Bendel 2-parameter equation (Equation 4.5)

(Buchner et al. 2002). These do allow for fewer data points, but will not produce as accurate a result as a Weibull fit.

$$f(E) = \frac{\alpha}{n}\left(\frac{E-\gamma}{n}\right)^{\alpha-1}.\exp\left[-\left(\frac{E-\gamma}{n}\right)^{\alpha}\right] \tag{4.3}$$

$$s = (24/A)^{14}[1-\exp\left(-0.18Y^{0.5}\right)]^4 \tag{4.4}$$

$$s = S[1-\exp\left(-1.18Y^{0.5}\right)]^4 \tag{4.5}$$

In the Weibull equation, α is the shape parameter, n is the scale parameter and γ is the location parameter. In the Bendel equations, $Y = (18/A)^{0.5}(E-A)$ and both A and E are in MeV. E is the proton energy and A is a fitting parameter. S is the the proton limiting cross section (the maximum).

The Weibull function has a cumulative density equation that can be manipulated into a specific form that is very useful when wanting to fit cross-section data. If the proton energies are quoted in LET, we can use Equation 4.6. Here, σ and σ_o represent the cross section, and the limiting cross section parameter respectively. l and l_o represent the LET and the LET fitting parameter. w is the scale parameter and s the shape parameter (Petersen 2011). Therefore, the parameters that need to be fitted for are σ_{lim}, l_o, w and s. It is important to note that more data points than fitting parameters are required in order to produce an accurate curve. Due to the fact that there are 4 parameters, a requirement of having 4 or more data points is imposed in order to be able to fit this curve.

$$\sigma = \sigma_{lim}\left[1-e^{-\left(\frac{l-l_o}{w}\right)^s}\right] \tag{4.6}$$

Once the fit equation has been selected (Weibull, lognormal or Bendel), the next step is to use the data points to calculate the parameters for the equation and plot the data points along with the fitted curve. The final curve should be similar to that of Figure 4.1. Note that this figure has a log-linear scale, and uses LET for the x-axis.

4.4 Calculating the Upset Rate

Once the tests have been performed and the upset cross-section curve has been produced, the upset rate for a mission can be estimated. The upset rate depends on two things: firstly, on how likely an upset is to occur for particles of different energies, and secondly, how many particles of each energy the device is likely to be exposed to during its mission. The first piece of information comes from the terrestrial tests and more specifically the upset cross-section. The second piece of information comes from a space radiation model.

A radiation model needs to be consulted in order to obtain spectra of the particles for a specific orbit and mission. This can be downloaded from any of the models on the SPENVIS platform. There are many models to choose from and the engineer will need to decide which model output they are going to use, as well as deciding whether they are going to combine the effects of trapped and solar protons, or just consider either one individually. Once the final spectrum has been obtained (either from a single model or a combination of models) it can be combined with the results from the terrestrial tests to get the expected upset rate for the mission.

The SPENVIS platform is able to estimate the upset rate of a certain device if the critical charge or the cross section is known from experiments. There are two methods that SPENVIS uses to estimate the direct-ionization upset rates. The Rectangular ParalleloPiped (RPP) method, and the Integral Rectangular ParalleloPiped method (IRPP).

The RPP method is used when the critical charge of the device is given, and the IRPP method is used when a cross section is given in the form of a Weibull function, Bendel function or a table of cross-section data. The IRPP method is a more accurate method of calculating the upset rate, due to the fact that the RPP model assumes a step function shape of the cross-section curve and the IRPP takes the whole shape of the curve into account. The IRPP model does however require having more than one data point in order to produce the Weibull or Bendel function.

When using the IRPP model, the upset rate (R) can be calculated using Equation 4.7, where $\frac{d\Phi}{dE}$ is the differential flux obtained from the model, and $\sigma_{SEU}(E)$ is the upset cross-section (Petersen 2011).

$$R = \int_{Emin}^{Emax} \frac{d\Phi}{dE} \sigma_{SEU}(E) dE \tag{4.7}$$

This equation represents a multiplication of the upset cross section with the flux at each energy value. The integral is present due to the fact that the rates over all energies need to be summed up in order to get a total upset rate for the specific mission. The rate will have units of upsets/unit time. The unit of time is determined by the mission duration that was specified when using the model of choice. For example, if a year-long mission was modelled, the rate will be in upsets per year. One can assume that this can be linearly scaled down and quoted as a value of upsets per week, per day, etc. SPENVIS will automatically quote the output as bit^{-1} (i.e. number of upsets for the total mission specified), $\text{bit}^{-1}s^{-1}$ (number of upsets per second) or $\text{bit}^{-1}day^{-1}$ (number of upsets per day).

Part II

Experimental Procedure

Chapter 5

Modelling Procedure

5.1 SPENVIS

In order to find a suitable model for the space environment, one has to consider various different aspects. There are many models to choose from on the SPENVIS platform, and the choice of model can greatly affect the outcome of an upset rate calculation. Due to this, the models under consideration should be very well understood, as well as each step in the modelling process.

Figure 5.1 is a graphical representation of the way the SPENVIS platform works. Once the user has created an account on the website, the first project can be created. Note that when creating an account, there is the option for either a normal or advanced user. The differences between these user categories will be discussed further on. The user is then taken to a page where the models can be selected. The models are organised into packages, and all the package names can be seen in Figure 5.2, which is what the user will see on the website. The list of models within each package can be seen once that package has been selected.

It is very important to note that certain models and packages depend on the output from other models. Due to this, some models may need to be run before others. This also means that those models will need to be re-run if parameters within the pre-required model are altered. The first package that is listed is the Coordinate generators. Here you can select between spacecraft orbits, geographical coordinate grids or switching to another planet (the default planet is Earth).

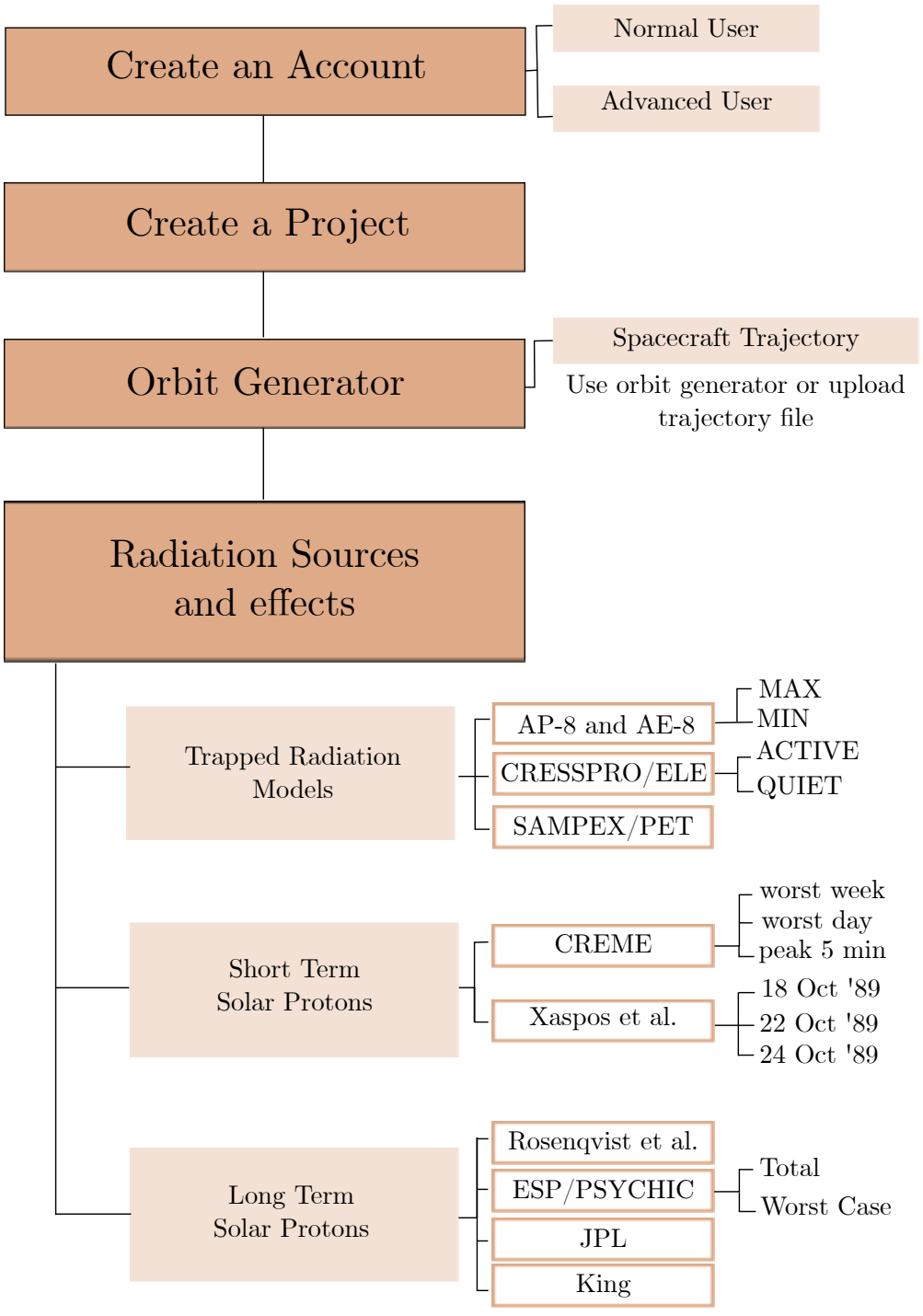

FIGURE 5.1: Graphical representation of the SPENVIS platform.

5.1.1 Using the Orbit Generator

The first step of the modelling process is to define the orbit of interest. The orbit generator is accessed once the spacecraft trajectories option has been selected. SPENVIS uses this information to personalise all subsequent model outputs so that they are specific to the orbit of interest. Therefore, the orbit needs to be specified before any of the radiation models can be run.

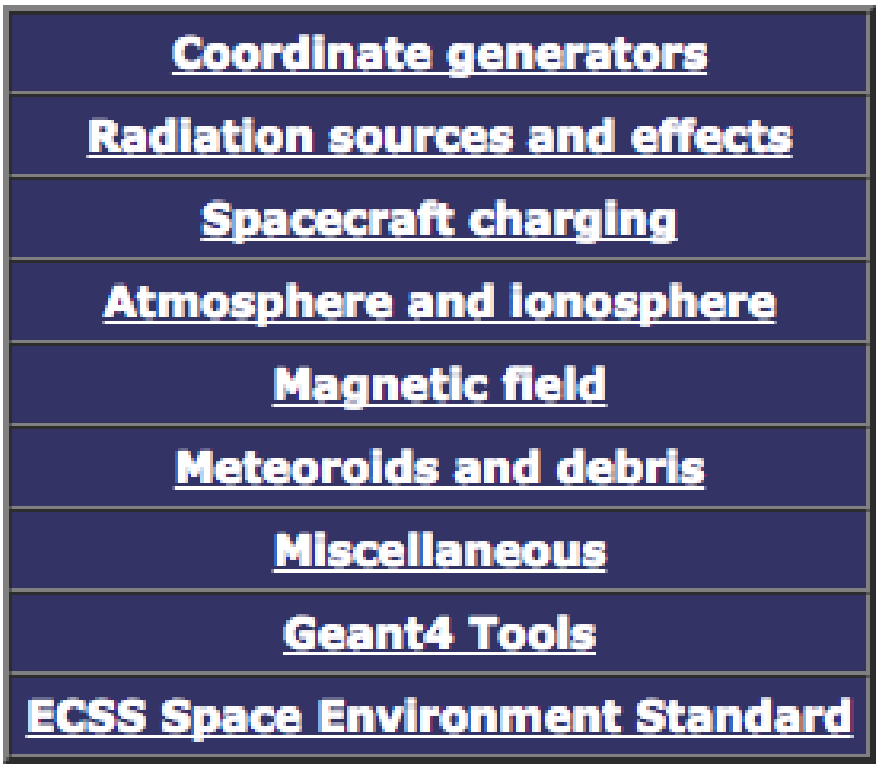

FIGURE 5.2: Package selection page on the SPENVIS platform.

The motion of any satellite will obey Kepler's three laws. They are as follows Kepler:

- The orbit is an ellipse with the planet at one of its foci.
- The radius vector of the satellite with respect to the planet as origin sweeps over equal areas in equal time.
- The ratio of the squares of the periods of two satellites is equal to the ratio of the cubes of the semimajor axes of their orbits.

SPENVIS calculates the orbit trajectory based on a number of inputs, and uses a numerical Runge-Kutta integration method Runge-Kutta. SPENVIS requires the following as inputs when specifying the orbit:

- Mission Duration (in years)
- Orbit Type (general, hyperbolic, heliosynchronous, near Earth interplanetary)
- Orbit Start (calendar date)
- Altitude
- Local Time of Ascending Node
- To represent the trajectory as a number of orbits, or as a number of days

All of these inputs are required in order for SPENVIS to generate an output file that fully represents the orbit of interest. Examples of graphical orbit outputs can be seen in Figures 5.3 and 5.4.

All plots are representative of the path the satellite would describe in 1 full day. These plots were produced on the SPENVIS platform to show the 3d view of the orbit. This is then the orbit that will be used in subsequent model runs to calculate the fluxes of particles. It is therefore important to ensure that the orbit is correct and accurate. Increasing the representative orbit to eight days, as opposed to 1 day, shows that more accurate spacecraft coordinates will be generated, and might therefore affect the accuracy of the model outputs. Eight-day orbits for the ISS and the heliosynchronous orbit can be seen in Figures 5.5 and 5.6.

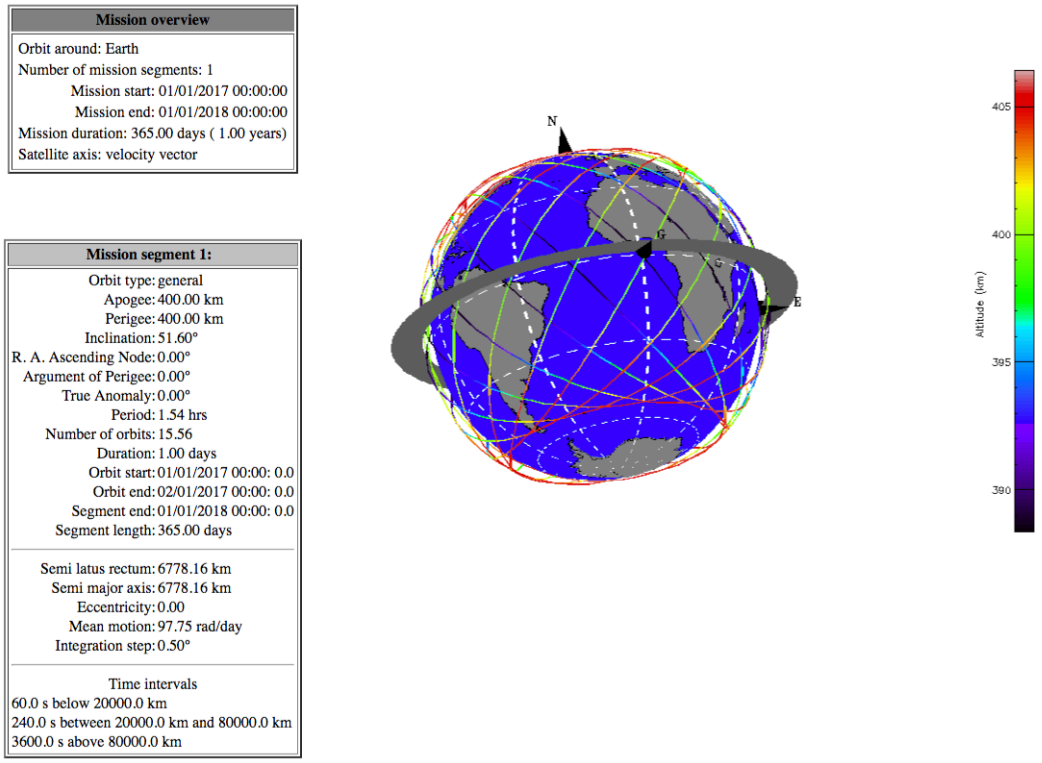

FIGURE 5.3: Orbit 1 - General 400km, 51.6 degree inclination orbit (International Space Station (ISS) type orbit).

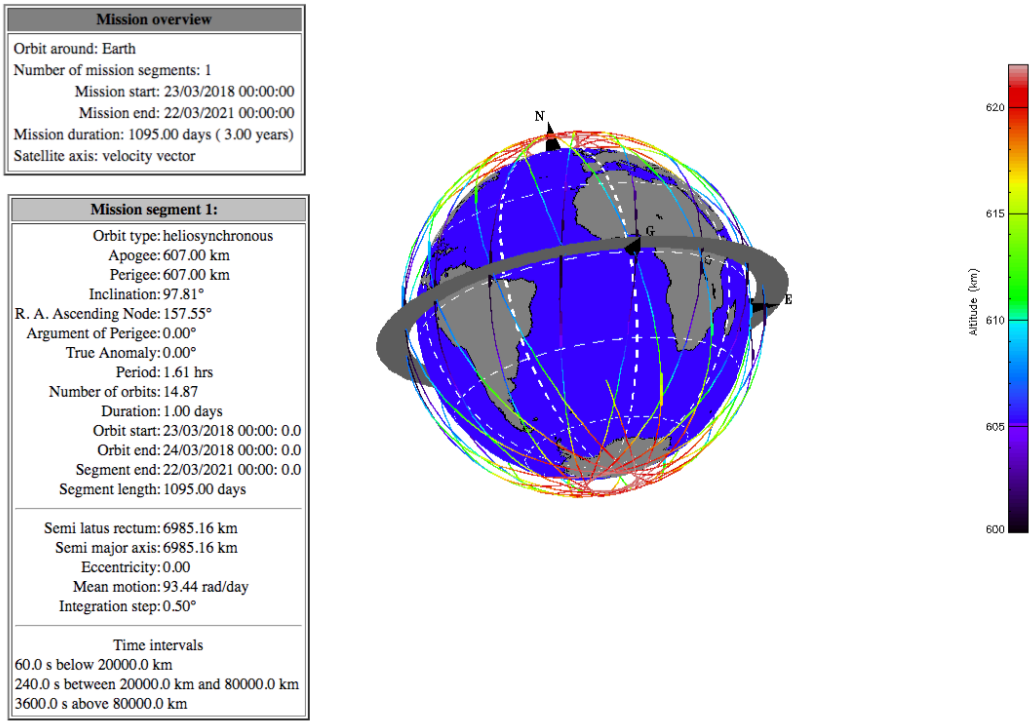

FIGURE 5.4: Orbit 2 - Heliosynchronous, 607km 97.8 degree inclination orbit.

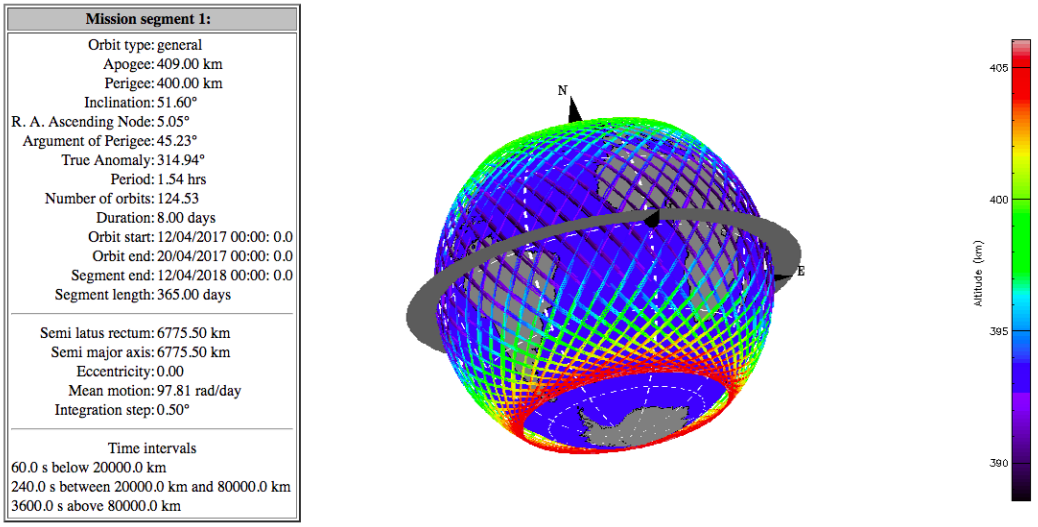

FIGURE 5.5: 8-day representation of an ISS type orbit.

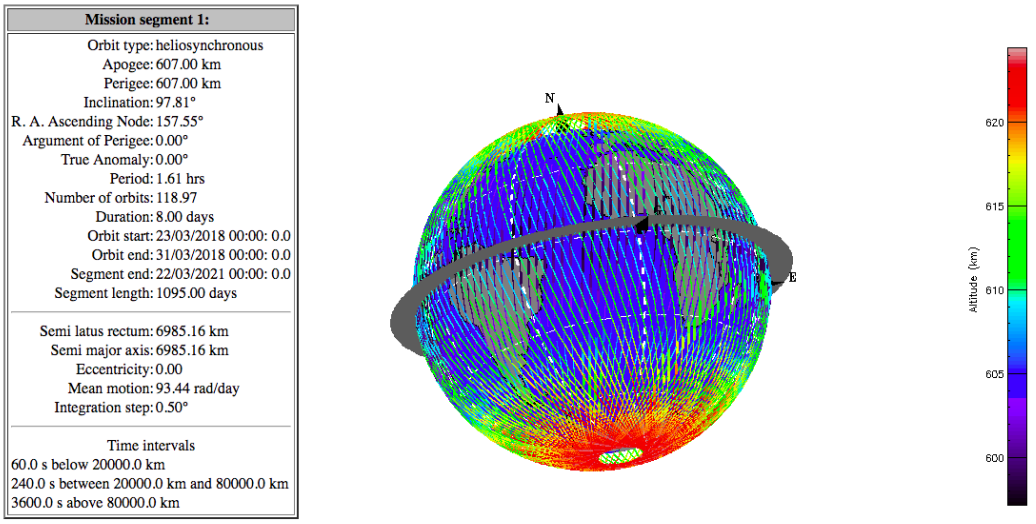

FIGURE 5.6: 8-day representation of a Heliosynchronous orbit.

5.1.2 Using Trapped Radiation Models

The next step of the modelling process is to choose the model from which to obtain predicted radiation levels. There are 4 sections under the Radiation Sources and Effects package:

- Trapped proton and electron fluxes
- Short-term solar particle fluxes
- Long-term solar particle fluences
- Galactic cosmic ray fluxes

Of the three trapped proton models (AP-8, CRESSPRO and SAMPEX/PET), two of them have additional parameters to choose from. AP-8 has the choice between solar max and solar min, and CRESSPRO has the choice between active and quiet. The selection between solar max and solar min for AP-8, allows the choice of data that was captured at specific points on the solar cycle. The active/quiet selection in the CRESSPRO model will determine whether the output will contain information that was captured without a solar storm at solar max (quiet), or during a solar storm (active). This is useful, as it allows one to make predictions based on the solar cycle and activity of the actual mission.

The SAMPEX/PET model does not have any extra parameters to choose from, and so the output from this model will only contain data that was captured at solar minimum.

Once a model has been selected and run, a plot of the averaged spectra can be produced on the SPENVIS platform. One can also choose to produce additional plots, namely a time plot, world map, 3D view (.png) and a 3D VRML plot. The time plot shows at which times during the orbit a certain flux will be present. The world map is a visual representation of the geographical regions over which the particle fluxes are present. The 3D plot shows the actual orbit and the fluxes observed along those lines.

5.1.3 Using Short-term Solar Models

The short-term solar models are used to calculate single event upsets. There are 3 models on the SPENVIS platform for short-term solar activity. These are the CREME-86, CREME-96 and Xaspos et al. models. With all 3 models, one has the option to select the ion range, which varies from hydrogen (H) to uranium (U). Due to the fact that we are interested in solar protons, the ions heavier than hydrogen were not added to the study.

CREME-96 has 3 cases which one can choose from: worst week, worst day and worst 5 minutes. These are averaged over 180 hours, 18 hours and 5 minutes respectively, and allow the user to decide which data set they want to look at.

When using the Xaspos et al. model, one first needs to select between October 1989 flare flux and mean composition, and October 1989 flare flux and worst-case composition. Whether the mean or the worst-case is selected, the user then has the option to look at each day individually (19th, 22nd or 24th of October).

Once again, SPENVIS can plot these outputs in a number of different ways, namely a time plot, world map, 3D view (.png) and a 3D VRML plot. The solar particle flux spectra can be downloaded as a .txt file. Outputs from all 3 CREME-96 cases, as well as the mean and worst-case of all 3 days for Xaspos et al. was downloaded and plotted on the same set of axes (using PYLAB) so that a comparison could be made.

5.1.4 Using Long-term Solar Models

When using the ESP-PSYCHIC models, there is the option to select an ion mass range, from hydrogen to uranium. This model is also divided into two sections, total fluence or worst-case event. The Rosenqvist et al., JPL and King models will only output proton data, and therefore one cannot select an ion range.

For all models, a confidence level of 95.0% was used, and Burrell statistics were used in the King model for both the number of ordinary events, and anomalously large events.

The same SPENVIS plots that were available for the trapped and short-term particles are available for the long-term solar protons, and the .txt files were downloaded and plotted against each other using PYLAB.

5.1.5 Combining These Effects

In order to be able to estimate the total fluences that a satellite in a specific orbit will be exposed to, the combination of these three effects had to be considered. The output for trapped radiation had the fewest number of data points (between 15 and 29 points, depending on the model) and the solar protons the most (75 points). In order to be able to combine these effects, we interpolated the output data points for the trapped radiation models. This was done using the INTERPOLATE package from SCIPY in PYTHON (available at *https://www.scipy.org/*). A one-dimensional interpolation was used to produce the extra points.

Once the extra points were produced, a plot was made to observe the interpolation. The one-dimensional interpolation can be done as a linear interpolation, or a zeroth, first, second or third order spline interpolation. In order to see which was best, the different types were run and the one that looked as though it represented the data in the best way was chosen. A linear interpolation was chosen and can be seen in Figure 5.7, where the red points represent the output from SPENVIS, and the yellow points represent the interpolated points.

A cubic interpolation can be seen in Figure 5.8.

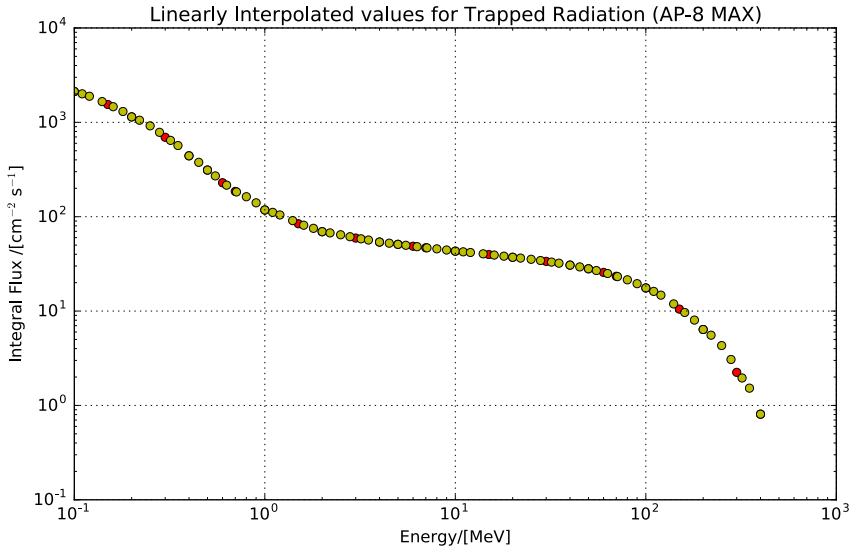

FIGURE 5.7: Linearly interpolated points for AP-8 MAX.

After this, a simple addition of the fluences at each energy value was performed in order to observe the overall spectra, taking into account both trapped and solar protons.

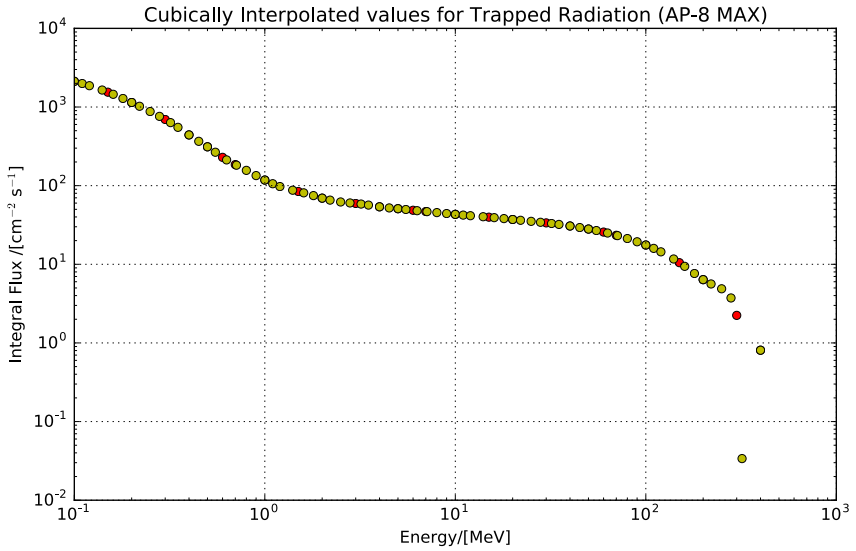

FIGURE 5.8: Cubic spline interpolated points for AP-8 MAX.

5.2 Comparing different SPENVIS outputs

We wanted to be able to understand how dramatic the effects would be for changing certain parameters within the models. Two different orbits within LEO were chosen in order to be able to compare the effects at different altitudes for these orbit types. The first orbit that was chosen was an International Space Station (ISS) type orbit. This orbit is of great interest to the space community, as not only are many satellites in similar orbits, but the ISS itself has so many electronic components on-board, as well as astronauts. It is therefore very important to understand and be able to quantify the radiation environment for this orbit. The details of the ISS orbit can be seen in Figures 5.3 and 5.5.

The other orbit that was chosen was a heliosynchronous 607km orbit. This is an orbit of particular interest for Earth observation applications. These types of satellites often have expensive state-of-the-art electronic components on-board, and so it is vital to be able to estimate what the space environment will be like during the mission. This will aid the electronic engineers in selecting components that they are confident will be able to survive in such an environment. The details of this orbit can be seen in Figures 5.4 and 5.6. These two orbits are also interesting to compare to one-another, as we will be able to see the difference between a lower altitude, low inclination orbit (ISS) and

a higher altitude, higher inclination orbit in which the effect of the radiation near the poles becomes a significant factor.

All models in SPENVIS were run for both orbits. This helps us to understand which parameters more greatly affect the output at different altitudes and orbit types.

5.2.1 Sensitivities to parameters

Changing the parameters within the models will affect the model outputs. In order to understand how dramatic this change is for each parameter, the models were run multiple times with a certain parameter being modified each time. The output from the SPENVIS model was saved as a .txt file and was plotted using PYTHON with the PYLAB module from the Matplotlib package matplotlib. The data was first cleaned up and sorted using the code that can be found in Appendix A, and then the necessary data was selected and plotted.

Changing the duration of the orbit trace could alter the results of the model. A 1-day representative orbit vs a multi-day representative orbit could change the accuracy of the results. The first step was to visualise the difference in the geographical representation and select an appropriate number of days for the orbit. As can be seen in Figure 5.3, there are at most 5 passages through the SAA that are accounted for. Figure 5.5 shows that the 8-day representation takes into account many more passages through the SAA and will therefore be more accurate. The orbit chosen needed to be one wherein a significant level of accuracy is present, but also avoiding very large amounts of data. We needed to decide on a particular number of days for the representative orbit for both the ISS and heliosynchronous orbits. The outputs from the trapped radiation models were consulted for both a single-day, and a multi-day orbit. These were then plotted on the same set of axes, and the percentage difference was calculated. The results were then summarised in a table (Tables 7.1 and 7.2).

The variation in the amount of radiation exposure during the solar cycle then needed to be considered. Each model was run at a solar maximum date (01/01/2013 to 01/01/2014) and at a solar minimum date (01/01/2008 to 01/01/2009) in order to see how this changed the output for each model. This was done for both orbit types and for all trapped, long-term and short-term solar models. Data that was downloaded to

compare radiation levels at solar max and solar min was plotted on the same set of axes to demonstrate the difference.

We also wanted to see what the effect would be if a mission date needed to be changed (for example, delayed by a year). This is very common in the space industry, as even just recently NASA's SLS/Orion has been pushed back from a 2018 launch to a 2019 launch SLSOrion. Of course, because of the change in activity levels of the sun (due to the solar cycle), a launch date change could change the original total radiation exposure profile for the mission. In order to see what effect this would have, we simulated a 1-year mission delay at a date near solar maximum, solar minimum and midway between solar min and max.

While using the long-term solar proton models for these different comparisons, it was found that no data was given at any solar minimum date (around 2008/2009 or 2021/2022), except for the King model. This is because all other models assume a zero fluence during solar minimum Xaspos2004. Due to this, no comparisons could be made for these models at those dates. If one upgrades to an ADVANCED user on the SPENVIS platform[1], it is possible to offset the solar maximum data by a specific number of years. 6 or 7 years from a solar maximum year would be a solar minimum year. This was done in order to see how the offset changes the outputs for these models.

All results from the modelling process are presented in Chapter 7. The most dramatic differences in the outputs were then used in subsequent calculations to calculate the upset rate predicted from these models for a specific electronic component. This was done in order to have a more in-depth understanding of exactly how the model choice and input parameters will affect the upset rate calculation for a mission. The methodology for this calculation is presented in Section 6.2 of Chapter 6.

[1]One can upgrade their user status to ADVANCED by clicking on MY ACCOUNT on *www.spenvis.oma.be/* and changing the "level" from NORMAL to ADVANCED

Chapter 6

Method for Calculating the Upset Rate

6.1 Obtaining Weibull Parameters from Cross-section Data

Unfortunately iThemba LABS was closed for maintenance for a portion of time over which this project was running. This led to beam time being in high demand once the facility was re-opened. Due to this, terrestrial testing could not be accomplished for this project and so we could not obtain our own cross-section data.

In order to be able to calculate an upset cross-section to see how different models affect the upset rate, we needed to gather this data elsewhere. Ryu et al. (Ryu et al. 2012) published a cross section curve for a Samsung Double Data Rate 2 (DDR2) Synchronous Dynamic Random Access Memory (SDRAM) device (part number K4T1G164QE) in their 2012 paper. The cross-section curve from this paper can be seen in Figure 6.1.

The data from this plot was read off using online software called WebPlotDigitizer that is able to generate coordinates from a downloaded image of a plot. This software was used to read off the SEU data from Figure 6.1. The coordinates obtained were uploaded into a PYTHON script and plotted. A code was then written to fit a Weibull function to this data (recall Equation 4.6). The code operated as a least-squares fit to find the parameters for the Weibull function based on some initial guess of the parameters. Due to the fact that the parameters can be found in the paper by Ryu et al. (Ryu et al.

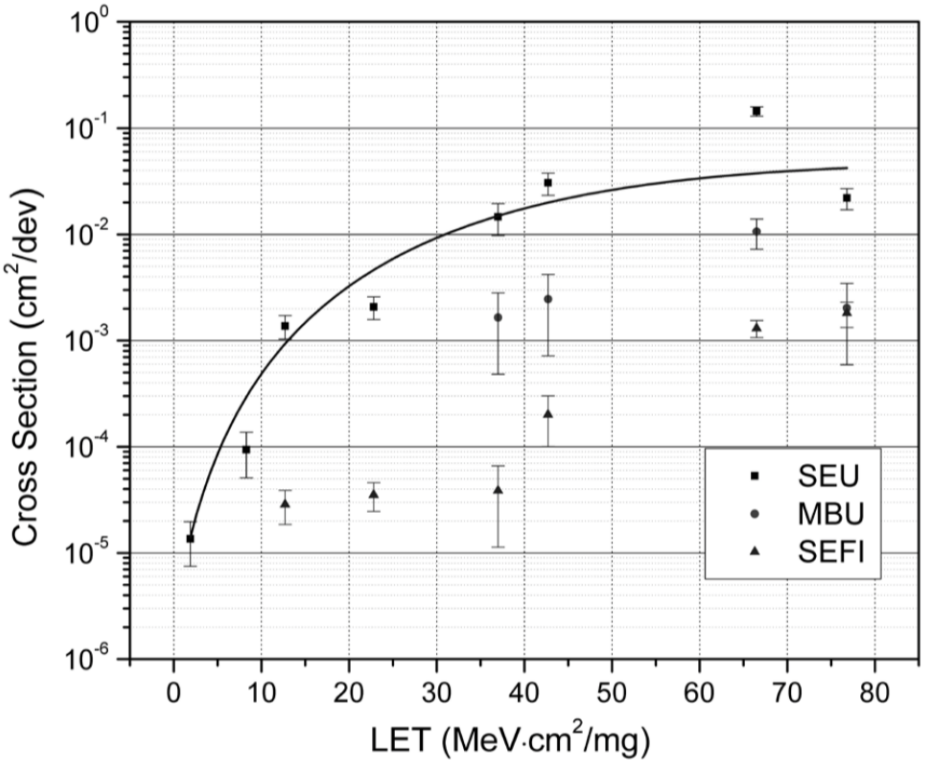

FIGURE 6.1: Cross-section plot of a DDR2 SDRAM device measured in a heavy-ion test by Ryu et al. (Ryu et al. 2012).

2012) we had a very good initial guess to implement in the code. This would not have been the case if we had been able to collect our own data, in which case, we would have had to determine the initial parameters by a trial and error approach. The code to fit a Weibull function to this data can be found in the Appendix B.

Due to the fact that it is sometimes not possible to obtain many data points from the upset cross-section experiments, we wanted to be able to understand how the number of data points affects the calculation of the Weibull parameters. In order to do this, we generated 3 different curves with decreasing numbers of data points. We started with the highest number (8), then generated a curve with 6 of the data points, and lastly we generated one with only 4 data points.

This same method was adopted for determining the parameters for a proton-induced upset cross-section curve. We used the cross section curve in the 2001 paper by C. Carmichael et al. (Carmichael et al. 2001). This can be seen in Figure 6.2. The DUT was a Virtex FPGA (part number XQVR300), that underwent a static proton test. Again, we found the parameters for this curve using different numbers of data points. We wanted to compare the results for 6 and for 4 data points. As can be seen in Figure

6.2, the x-axis has values of Proton energy (from the proton beam) as opposed to LET as in Figure 6.1. This means that the onset parameter (l_o) from Equation 4.6 becomes E_o.

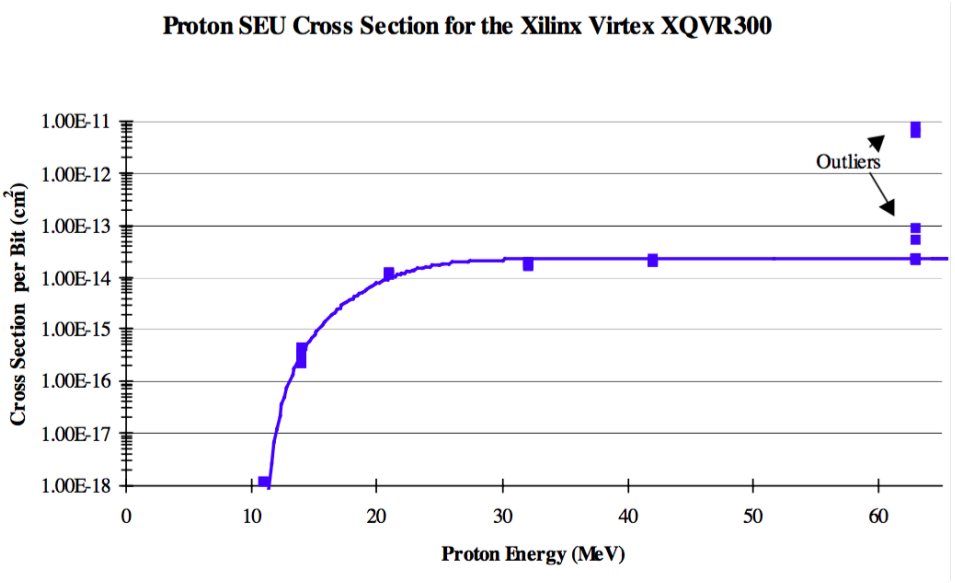

FIGURE 6.2: Cross-section plot of a Virtex FPGA device as measured in a proton test by Carmichael et al. (Carmichael et al. 2001).

6.2 Calculating the Upset Rate Using SPENVIS

Once all four parameters (σ_{lim}, l_o (or E_o for protons), w and s) were obtained, we were then at a point where we could use SPENVIS' built-in upset cross section calculator. This can be found under the SINGLE EVENT EFFECTS section of the models, and the input page can be seen in Figure 6.3. As can be seen in the figure, two devices can be analysed at the same time, as well as taking into account trapped, solar and galactic cosmic ray model outputs all together. A user can add information about the device by selecting EDIT on the right hand side. Here, the user has the choice of uploading device data in the form of Bendel function parameters, Weibull function parameters, PROFIT parameters or experimental data. One can also decide whether the output should contain the upset rate from direct ionisation due to heavy ions, proton-induced ionisation or the combination of both.

It is important to note here that SPENVIS will gather information from the output of whichever radiation environment model was last used. It uses this in combination with

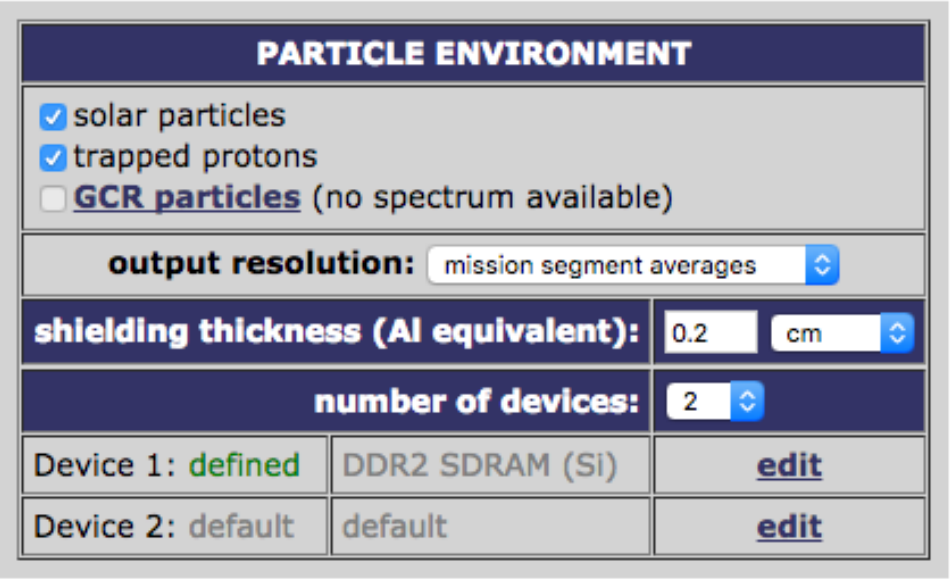

FIGURE 6.3: SPENVIS short-term single event upsets page.

the device characteristics to estimate the upset rate for a specific device, using a specific model, for a specific mission.

Once the model has been run, the upset rates can be gathered from the report file. The report file contains a segment-averaged value for upset rates, as well as a total upset rate for the entire mission. The upset rates are quoted in units of bit^{-1}, $\text{bit}^{-1}\text{s}^{-1}$ or $\text{bit}^{-1}\text{day}^{-1}$. This is useful because it gives the user all the information for knowing how many upsets are predicted for the total mission duration, each second, or each day.

In order to understand the effect on the upset rate calculation from changing different model parameters, we decided to compare best and worst case scenarios for each orbit. We also wanted to see how the solar cycle affects this calculation and so we used models for different positions on the cycle.

The best and worst case scenarios for the ISS and heliosynchronous orbit were chosen as follows:

- Best Case: SAMPEX/PET, King and Xaspos et. al (19 October)
- Worst Case: CRESSPRO quiet, ESP Total Fluence, CREME Peak 5 minute

The best case scenario was chosen based on the fact that these models had the lowest fluences for trapped, long-term solar protons and short-term solar protons, respectively.

The worst case scenario was chosen by selecting the models with the highest fluences. The best and worst case scenarios were modelled for a 3 year orbit from 01/01/2018 to 01/01/2021.

To see the effect of the solar cycle on the SEU rate, we selected the model with the largest difference between solar max and solar min. These are the short-term solar models for the years 2009 and 2013. We ran the Xaspos et al. model (19 October 1989) for a 1-year orbit from 01/01/2009 and from 01/01/2013. We also looked at the differences between AP-8 max and AP-8 min. In addition to this, we looked at the effect of a date change at solar maximum (2013 and 2014) for a long-term model. We chose a long-term model, as this had the most dramatic difference for the date change at solar maximum. ESP-PSYCHIC (total fluence) was run for a year-long orbit from 01/01/2013 and from 01/01/2014.

Lastly, we compared the differences between just looking at trapped radiation, just looking at solar particles, and looking at a combination of the two. These were also done for the 3-year orbit from 01/01/2018 to 01/01/2021.

Part III

Results, Discussion and Conclusions

Chapter 7

Results from the Modelling Process

When using the SPENVIS platform, even just for a straight-forward output of the radiation spectra for an orbit, one is confronted with the choice of different radiation types. The first step for a user is to decide which type of radiation they are mostly concerned with (e.g. trapped, long-term solar, short-term solar, galactic cosmic rays or even a combination of these). The next step is to decide on the model that they believe will output reliable predictions for their mission type. This is not a straight-forward task, as each of the models output results that are different to the next, and can even vary greatly within themselves depending on which parameters are chosen.

If one begins by considering just trapped radiation, an output similar to that of Figure 7.1 could be produced on the platform itself. However, this is just one of the five choices of trapped radiation models. In order to see how each model differs from the next, Figure 7.2 was plotted. This figure was produced by using data for an ISS-type orbit from 1 January 2017 to 1 January 2018. This date range is during a mid-solar cycle. The data used in the plot was obtained from SPENVIS, each with a threshold flux for exposure at 1 $cm^{-2}s^{-1}$.

As can be seen in the figure, AP-8 MIN has a higher integral flux than AP-8 MAX. This agrees with theory, as the neutral atmosphere expands at solar maximum, so fewer charged particles should be observed. However, CRESSPRO shows a very high integral flux. CRESSPRO data was collected at solar maximum, so one would expect the output

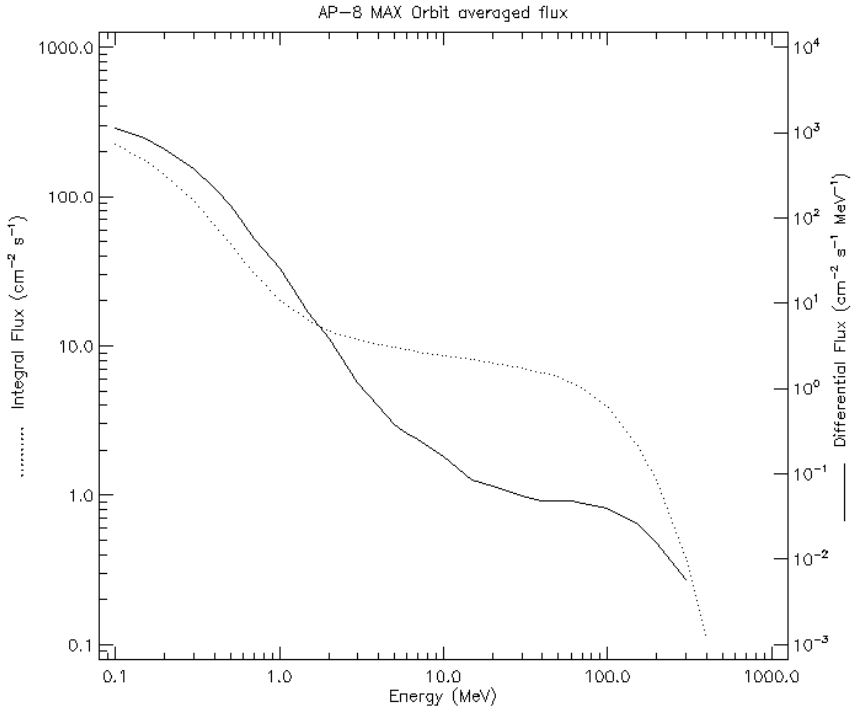

FIGURE 7.1: Orbit averaged flux from the AP-8 MAX model.

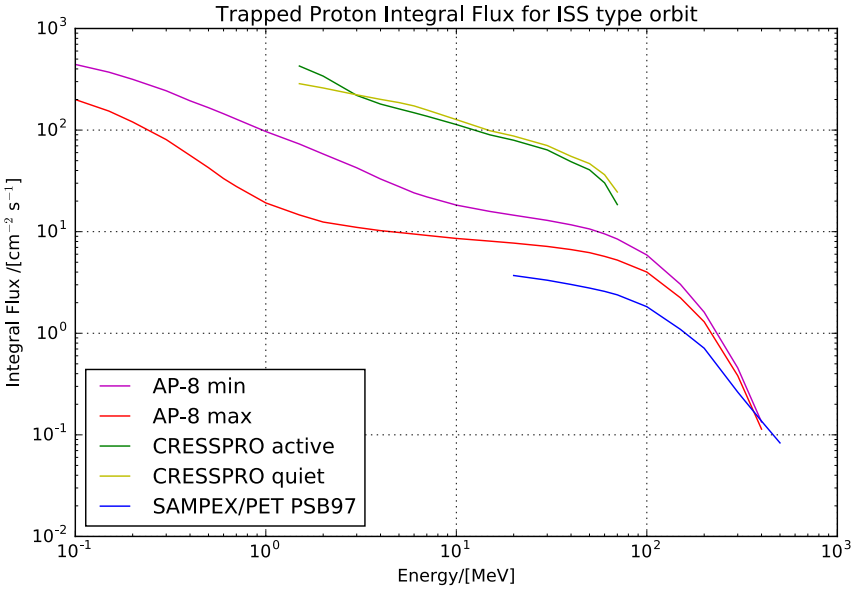

FIGURE 7.2: Trapped proton fluences for different models - 01/01/2017 to 01/01/2018.

from this model to be have a lower fluence than AP-8 MIN if it is to agree with theory. The most important thing to note, however, is how different each of the outputs are to eachother. The output from the CRESSPRO models are more than 33 times greater than that of the SAMPEX/PET model for protons in the 10 MeV range. This is an

exceptionally large discrepancy, which will greatly affect an upset rate calculation for a specific mission.

Figure 7.3 shows the output from the long-term solar proton models within SPENVIS for an ISS-type orbit. By looking at the figure, one might conclude that the differences between the models are less dramatic than that of the trapped proton models. However, the output from the ESP model is around 50 times greater than that of the King model at energies lower than 10 MeV. At high energies, ESP and JPL fluences are around 8000 times greater than King and Rosenqvist et al. Once gain, this could cause very different results when one uses these models to calculate the upset rate expected for a particular electronic device.

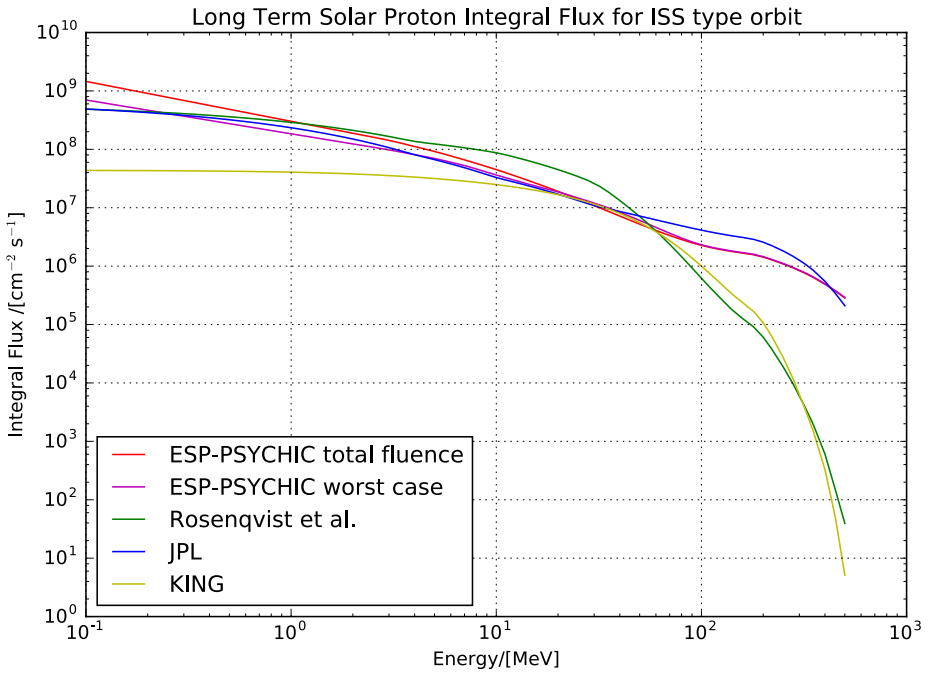

FIGURE 7.3: Long-term solar proton fluences for different models - 01/01/2017 to 01/01/2018.

The short-term solar proton models also differ quite dramatically in their output. Figure 7.4 shows this. The outputs from the Xaspos model were exactly the same for the mean and worst-case for each individual date. Due to this, only the worst case data was plotted. There are very large differences in the output values from the models at low energies. The CREME-96 peak 5-min averaged flux is almost 5000 times more intense than the Xaspos 19 October output at energies less than 10 MeV. The difference remains quite substantial, and the models only start to agree on fluences once the energies get

as high as 500 MeV. This makes it very difficult for an engineer, as selecting one model over another could lead to either an overestimation or an underestimation of the effect of potential solar events during a mission lifetime.

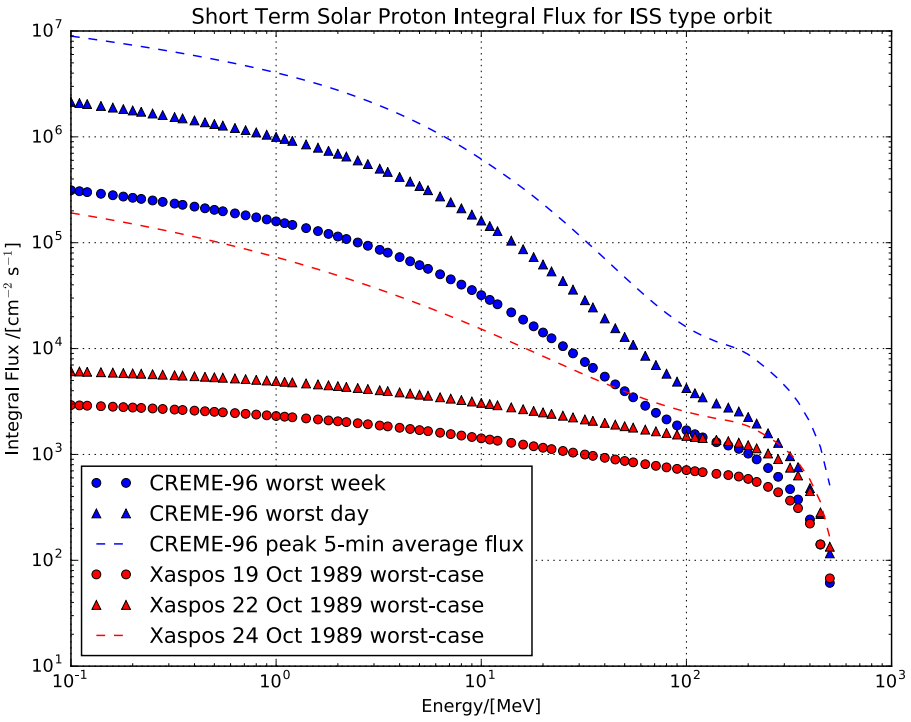

FIGURE 7.4: Short-term solar proton fluences for different models - 01/01/2017 to 01/01/2018.

7.1 Effects of Changing the Orbit Accuracy

For the heliosynchronous orbit, we found that an 8-day orbit covered the entirety of the trajectory around the Earth. This means that the orbit of the eighth day ended where the first day began. This would clearly output the most accurate results, as it would accurately represent the number of times the satellite passed through the SAA. However, SPENVIS did not output any data from the models for this orbit. This could be due to the fact that the program would take too long to run and the size of the data output would be too large. We therefore had to find a middle ground, where the data would be more accurate than a 1-day trajectory, but not take too long to run. A 3-day representative trajectory was chosen. This trajectory is depicted in Figure 7.5.

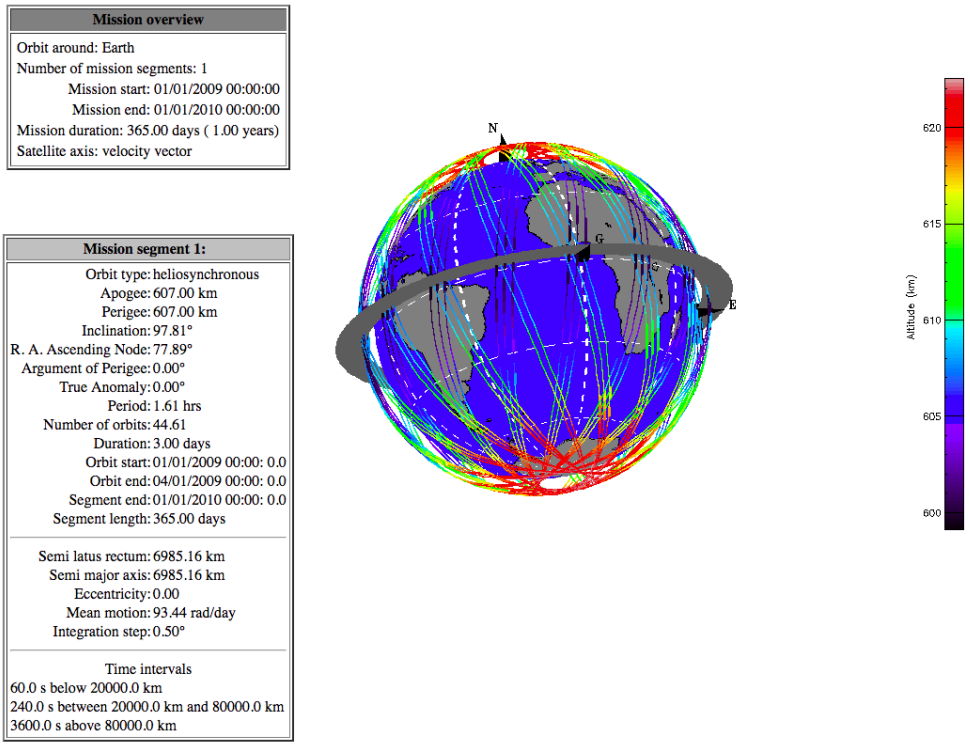

FIGURE 7.5: 3-day representation of a heliosynchronous orbit.

After running the trapped radiation models for both a 1-day and a 3-day representation of the ISS and heliosynchronous orbits, some discrepancies were found. Figures 7.6 and 7.7 demonstrate the differences in the output values from the trapped radiation models for a 1-day and a 3-day orbit. Figure 7.6 is for the heliosynchronous orbit, and one can see that the largest differences lie in the low energy end of the spectrum. This is the same for the ISS-type orbit in Figure 7.7.

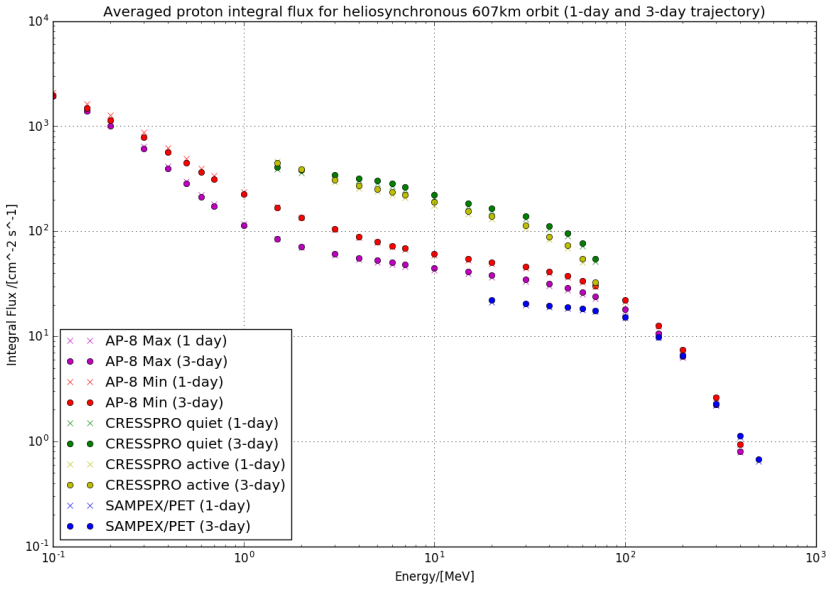

FIGURE 7.6: Trapped proton fluences for a 1-day orbit vs a 3-day orbit (Heliosynchronous 607km).

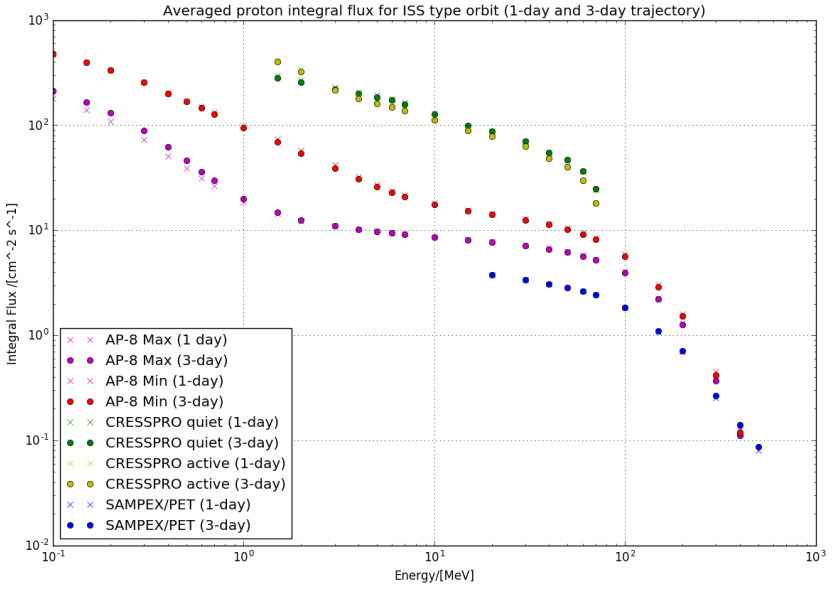

FIGURE 7.7: Trapped proton fluences for a 1-day orbit vs a 3-day orbit (ISS-type orbit).

The largest difference for the heliosynchronous orbit was a 10.15% difference at 0.3MeV for AP-8 MIN. For the ISS-type orbit, the largest difference was 21.9% at 0.3MeV as well, however, this was using the AP-8 MAX model. Tables 7.1 and 7.2 summarise the differences.

Energy /[MeV]	Integral Flux **1-day** /[cm^{-2} s^{-1}]	Integral Flux **3-day** /[cm^{-2} s^{-1}]	Difference /[cm^{-2} s^{-1}]	Percentage Difference /[%]
0.1	2102.3	1961	141.3	6.72
0.15	1619.3	1481	138.3	8.54
0.2	1272.3	1147.3	125	9.82
0.3	870.68	782.33	88.35	**10.15**
0.4	625.09	563.81	61.28	9.80
0.5	490.19	446.76	43.43	8.86
0.6	396.38	365.17	31.21	7.87
0.7	338.98	314.35	24.63	7.27
1	238.12	225.9	12.22	5.13

TABLE 7.1: Differences between AP8-MIN for a 1-day and 3-day orbit trajectory (Heliosynchronous 607km).

Energy /[MeV]	Integral Flux **1-day** /[cm^{-2} s^{-1}]	Integral Flux **3-day** /[cm^{-2} s^{-1}]	Difference /[cm^{-2} s^{-1}]	Percentage Difference /[%]
0.1	179	211.69	32.69	18.26
0.15	138.76	166.32	27.56	19.86
0.2	109.14	132.15	23.01	21.08
0.3	72.744	88.674	15.93	**21.90**
0.4	50.958	61.796	10.838	21.27
0.5	39.144	46.372	7.228	18.47
0.6	31.07	35.881	4.811	15.48
0.7	26.234	29.822	3.588	13.68
1	18.437	20.024	1.587	8.61

TABLE 7.2: Differences between AP8-MAX for a 1-day and 3-day orbit trajectory (ISS-type Orbit).

We can therefore see that up to a 22% difference (or error) in the output value is possible, simply by choosing a representative orbit that does not cover a large enough range of the satellite positions. It is therefore very important for the user to decide whether this 22% falls within their design margins, or if they need to look at a more accurate orbit representation.

7.2 Solar Cycle Effects on Models

7.2.1 Spectra at Solar Maximum Date vs Solar Minimum Date

Plotting data that was collected for an orbit at a time of solar max (the year 2013) and solar min (the year 2008) does not show any differences in the output for trapped radiation models (See Figures 7.8 and 7.9). It is therefore clear that the trapped radiation models are independent of the date specified when defining the orbit. This is an understandable result, as the trapped models are stated as being static models. AP-8 has a solar cycle dependence, which does not mean that the date of the mission will determine whether solar maximum or solar minimum data is consulted. Instead it is apparent that this solar-cycle dependence only refers to the fact that one can choose between AP-8 MAX and AP-8 MIN.

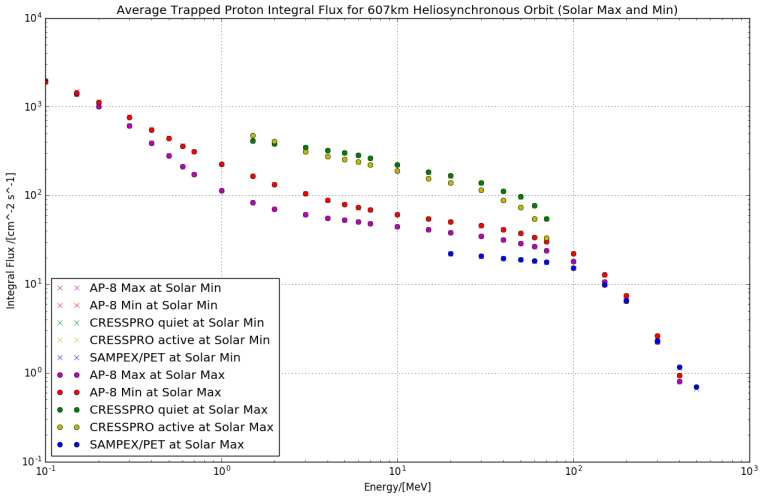

FIGURE 7.8: The effect of choosing different dates on the solar cycle for trapped radiation models (heliosynchronous orbit).

There are however very minor differences at low energies for AP-8 MAX (ISS) and AP-8 MIN (heliosynchronous). The difference in the fluxes can be seen in Table 7.4. The highest difference is one of 2.58% at 0.2 MeV and so one can conclude that these minor differences are not statistically significant. They might arise due to the fact that the orbit data generated could begin at a different position with respect to the Earth for different years.

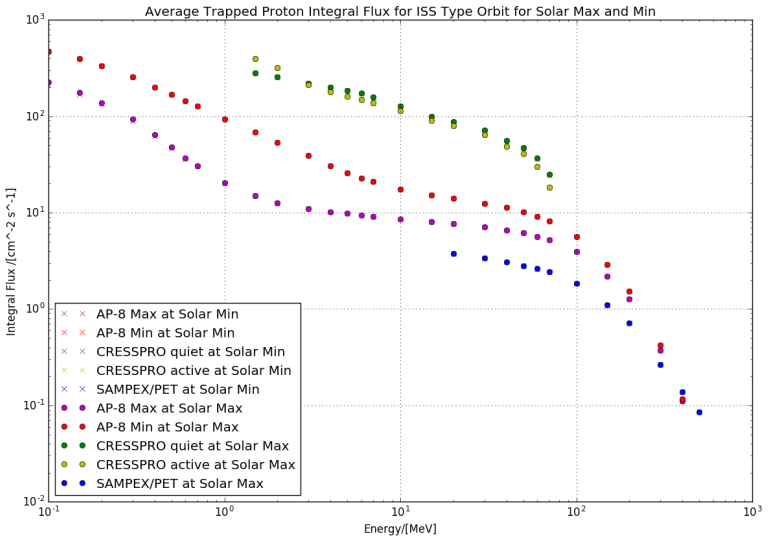

FIGURE 7.9: The effect of choosing different dates on the solar cycle for trapped radiation models (ISS-type orbit).

Energy /[MeV]	Integral Flux **at Max** /[cm^{-2} s^{-1}]	Integral Flux **at Min** /[cm^{-2} s^{-1}]	Difference /[cm^{-2} s^{-1}]	Percentage Difference /[%]
0.1	1918.6	1961.00	42.4	2.16
0.15	1444.7	1481.00	36.3	2.45
0.2	1117.6	1147.30	29.7	2.58
0.3	763.95	782.33	18.38	2.35
0.4	552.41	563.81	11.4	2.02
0.5	439.75	446.76	7.01	1.57
0.6	360.85	365.17	4.32	1.18
0.7	310.93	314.35	3.42	1.09

TABLE 7.3: Differences between AP8-MIN at solar maximum and minimum dates for Heliosynchronous orbit.

Energy /[MeV]	Integral Flux **at Max** /[cm^{-2} s^{-1}]	Integral Flux **at Min** /[cm^{-2} s^{-1}]	Difference /[cm^{-2} s^{-1}]	Percentage Difference /[%]
0.1	225.07	211.69	13.38	5.94
0.15	175.81	166.32	9.49	5.34
0.2	138.84	132.15	6.69	4.82
0.3	92.984	88.674	4.31	4.64
0.4	64.467	61.796	2.671	4.14
0.5	48.196	46.372	1.824	3.78
0.6	37.128	35.881	1.247	3.36
0.7	30.694	29.822	0.872	2.84

TABLE 7.4: Differences between AP8-MAX at solar maximum and minimum dates for an ISS-type orbit.

Figures 7.10 and 7.11 are obtained by running the MAX and MIN AP-8 models at the exact same input date. This demonstrates that although AP-8 MAX and MIN are static models and do not depend on the input date, the difference between them clearly takes into account the difference between the two extremes of the space environment at solar minimum and at solar maximum. Figure 7.11 clearly has much more severe radiation along the orbital lines due to the increased radiation intensity near the SAA.

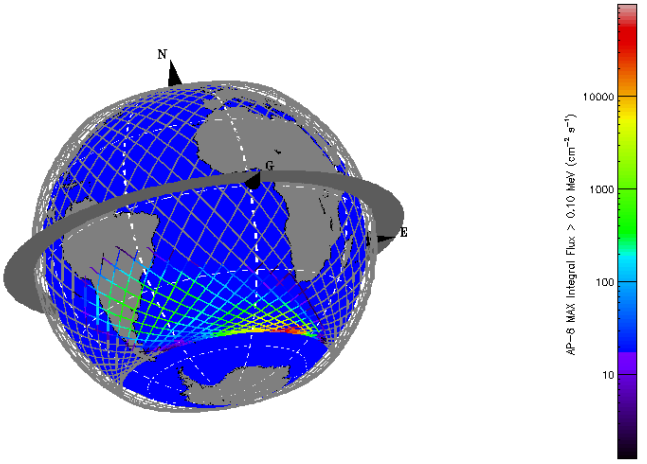

FIGURE 7.10: 3D representation of the output for AP-8 MAX with an ISS-type orbit.

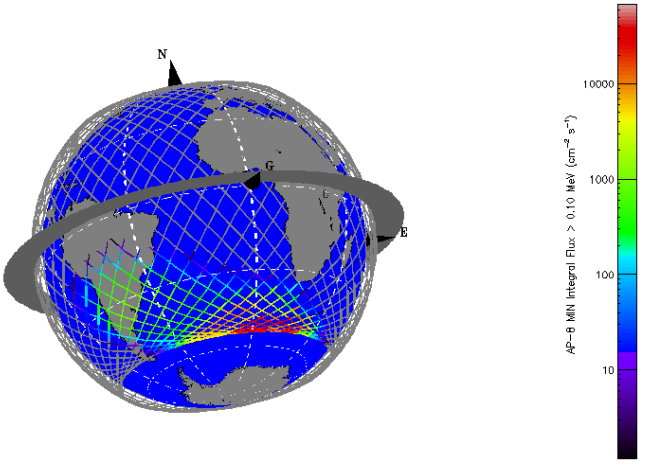

FIGURE 7.11: 3D representation of the output for AP-8 MIN with an ISS-type orbit.

This is seen even more clearly if one looks at the 2D ground track of the orbit on the Earth. In Figures 7.12 and 7.13 one can clearly see the shift in the regions of high radiation intensity. Note that in both the 3D and the 2D figures, the fluences are for protons of energies greater than 0.1 MeV.

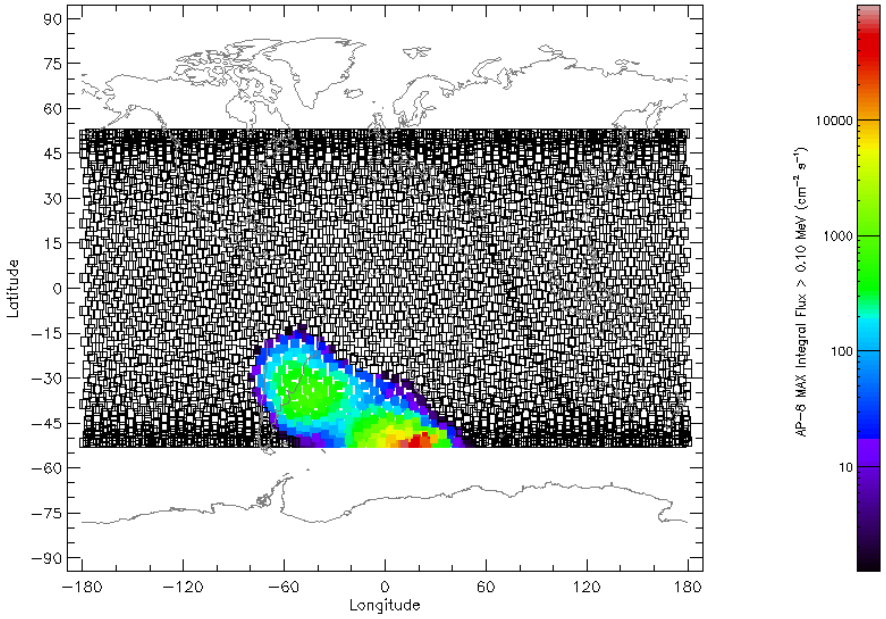

FIGURE 7.12: 2D map of the output for AP-8 MAX with an ISS-type orbit.

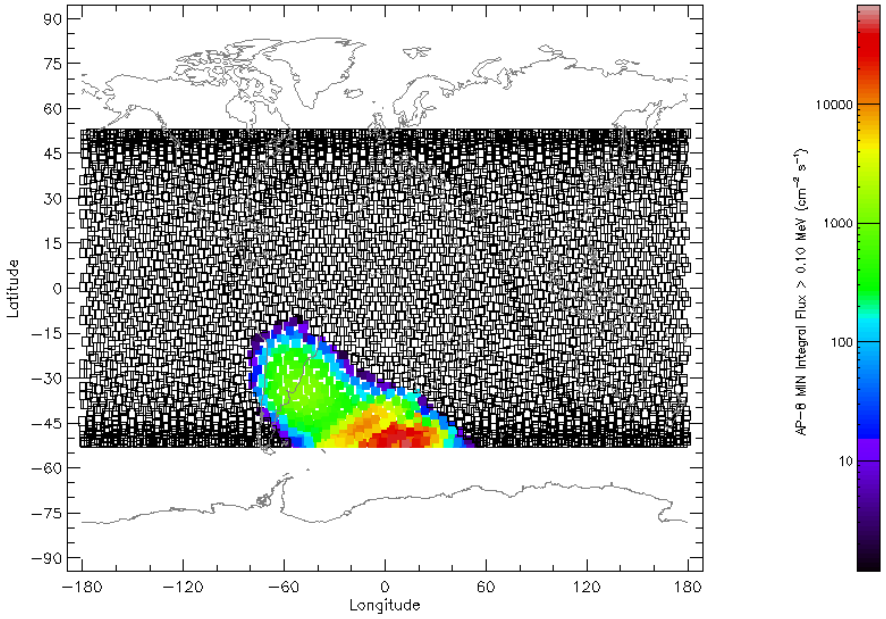

FIGURE 7.13: 2D map of the output for AP-8 MIN with an ISS-type orbit.

The case is quite different for the solar proton models. Data from a solar maximum date and a solar minimum date was downloaded for the short-term solar proton models for the ISS-type orbit. The output can be seen in Figure 7.14. As is apparent from this plot, there is quite a substantial difference between solar maximum and solar minimum. This is what is expected, as the solar activity changes dramatically between solar maximum and solar minimum. However, an unexpected result is that the solar minimum date (2009) actually has a higher fluence at every energy level than the solar maximum date (2013). This is the case for both the CREME and the Xaspos et al. models. One would expect the fluence to be greater during a solar maximum, as there will be a higher probability of a solar event occurring during this period of time.

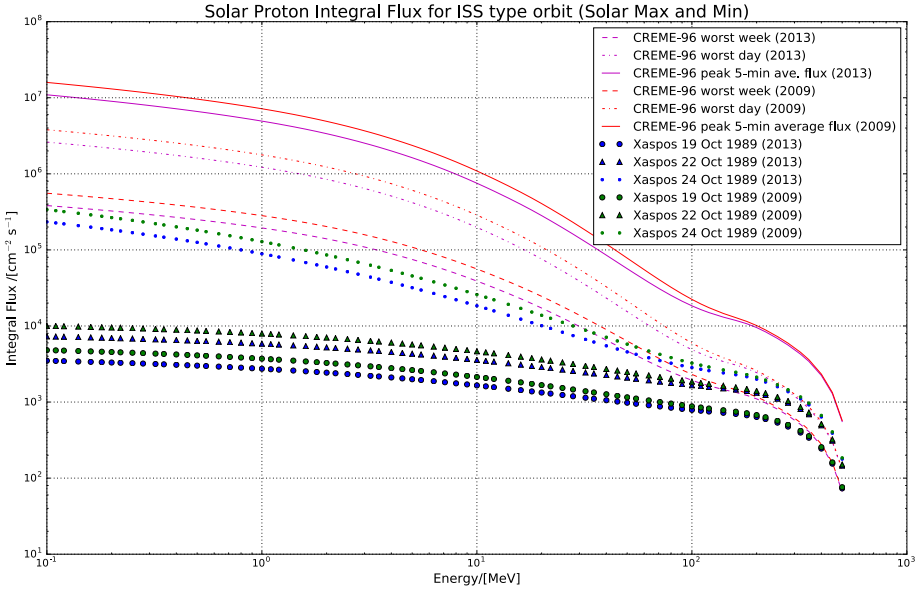

FIGURE 7.14: Plot to show fluences for a solar maximum and minimum date (ISS-type orbit).

For the long-term solar proton models, an analysis of the difference between the output data at a solar maximum date vs a solar minimum date could not be carried out. This is due to the fact that all models (except King) will output a zero value for solar minimum. An attempt to obtain solar minimum data for the other long-term solar models was made, and is discussed in section 7.2.3.

7.2.2 Mission Date Change Near Maximum, Minimum and Mid-cycle

As mentioned above, a date change will have no effect on the trapped radiation models, as the output is independent of the dates specified for the orbit. Therefore, if there happens to be a mission date change, the trapped models do not need to be re-run.

However, when one looks at the output from the short-term solar models, we do see a difference. Figures 7.15 and 7.16 show the effect of a 1-year mission delay at solar maximum and minimum respectively. The solar maximum dates chosen were the years 2013 and 2014, and the solar minimum dates, 2008 and 2009. As can be seen in the figures, the largest difference occurs near solar maximum, and at low energies. This corresponds to a 27% difference in the predicted fluences. For solar minimum, there is a 11% difference. These are both substantial differences, and could cause a change in the calculated upset rate. At mid-solar cycle (between solar maximum and solar minimum), only a 0.02% difference was observed, and so a date change here would not have too much of an effect in the model outputs, and therefore an upset-rate calculation.

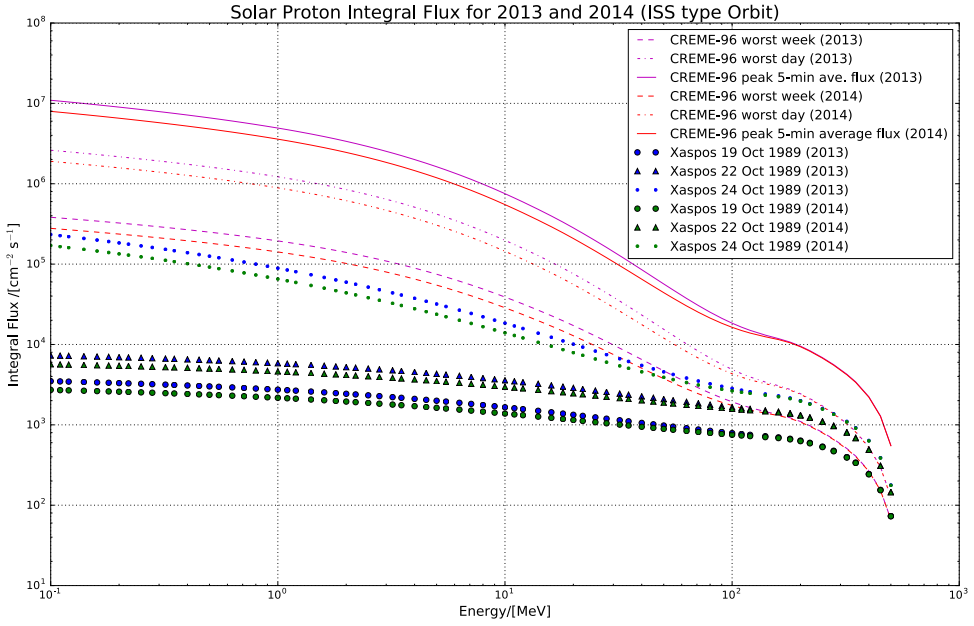

FIGURE 7.15: Plot to show the effect of a mission date change near solar maximum (ISS-type Orbit).

Table 7.5 summarises the differences observed for date changes for the short-term solar proton models.

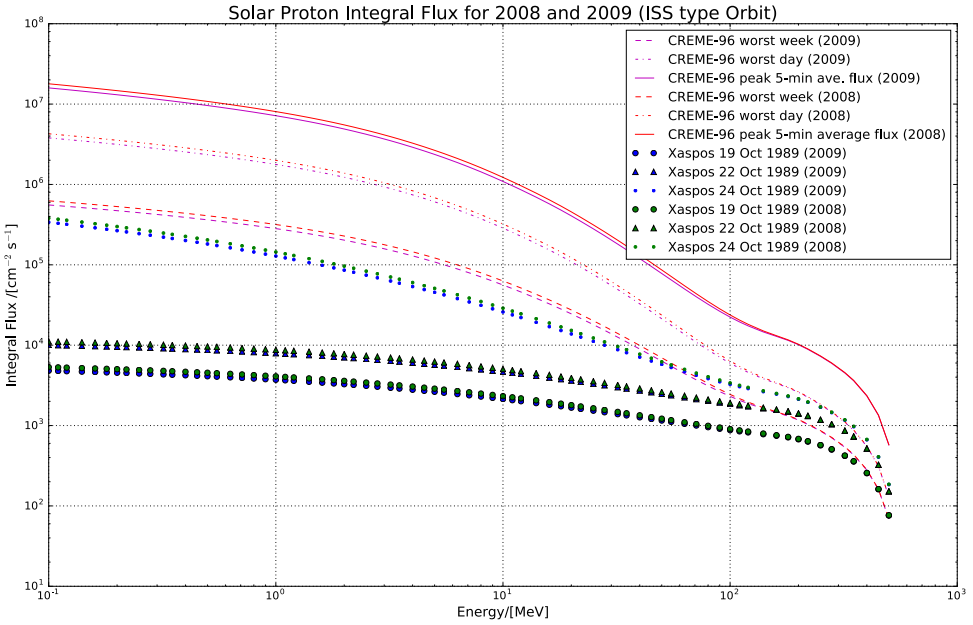

FIGURE 7.16: Plot to show the effect of a mission date change near solar minimum (ISS-type Orbit).

Solar Cycle	Energy /[MeV]	Integral Flux **Year 1** /[cm^{-2} s^{-1}]	Integral Flux **Year 2** /[cm^{-2} s^{-1}]	Difference /[cm^{-2} s^{-1}]	Percentage Difference /[%]
Maximum	0.1	382520	278530	103990	27.19
	0.11	374520	272710	101810	27.18
	0.12	367230	267410	99820	27.18
	0.14	354330	258020	96310	27.18
	0.16	343200	249930	93270	27.18
	0.18	333420	242820	90600	27.17
	0.20	324710	236480	88230	27.17
Minimum	0.1	555880	625210	69330	11.09
	0.11	544240	612120	67880	11.09
	0.12	533640	600200	66560	11.09
	0.14	514870	579080	64210	11.09
	0.16	498690	560870	62180	11.09
	0.18	484470	544870	60400	11.09
	0.20	471790	530610	58820	11.09

TABLE 7.5: The effect of a mission date change for **short-term solar** proton models.

The long-term solar proton models also show changes for a year-long mission delay. The dates chosen were 2013 and 2014 for a delay near solar maximum, and the years 2016 and 2017 for mid-solar cycle. As can be seen in Figures 7.17 and 7.18, the differences occur over most energy ranges, and only seem to agree above 2x10^2 MeV in Figure 7.17. For solar maximum, this difference is around 27% for most energy ranges. At mid-solar

cycle, the difference is a maximum of 26% at low energies. Therefore, the output from an upset rate calculation using long-term solar models will differ quite substantially for a date change of one year, depending on where one is in the solar cycle. These results are summarised in Table 7.6.

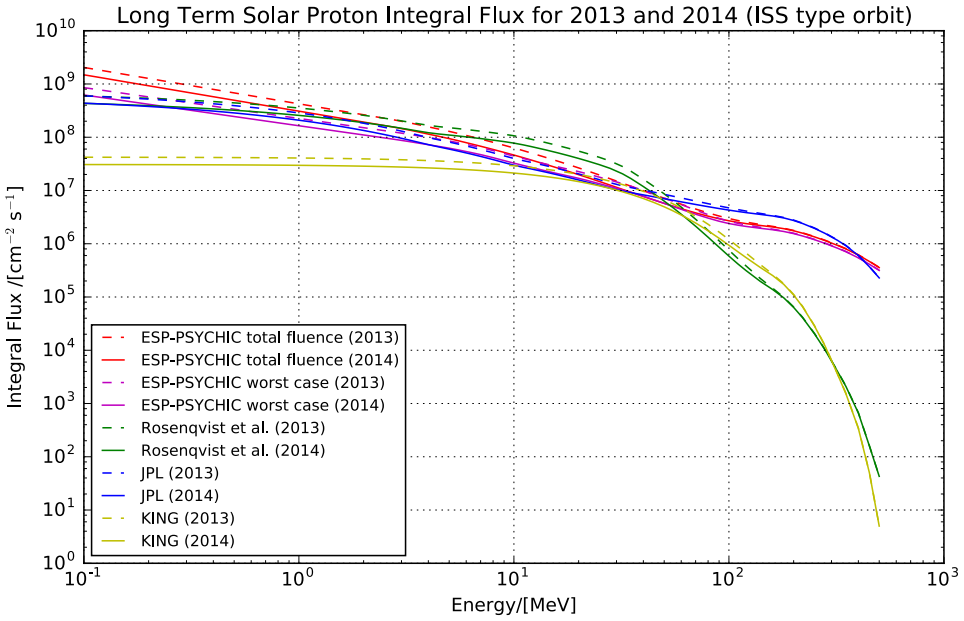

FIGURE 7.17: The effect of a mission date change near solar maximum (ISS-type orbit).

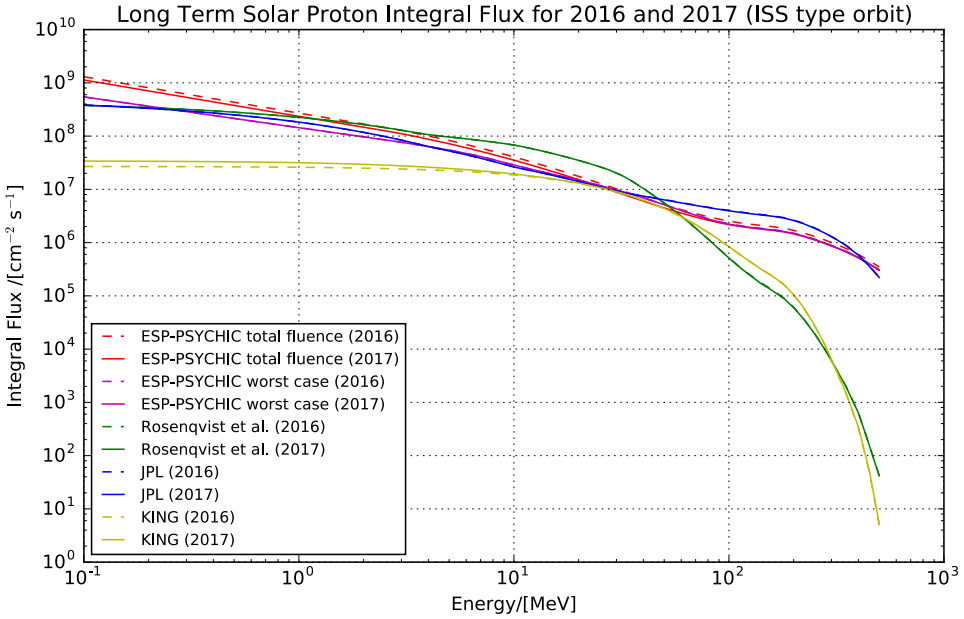

FIGURE 7.18: The effect of a mission date change near mid-solar cycle (ISS-type orbit).

Solar Cycle	Energy /[MeV]	Integral Flux **Year 1** /[10^4 cm^{-2} s^{-1}]	Integral Flux **Year 2** /[cm^{-2} s^{-1}]	Difference /[cm^{-2} s^{-1}]	Percentage Difference /[%]
Maximum	0.1	148610	204270	55660	27.25
	0.11	139370	191560	52190	27.24
	0.12	131360	180550	49190	27.24
	0.14	118150	162380	44230	27.24
	0.16	107780	148130	40350	27.24
	0.18	99437	136660	37223	27.24
	0.20	92543	127180	34637	27.23
Middle	0.1	3390.4	2687.2	703.2	26.17
	0.11	3387.7	2686.2	701.5	26.11
	0.12	3385	2685.2	699.8	26.06
	0.14	3379.7	2683.2	696.5	25.96
	0.16	3374.4	2681.3	693.1	25.85
	0.18	3369.1	2679.3	689.8	25.75
	0.20	3363.8	2677.3	686.5	25.64

TABLE 7.6: The effect of a mission date change for **long-term solar** proton models.

7.2.3 Obtaining Long-Term Solar Proton Data at Solar Minimum

Unfortunately, a normal SPENVIS user cannot obtain data for long-term solar protons at solar minimum (except for King). If one is to run any of the long-term solar proton models at a solar minimum date, all models (except King) output zero values. Due to this, none of the comparisons in subsections 7.2.1 and 7.2.2 contain predictions for the long-term protons at solar minimum. In order to obtain such predictions, one would need to upgrade to an advanced user in SPENVIS. It is however not advisable to upgrade to an advanced user until a good understanding of the SPENVIS platform and the models is obtained. This is because there are many extra parameters that can be altered and overridden, which could lead to very confusing and incorrect results and interpretations. Using the SPENVIS platform in the incorrect manner may also result in a user accidentally requesting too much data from the system, and this could lead to an overburden of the SPENVIS servers.

If we are to look at the output from the King model at solar minimum (Figure 7.19), we see that there is a fairly significant amount of radiation that this model predicts. This is interesting, as the other models assume a zero flux at this particular date.

If one is to upgrade to an advanced user, there is the option to offset the data by any of 0 to 7 years. In order to see the effect of this offset, data was downloaded for the

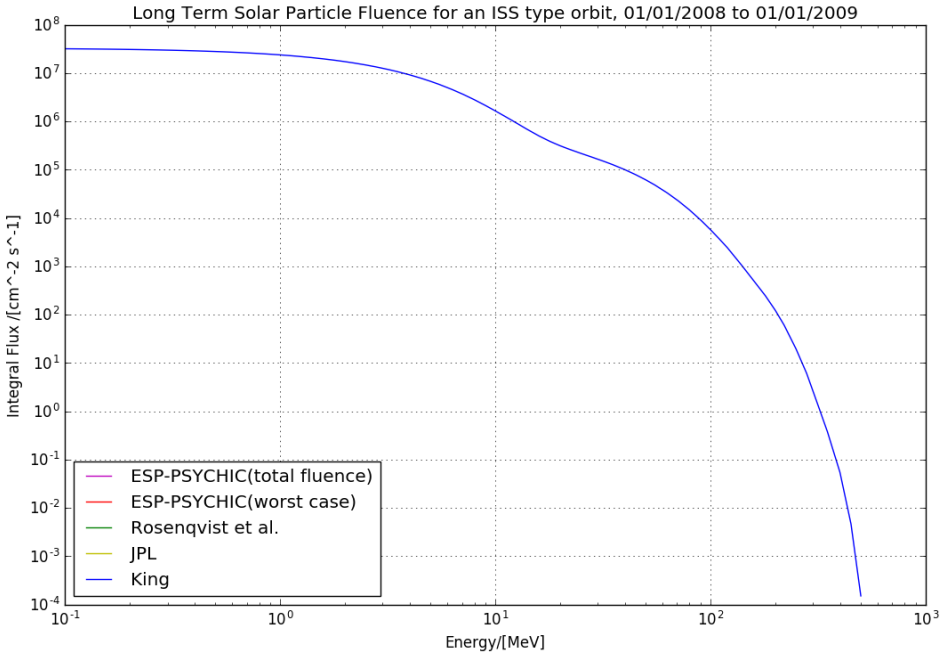

FIGURE 7.19: Long-term solar proton models at a solar minimum date.

JPL model for all 8 offset options (i.e. a 0 year, 1 year, 2 year, ..., 7 year). The results obtained were that all the data for the offsets from years 0 to 6 contained the exact same values, but the 7-year offset output was all zeros. The output from the 6-year offset (which is the same data as 0-5 year offsets) was then plotted against the King model output for solar minimum. We can see in Figure 7.20 that the JPL 6-year offset predicts a much higher flux than King does for solar minimum.

The 6-year offset data was then plotted along with the long-term **solar maximum** data, and this can be seen in Figure 7.21. Here we see that this offset data seems to fit better with these solar maximum models, but it still has a much higher flux than that of the JPL solar maximum. This therefore makes it very difficult to understand how the offsetting of the data actually works. If one is to offset the data towards a period of solar minimum, a very high flux is obtained. Yet without the advanced user capabilities, this value is assumed to be zero and therefore contradicts the offset output. It is also intriguing as to why the output from all the different offset years (except the 7-year offset) is exactly the same, instead of gradually changing with each year by which it is offset by.

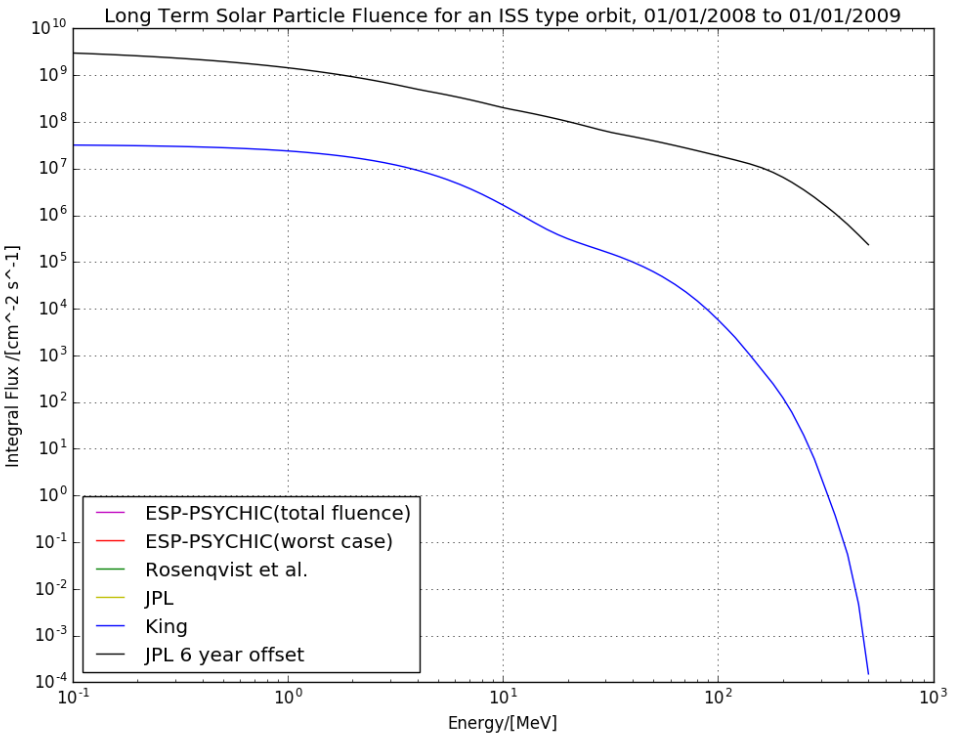

FIGURE 7.20: Long-term solar proton models at a **solar minimum** date, including the JPL 6-year offset data.

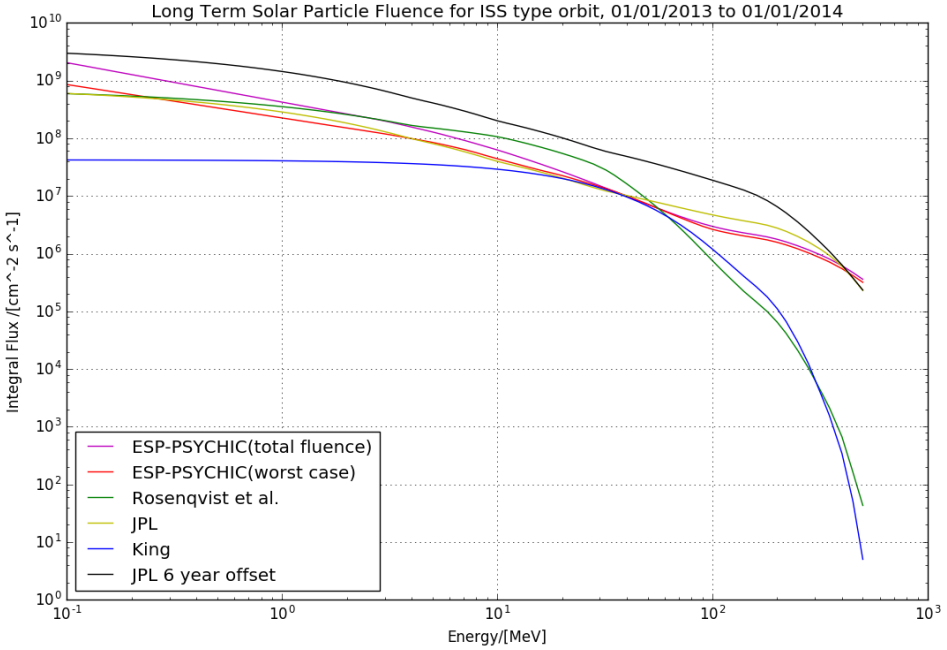

FIGURE 7.21: Long-term solar proton models at a **solar maximum** date, including the JPL 6-year offset data.

Chapter 8

Results from the Upset Rate Calculation

8.1 Fitting a Weibull Function to the Cross-section Data

The plots obtained from fitting a Weibull function to the Samsung DDR2 SDRAM device (part number K4T1G164QE) irradiated by Ryu et al (Ryu et al. 2012) can be seen in Figures 8.1, 8.2 and 8.3. Here, we see that the shape of the curve changes depending on how many data points were used in the fit. The values of the parameters therefore also change, and these are summarised in Table 8.1.

Number of Data Points	σ_{lim} [cm^{-2}]	l_o [MeV.cm^{-2} mg^{-1}]	w	s
8	0.054	2.032	36.76	2.913
6	0.063	2.032	41.066	3.820
4	0.062	-0.604	41.066	2.836

TABLE 8.1: A summary of the Weibull parameters obtained when using different numbers of data points **(DDR2 DSRAM device)**.

The plots obtained from fitting a Weibull function to the Virtex FPGA device (part number XQVR300) irradiated by Carmichael et al. (Carmichael et al. 2001) can be seen in Figures 8.4 and 8.5. The differences in the Weibull parameters obtained from these two fits can be found in Table 8.2.

By looking at Figures 8.1 through to 8.3 we see that the data very clearly follows a curved shape. This makes it very apparent that if we were to have used the RPP

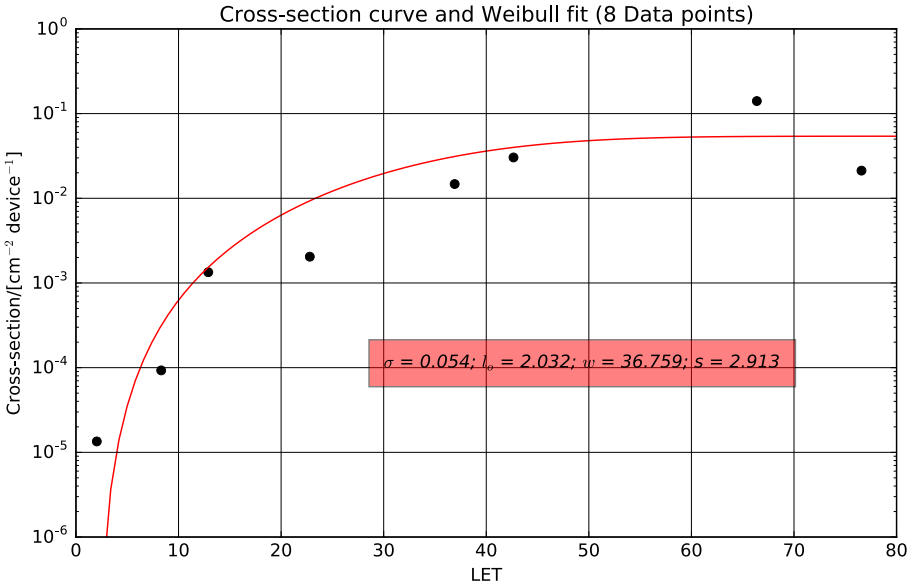

FIGURE 8.1: Cross-section curve and parameters **for heavy ions** obtained from fitting a Weibull function to the 8 data points published by Ryu et al. (Ryu et al. 2012) from their measurements of a Samsung DDR2 SDRAM device irradiated with heavy ions.

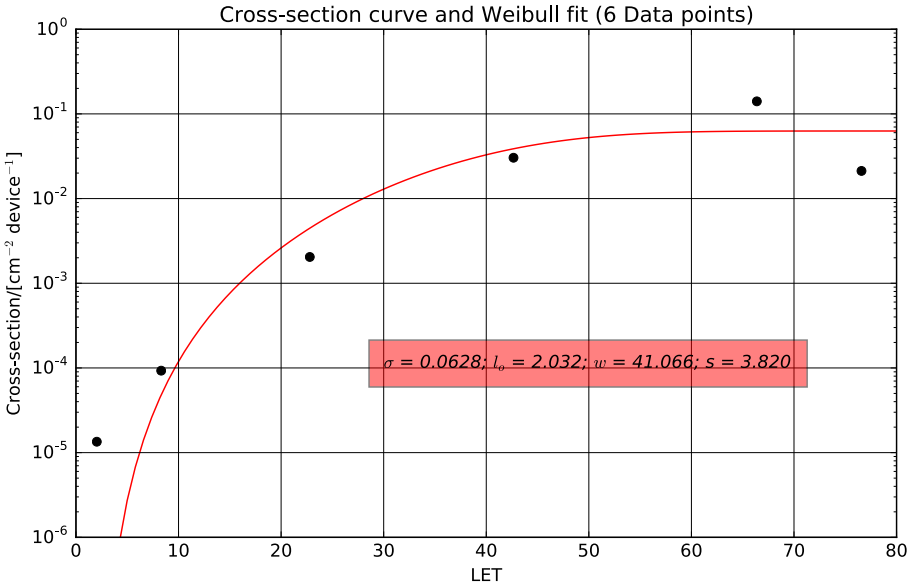

FIGURE 8.2: Cross-section curve and parameters **for heavy ions** obtained from using only 6 of the data points from Ryu et al. (Ryu et al. 2012) in Figure 8.1.

method (wherein a step function shape of the cross section plot is assumed) we would have been greatly simplifying the situation, and this could have led to inaccurate results when calculating the upset rate. In contrast, the Virtex FPGA device data has a much steeper gradient and is more consistent with a step function.

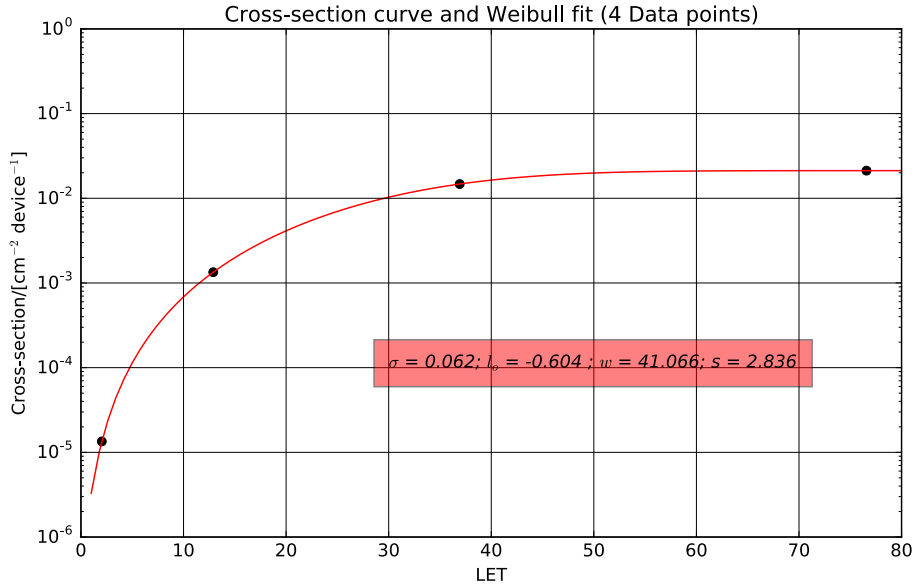

FIGURE 8.3: Cross-section curve and parameters **for heavy ions** obtained from using only 4 of the data points from Ryu et al. (Ryu et al. 2012) in Figure 8.1.

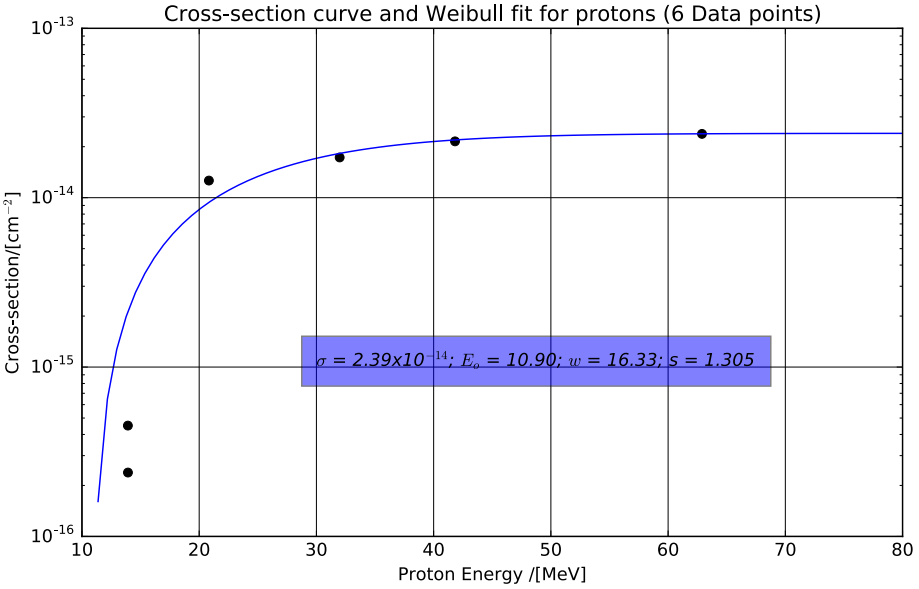

FIGURE 8.4: Cross-section curve and parameters **for protons** impinging on a Virtex FPGA device obtained from using 6 data points published by Carmichael et al. (Carmichael et al. 2001).

8.2 Upset Rate Predictions

After the Weibull parameters were calculated, these were added into the SPENVIS single event effects packages to obtain an estimate of the upset rate.

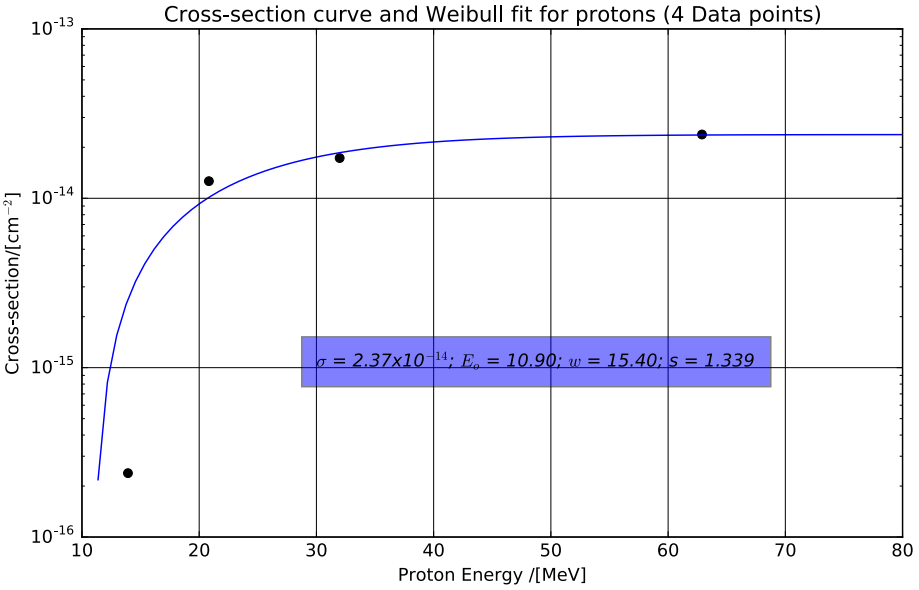

FIGURE 8.5: Cross-section curve and parameters **for protons** obtained from using only 4 data points from the data published by Carmichael et al. (Carmichael et al. 2001) as shown in Figure 8.4.

Number of Data Points	σ_{lim} [cm^{-2}]	E_o [MeV]	w	s
6	2.39x10^{-14}	10.90	16.33	1.31
4	2.37x10^{-14}	10.90	15.40	1.34

TABLE 8.2: A summary of the Weibull parameters obtained when using different numbers of data points **(Virtex FPGA)**.

8.2.1 Best and Worst Case Model Combinations for Calculating the Upset Rate

In Table 8.3 we have summarised the results obtained from the best-case models and worst-case models. When we decided on the best-case models, we chose the models that had the highest fluences for that particular orbit. If we look at the results in Table 8.3 we see that the predicted upset rate is much greater for the worst-case model selection. This is what is expected due to the fact that a higher fluence (more particles) will result in a better likelihood of a particle hitting a sensitive region, thereby causing an upset. We can see that there is a difference of a factor of 1000 for the SDRAM device, and a factor of 100 for the FPGA device for the different model combinations. This demonstrates that the **model selection** can very greatly affect the upset rate calculation, and so one needs to be aware of this when selecting a model. By using the worst case models,

the engineer will obtain a more conservative higher estimate for the upset rate and will therefore either need to implement mitigation techniques or select a different device.

Device	Case	bit^{-1}	$bit^{-1}\ s^{-1}$	$bit^{-1}\ day^{-1}$
DDR2 SDRAM	Best	3.499	$3.699x10^{-8}$	$3.196x10^{-3}$
	Worst	$3.792x10^{3}$	$4.008x10^{-5}$	3.463
Virtex FPGA	Best	$7.410x10^{-4}$	$7.836x10^{-12}$	$6.771x10^{-7}$
	Worst	$4.130x10^{-2}$	$4.369x10^{-10}$	$3.770x10^{-5}$

TABLE 8.3: The effect on the upset rate calculation for a best and worst case model choice **(heliosynchronous orbit)** for the two test devices considered in this study.

8.2.2 The Effect of the Solar Cycle on the Upset Rate

Table 8.4 shows the upset rates calculated for the ISS orbit at a solar maximum date and at a solar minimum date. Here we see that there are very few upsets predicted at both stages of the solar cycle, and that there isn't too great a difference between the two dates. This is due to the fact that the ISS is at a low altitude, and so it hardly passes through the SAA. This orbit also doesn't go anywhere near the poles, and so a lot of radiation is avoided that way. This is what was expected, as the ISS itself not only has many electronic components on-board, but is also carrying astronauts and so it was inserted into this orbit in order to expose it to as little radiation as possible. The altitude the ISS is at also means it is very well shielded from any solar protons, and this (in combination with avoiding the poles and the SAA) means that it is not too greatly affected by the change in the sun's activity throughout the solar cycle.

We see that for the heliosynchronous orbit in Table 8.5 the upset rates are slightly larger, but still very low. There also does not seem to be too much of a difference between the solar maximum date and the solar minimum date. We would expect the higher heliosynchronous orbit to have more of a solar cycle dependence than the ISS type orbit as this particular orbit is deeper in the Van Allen belts at the SAA, and passes over the poles too.

We can get an idea of how the solar cycle will affect the trapped radiation SEU rates by looking at the two models AP-8 MAX and AP-8 MIN. Table 8.6 shows that there is quite a significant difference between the two model outputs. AP-8 MIN has a higher upset rate, as expected due to the fact that there is a greater presence of charged particles during solar minimum. This is unlike the situation with the solar proton models, where

Device	Solar State	bit^{-1}	$bit^{-1}\ s^{-1}$	$bit^{-1}\ day^{-1}$
DDR2 SDRAM	Max (2013)	$5.067x10^{-2}$	$1.607x10^{-9}$	$1.388x10^{-4}$
	Min (2009)	$5.052x10^{-2}$	$1.602x10^{-9}$	$1.384x10^{-4}$
Virtex FPGA	Max (2013)	$3.646x10^{-6}$	$1.156x10^{-13}$	$9.991x10^{-9}$
	Min (2009)	$3.690x10^{-6}$	$1.170x10^{-13}$	$1.101x10^{-8}$

TABLE 8.4: The effect on the upset rate calculation for a solar proton model run at a solar maximum date and one at a solar minimum date **(ISS type orbit)**.

Device	Solar State	bit^{-1}	$bit^{-1}\ s^{-1}$	$bit^{-1}\ day^{-1}$
DDR2 SDRAM	Max (2013)	1.169	$3.708x10^{-8}$	$3.203x10^{-3}$
	Min (2009)	1.167	$3.702x10^{-8}$	$3.199x10^{-3}$
Virtex FPGA	Max (2013)	$6.118x10^{-5}$	$1.940x10^{-12}$	$1.676x10^{-7}$
	Min (2009)	$6.107x10^{-5}$	$1.937x10^{-12}$	$1.673x10^{-7}$

TABLE 8.5: The effect on the upset rate calculation for a solar proton model run at a solar maximum date and one at a solar minimum date **(Heliosynchronous orbit)**.

a significant difference was not observed for a solar maximum date and solar minimum date (Tables 8.4 and 8.5).

Device	Model	bit^{-1}	$bit^{-1}\ s^{-1}$	$bit^{-1}\ day^{-1}$
DDR2 SDRAM	AP-8 MAX	$1.752x10^{-1}$	$5.555x10^{-9}$	$4.799x10^{-4}$
	AP-8 MIN	$7.705x10^{-1}$	$8.144x10^{-9}$	$7.073x10^{-4}$
Virtex FPGA	AP-8 MAX	$2.592x10^{-5}$	$8.220x10^{-13}$	$7.102x10^{-8}$
	AP-8 MIN	$1.033x10^{-4}$	$1.092x10^{-12}$	$9.434x10^{-8}$

TABLE 8.6: The effect on the upset rate calculation by using the trapped radiation models AP-8 MAX and AP-8 MIN **(heliosynchronous orbit)**.

Table 8.7 shows the change in the upset rate calculation for a possible date change near solar maximum. As can be seen, the effect is not too dramatic, and so the calculations would probably not need to be re-run if there was a 1-year mission delay at solar max. Recalling from Section 7.2.2, the change at solar max was the greatest of all the fluence differences. So if we conclude that this does not have a great enough effect on the SEU rate to warrant a re-calculation, then we can conclude that a 1-year mission delay at any point on the solar cycle will not have a substantial effect on the SEU rate. For the heliosynchronous orbit, the models produced the exact same values for the SEU for years 2013 and 2014 (as seen in Table 8.8, and so even a slightly higher LEO orbit (607km) passing over the poles will not be greatly affected by a 1-year mission delay.

Tables 8.9 and 8.10 demonstrate the difference in the upset rate between a situation wherein only the a trapped model is used, and one wherein only a solar proton model is used. We see here that it is important to consider both the trapped and the non-trapped

Device	Year	bit^{-1}
DDR2 SDRAM	2013	1.0081x10^{-1}
	2014	1.112x10^{-1}
Virtex FPGA	2013	1.668x10^{-6}
	2014	1.685x10^{-6}

TABLE 8.7: The effect on the long-term upset rate calculation for a mission date change near solar maximum **(ISS type orbit)**.

Device	Year	bit^{-1}
DDR2 SDRAM	2013	2.496
	2014	2.496
Virtex FPGA	2013	3.468x10^{-5}
	2014	3.468x10^{-5}

TABLE 8.8: The effect on the long-term upset rate calculation for a mission date change near solar maximum **(Heliosynchronous type orbit)**.

radiation, due to the fact that the upset rates are so similar for both radiation types. This means that if one were to only consider trapped models, one could potentially be underestimating the total possible upsets by almost 40%. An engineer therefore needs to take both trapped radiation and solar particles into account, even for low-altitude orbits.

Device	Model	bit^{-1}	bit^{-1} s^{-1}	bit^{-1} day^{-1}
DDR2 SDRAM	Trapped	2.442x10^{-1}	2.582x10^{-9}	2.231x10^{-4}
	Solar	1.545x10^{-1}	1.663x10^{-9}	1.411x10^{-4}
Virtex FPGA	Trapped	2.893x10^{-5}	3.058x10^{-13}	2.642x10^{-8}
	Solar	1.070x10^{-5}	1.131x10^{-13}	9.773x10^{-9}

TABLE 8.9: The upset rate calculation for trapped models and short-term solar models individually for an **ISS-type orbit**.

Device	Model	bit^{-1}	bit^{-1} s^{-1}	bit^{-1} day^{-1}
DDR2 SDRAM	Trapped	7.705x10^{-1}	8.144x10^{-9}	7.036x10^{-4}
	Solar	3.499	3.699x10^{-8}	3.196x10^{-3}
Virtex FPGA	Trapped	1.033x10^{-4}	1.091x10^{-12}	9.434x10^{-8}
	Solar	1.833x10^{-4}	1.937x10^{-12}	1.674x10^{-7}

TABLE 8.10: The upset rate calculation for trapped models and short-term solar models individually for a **heliosynchronous orbit**.

8.2.3 The Effect of the Number of Data Points on the Upset Rate Calculation

Lastly, the upset rates in Tables 8.11 and 8.12 were produced by using the same models for the same dates (3-year mission, starting on 01/01/2018). These tables show the effect on the SEU rate of the number of cross-section data points used to generate a Weibull fit. The highest number of data points will have different fitting parameters to the lowest number of points, and so the calculation of the upset rate will differ. As can be seen from both tables, the number of data points greatly affects the SEU rate of the DDR2 SDRAM device. This is the device where the cross section curve was obtained by direct ionisation from heavy ions. From this we can conclude that it is very important to attempt to gather as many data points for the rising portion of the cross-section curve. The Virtex FPGA, which was irradiated only with a proton beam, shows less of a dramatic dependence on the number of data points. This may be due to the fact that the Virtex FPGA data has a much steeper slope and more greatly resembles a step function. Fewer data points are required to model this step-like behaviour, as long ad the data points cover the rising portion of the curve.

Device	Number of points	bit^{-1}	$bit^{-1}\ s^{-1}$	$bit^{-1}\ day^{-1}$
DDR2 SDRAM	8	$3.987x10^{-1}$	$4.215x10^{-9}$	$2.231x10^{-4}$
	4	1.440	$1.522x10^{-9}$	$1.315x10^{-4}$
Virtex FPGA	6	$3.963x10^{-5}$	$4.189x10^{-13}$	$3.619x10^{-8}$
	4	$3.960x10^{-5}$	$4.187x10^{-13}$	$3.617x10^{-9}$

TABLE 8.11: The effect on the upset rate calculation of using Weibull parameters derived from fitting a different number of data points **(ISS-type orbit)**.

Device	Number of points	bit^{-1}	$bit^{-1}\ s^{-1}$	$bit^{-1}\ day^{-1}$
DDR2 SDRAM	8	4.270	$4.513x10^{-8}$	$3.899x10^{-3}$
	4	$1.544x10^{1}$	$1.632x10^{-7}$	$1.409x10^{-2}$
Virtex FPGA	6	$2.866x10^{-4}$	$3.029x10^{-12}$	$2.618x10^{-7}$
	4	$2.872x10^{-4}$	$3.036x10^{-12}$	$2.623x10^{-7}$

TABLE 8.12: The effect on the upset rate calculation of using Weibull parameters derived from fitting a different number of data points **(Heliosynchronous orbit)**.

Chapter 9

Conclusions and Recommendations

9.1 Findings

A detailed step-by-step account of the use of the SPENVIS platform has been presented. This was done in an attempt understand how best to use the different radiation models in SPENVIS to calculate upset rates expected for low-Earth missions in different orbits and at different phases in the solar cycle. We did this by comparing model outputs for different input parameters and using these outputs to calculate upset rates for two different electronic devices. In doing so, we were able to understand the effect of varying each input parameter on the upset rate calculation.

After using the SPENVIS platform and comparing the outputs of several models, one can see that there can be large differences of up to a factor of 1000 in the output depending on which model is chosen, and even on which parameters are chosen for each of the models. This can make it very difficult when trying to select a reliable output on which further calculations can be based. We found that having a fair understanding of the radiation environment, especially of the Van Allen Belts and the south Atlantic anomaly, and of the distribution of the different species of particles in these regions will greatly assist the user when attempting to gather information from the SPENVIS platform.

We found that changing the input date in the coordinate generators package does not make a significant difference to the calculation of the SEU rates. This is particularly true for the trapped radiation models, as we found that the input date does not have any effect at all on the model output. Due to this, we conclude that it is important to understand fully the state of the solar cycle at the projected mission date, as well as exactly what this will mean for trapped radiation (for example, the fluence for trapped radiation goes up at solar min) and for non-trapped radiation (for example, more solar wind and a greater likelihood of solar weather events at solar max).

By running the models at a solar maximum date and a solar minimum date, we found that if the specific mission is at solar minimum, the only long-term model that will output data is the King model. All other models assume a zero fluence at solar minimum and will therefore output zero values for all input dates which fall on solar minimum. SPENVIS allows an “advanced" user to offset the long-term solar proton data by a specific number of 1-7 years, but in doing so, we found that each of the offset years 1-6 yielded exactly the same values, and the 7th year output was all zeros.

For our calculation of device upset rates, we made use of published data for direct ionisation tests (from heavy ions) in a DDR2 SDRAM device (Ryu et al. 2012) and for proton-induced upsets in a Virtex FPGA device (Carmichael et al. 2001). In order to assess the sensitivity of the Weibull parameter fits to the number of data points, we performed the Weibull fits for the total number of published data points (8 for the DDR2 SDRAM device and 6 for the FPGA respectively) and then repeated the fits for successively fewer data points. For the FPGA device we found that an adequate fit could be achieved with only 4 (out of 6) data points. This however was not the case for the device tested with direct ionisation (DDR2 DSRAM), and so it is good that the original paper ((Ryu et al. 2012)) had 8 data points to work with. The accuracy of the Weibull parameter determination relies heavily on the shape of the curve, so the device with a steeper, more step-like shape (proton induced upsets in the Virtex FPGA) can be described using fewer data points, whereas the DDR2 SDRAM device has a more gradually curving slope and so more data points are required to represent this portion of the curve accurately.

We have found that if the user decides to consider only trapped radiation or only solar protons, the upset rate could be underestimated by approximately 50% of its total value.

We found this to be true even at a low-altitude, low-inclination orbit like that of the ISS.

One of our most important findings was to see exactly how important it was to know how the model choice would affect the upset rate calculation. The difference between our “best case" and “worst case" model selection was as large as a factor of 100 for proton ionisation and 1000 for direct ionisation. This means that, above all, model choice had the most significant influence on the predicted upset rates. There was almost a 100% difference between the best and worst case model combinations. This is far greater than the difference between only looking at trapped models or only looking at solar models (a maximum difference of 63%) and also greater than the difference due to the number of data points used to obtain the Weibull parameters (the maximum difference being 56% between 6 and 4 data points).

Overall, a much greater understanding of the modelling process using the SPENVIS platform has been obtained. Combining a model with terrestrial test data in order to obtain an estimate for a SEU rate has been well analysed and different situations have been compared. We have found that are many small errors that could be made by someone using the platform who does not fully understand how it works. An in-depth comparison between the SEU rates due to different models and different parameters within the models has been made as an attempt to inform other users of the importance of knowing how to use the platform properly.

9.2 Guidelines for the use of SPENVIS for Upset Rate Calculations

Based on our findings above, we offer a number of guidelines for novice SPENVIS users when using the platform for designing space missions and calculating upset rates. These are categorised into four main parts: before using the SPENVIS platform, while using the SPENVIS platform, terrestrial tests, and design considerations.

9.2.1 Before using the SPENVIS platform

Obtain a good understanding of the radiation environment.
It very important for one to understand both the trapped and the non-trapped radiation sources as well as how each will contribute to the total radiation a satellite will experience in orbit. Once the user is able to conceptualise and visualise the radiation environment, he or she will be better equipped to select certain parameters, make choices between models and draw conclusions from the model outputs. A good understanding of how the altitude and inclination of the orbit will affect its vulnerability with respect to all the sources of radiation will also greatly assist in using the platform and interpreting the outputs.

Understand the solar cycle and its effect on the radiation environment.
Before using the platform, one should be well aware of where in the solar cycle the mission is planned for, and what this means for the predicted radiation environment. This is particularly important when using the trapped radiation models, as the input date from the orbit generator does not affect the trapped models. This means that the user would have to select between solar max/min for AP-8. The user should also note that both the CRESSPRO active and quiet models are representative of a period of solar maximum. An understanding of the solar cycle will also help when selecting a solar model, as the user will have a better understanding of how active the sun would be, and can therefore make choices based on how many solar events would be likely to occur (particularly with all the short-term models, and the King long-term model).

Before selecting a model, be sure to know how each model works, the assumptions made and how the data was collected .
This can be done by utilising SPENVIS' help files which are very informative while still remaining concise. If more information is required, all sources are referenced in the help file as well. Knowing more about a model will help the user to be able to decide whether it is reliable and accurate for their particular orbit and mission. For example, choosing a model where the data was collected only over a solar maximum period would not be a good choice for a mission over solar minimum.

Understand how an upset occurs within an electronic device.
One needs to understand what is meant by the upset cross-section curve, as well as the

difference between direct and indirect ionisation. This will help when interpreting test data as well as when calculating the upset rate.

9.2.2 While using the SPENVIS platform

Use a multi-day orbit.

When using the SPENVIS platform, there are a few things that the user should take into account. A multi-day orbit is highly advised when using the orbit generator. A 3-day orbit will not increase the run-time by too much, and will therefore not overload the SPENVIS servers. It will however increase the accuracy of all the subsequent model output data, especially for orbits where passages through the SAA occur.

Do not re-calculate model outputs for a 1-year mission delay.

If the mission is to be delayed by a year or two, no matter what point along the solar cycle it is on, the models do not need to be re-run and the upset rate calculation does not need to be redone either. It is advised however that for longer delays that the calculation is redone, as the mission could then change from being at solar min to a mid solar cycle for example, and will then have different outputs.

Select models for both trapped and non-trapped radiation.

When running the upset rate calculation, it is very important to select models for both trapped and non-trapped radiation in order to avoid underestimating the total radiation profile due to the combination of both sources. The most important part of the entire upset rate calculation is determining which model to use. The user needs to know exactly why one model is chosen over another, and should understand the effects of that selection. It is advised to conduct a best and worst case model choice for the specific orbit and a given electronic component in order to be able to account for the fact that a different model may have more accurately represented the space environment during the actual mission. By doing so, the engineer can decide whether to design conservatively or to design in a way which is more cost-effective.

9.2.3 Terrestrial Laboratory Tests

Perform a total-dose test before conducting SEU tests.

It is advised to conduct a TID test in order to ensure that the maximum allowable

radiation exposure is well known so that one does not allow the device to reach this point during the SEU tests.

Test for both heavy ions and protons.

During laboratory tests at a particle accelerator, it is highly recommended to test for both proton-induced upsets, as well as direct ionisation from heavy ions. Heavy ion experiments are much more difficult than proton experiments, and therefore a satellite designer or electronic engineer might choose to forego the heavy ion tests and focus on proton upsets only. This is not advised, as both direct ionisation by heavy ions and proton ionisation play a significant role in the total upset rate.

Use the IRPP method for calculating upset rates from cross-section data.

When the cross-section data points have been obtained from a laboratory test and one is attempting to obtain Weibull/Bendel parameters, it is important to note that having a good idea of the parameters before-hand will be of assistance if a least-squares fit is being used. σ_{lim} is usually the y-axis asymptote. l_o or E_o is the value on the x-axis where σ=0 (x-intercept) in the equation $\sigma = \sigma_{lim}\left[1 - e^{-\left(\frac{l-l_o}{w}\right)^s}\right]$ or $\sigma = \sigma_{lim}\left[1 - e^{-\left(\frac{E-E_o}{w}\right)^s}\right]$ respectively. The other parameters can be found by trial and error, as they are not as easy to guess from the plotted data points. If the curve is being fitted in python, there is a function within the scipy stats package that can fit a Weibull function to a data set. Take note however that it is the cumulative density version of the Weibull function that needs to be fitted to the data. We would also suggest using a Weibull/Bendel fit, thereby using the IRPP method as opposed to the RPP method. The RPP method assumes a step-function shape of the cross-section and is not accurate as it will not take into account the curved portion of the cross section curve. This may lead to an over or under estimation of the upset rate.

9.2.4 Design Considerations

Implement software techniques to mitigate the effects of upsets.

The engineer may decide to use mitigation techniques such as Triple Modular Redundancy (TMR) or scrubbing. This would be done if the upset rate for a device is larger than what can be tolerated and the client would like to attempt to manage these upsets in the software. The selection of a specific electronic component or not due to its upset rate is determined by how many errors the satellite operator is willing to accept. By

using COTS components, there is a greater likelihood of errors occurring, but the manufacturing cost is reduced significantly. It is therefore up to the client to decide whether it is more important for the design to be based around being conservative and safe, or for it to be more affordable.

9.3 Future Work

The results discussed in this dissertation are only applicable to LEO missions, as these are the types of orbits we analysed. An extension to other orbit types such as geostationary, medium Earth orbit and high Earth orbit is advised for future studies. It is also suggested to compare the results from the trapped radiation models used in this project to the output of AP-9 once it is available on the SPENVIS website. A comparison with other software such as OMERE is also advised, in order to compare this with SPENVIS.

Finally, as this work is conducted in the context of the small satellite community in South Africa, we close with some remarks on how this work could be taken forward within the community. The modelling approach discussed in this dissertation is both underpinned and validated by laboratory tests. Hence, a logical next step would be to carry out laboratory-based investigations of carefully selected electronic components. An in-depth analysis of the laboratory testing procedure could be conducted at a facility such as iThemba LABS, a nuclear accelerator facility near Cape Town, South Africa. Here, one could look at performing radiation hardness assurance testing for electronic components using a proton beam in order to increase South Africa's expertise in this field. This would also be an opportunity to enhance the local space industry, as government entities and commercial space companies would be able to test new electronic components that have not been flown in space before, thereby increasing their competitive edge in the market. iThemba LABS also has the ability to increase its proton beam energy to 200 MeV, which would also allow for testing of latchups at this facility, thereby broadening the radiation effects testing capabilities within the country.

Appendix A

Code to extract only the model output data from the SPENVIS .txt file

```
#Read in SPENVIS .txt file
#Clean up the file so that only the data is present


inputfiles=['spenvis_tri.txt','spenvis_tri2.txt','spenvis_tri3.txt',
'spenvis_tri4.txt', 'spenvis_tri5.txt']

for kk in range(len(inputfiles)):
    inname=inputfiles[kk]
    infile = open(inname, "r")
    outname = inname.strip('.txt')+'_out.txt'
    outfile = open(outname, "w")

    energy=""
    iflux=""
    dflux=""

    for line in infile:
       # print(line)
        if line[0:2] == '  ':
            energy = line[2:12]
            iflux = line[15:25]
            dflux = line[28:38]

            newline= energy + '\t' + iflux + '\t' + dflux +'\n'

            outfile.write(newline)
            print(newline)
        if (line[0:15] == "'End of Block'"):
            print(line)
            break

    outfile.close()
```

Appendix B

Weibull Fit Code

```
#Code to fit a Weibull function to Direct Ionisation Cross-section
data
#using a least-squares method to find the 4 parameters

import scipy.optimize as optimize
import pylab as pl
import numpy as np


x= np.array([2.0321931589537208, 8.309859154929576,
12.897384305835011, 22.796780684104625, 36.92152917505031,
42.6559356136821, 76.57947686116702, 66.37826961770625])

y=np.array([0.00001345436418537924, 0.00009285748170187538,
0.0013398380708052244, 0.0020436306827435378, 0.014724762197753382,
0.03034537825451455, 0.021205017333106264, 0.14064970739301882])


def resid(p, yy, xx):
    err=abs(yy - p[0]*(1.-np.exp(-((xx-p[1])/p[2])**p[3])))
    return err

p0=np.array([0.03, 0.5, 47.3, 1.7])
fit=optimize.leastsq(resid, p0, args=(y,x))

coeffs=fit[0]


xxx=np.linspace(1,80,100);
yyy=coeffs[0]*(1.-np.exp(-((xxx-coeffs[1])/coeffs[2])**coeffs[3]))

#to add the text box
fig = pl.figure(figsize=(10,6))
ax = fig.add_subplot(111)

pl.plot(x, y, 'ko')
pl.yscale('log')


pl.plot(xxx, yyy, 'r-')
pl.title('Cross-section curve and Weibull fit (8 Data points)')
pl.xlabel('LET')
pl.ylabel('Cross-section/[cm$^{-2}$ device$^{-1}$]')
pl.yscale('log')
pl.rc('grid', linestyle="-", color='black')
pl.grid(True)
pl.ylim((1e-6,1))
```

```
print('coefficiens are: sigma =', coeffs[0], 'lo=' ,coeffs[1], 'w=',
coeffs[2], 's=', coeffs[3] )


#adding red text box at coordinates (40; 1e-4)
ax.text(30, 1e-4, '$\sigma$ = 0.054; $l_o$ = 2.032; $w$ = 36.759; s =
2.913', style='italic',
        bbox={'facecolor':'red', 'alpha':0.5, 'pad':10})


pl.show()
```

Bibliography

Allen, J. V. (1961), *Radiation belts around the Earth*, Freeman.

Benton, E. & Benton, E. (2001), 'Space radiation dosimetry in low-earth orbit and beyond', *Nuclear Instruments and Methods in Physics Research Section B: Beam Interactions with Materials and Atoms* **184**(1), 255–294.

Brautigam, D. & Bell, J. (1995), Crresele documentation., Technical report, DTIC Document.

Brautigam, D., Gussenhoven, M. & Mullen, E. (1992), 'Quasi-static model of outer zone electrons', *IEEE transactions on nuclear science* **39**(6), 1797–1803.

Buchner, S., Marshall, P., Kniffin, S. & LaBel, K. (2002), 'Proton test guideline development–lessons learned', *NASA/Goddard Space Flight Center, NEPP* .

Caffrey, M., Graham, P., Johnson, E., Wirthlin, M. & Carmichael, C. (2002), Single-event upsets in SRAM FPGAs, *in* 'Proceedings of the 5th Annual International Conference on Military and Aerospace Programmable Logic Devices (MAPLD)', Citeseer, p. 8.

Carmichael, C., E.Fuller, Fabula, J. & Lima, F. (2001), 'Proton testing of SEU mitigation methods for the Virtex FPGA', *Proc. of Military and Aerospace Applications of Programmable Logic Devices MAPLD* .

Chen, F. (2012), *Introduction to plasma physics*, Springer Science & Business Media.

Cravens, T. (2004), *Physics of Solar System Plasmas*, Cambridge University Press.

Dodd, P. & Massengill, L. (2003), 'Basic mechanisms and modeling of single-event upset in digital microelectronics', *IEEE Transactions on Nuclear Science* **50**(3), 583–602.

E. Johnson, M. W. & Caffrey, M. (2002), Single-event upset simulation on an FPGA, *in* 'Proceedings of the International Conference on Engineering of Reconfigurable Systems and Algorithms (ERSA)', CSREA Press, pp. 68–73.

European Space Agency (ESA) (2012), 'South atlantic anomaly'.
URL: *http://www.esa.int/spaceinimages/Images/2012/09/South_Atlantic_Anomaly*

European Space Agency (ESA) (2014), 'Radiation environment'.
URL: *http://www.esa.int/Our_Activities/Space_Engineering_Technology/Space_Environment/Radiation_environment*

Feynman, J., Spitale, G., Wang, J. & Gabriel, S. (1993*a*), 'Interplanetary proton fluence model: JPL 1991', *Journal of Geophysical Research: Space Physics* **98**(A8), 13281–13294.

Feynman, J., Spitale, G., Wang, J. & Gabriel, S. (1993*b*), 'Interplanetary proton fluence model: Jpl 1991', *Journal of Geophysical Research: Space Physics* **98**(A8), 13281–13294.

Group, A. T. (2015), 'Displacement damage'.
URL: *http://wpo.altertechnology.com/displacement-damage/*

Hathaway, D. (2016), 'Solar cycle 22, 23 and 24'.
URL: *https://solarscience.msfc.nasa.gov/predict.shtml*

Hensley, F., Major, G., Edel, C., Hauswald, H. & Marc, M. B. (2014), 'Technical and dosimetric aspects of the total skin electron beam technique implemented at heidelberg university hospital', *Reports of Practical Oncology & Radiotherapy* **19**(2), 135–143.

Heynderickx, D., Quaghebeur, B., Wera, J., Daly, E. & Evans, H. (2004), 'New radiation environment and effects models in the european space agency's space environment information system (SPENVIS)', *Space Weather* **2**(10).

Hitek, P. (2016), 'BJT vs MOSFET'.
URL: *http://panamahitek.com/tag/bjt-vs-mosfet/*

Hutchinson, I. (2001), *Introduction to Plasma Physics*.

iThembaLABS (2017), 'About iThemba'.
URL: *http://tlabs.ac.za/*

J. Feynman, T.P. Armstrong, L. D.-G. S. S. (1990), 'New interplanetary proton fluence model', *Journal of Spacecraft and Rockets* **27**(403).

King, J. (1974), 'Solar proton fluences for 1977-1983 space missions', *Journal of Spacecraft and Rockets* **11**(6), 401–408.

Maurer, R., Fraeman, M., Martin, M., Roth, M. & Roth, D. (2008), 'Harsh environments: Space radiation environment, effects and mitigation', *Johns Hopkins APL technical digest* **28**(1), 17.

Meffert, J. & Gussenhoven, M. (1994), Crrespro documentation, Technical report, DTIC Document.

NOAA (1994), *Solar Geophysical Data,*, number 603, NOAA, Boulder, CO.

Nwosa, C. (2011), 'Orbital environemnt risk assessment for sumbandilasat'.

Pease, R., Johnston, A. & Azarewicz, J. (1988), 'Radiation testing of semiconductor devices for space electronics', *Proceedings of the IEEE* **76**(11), 1510–1526.

Petersen, E. (2011), *Single event effects in aerospace*, John Wiley & Sons.

Rosenqvist, L., Hilgers, A., Evans, H., Daly, E., Hapgood, M., Stamper, R., Zwickl, R., Bourdarie, S. & Boscher, D. (2005), 'Toolkit for updating interplanetary proton cumulated fluence models', *Journal of spacecraft and rockets* **42**(6), 1077–1090.

Ryu, K., Park, M., Chae, J., Lee, I., Uchihori, Y., Kitamura, H. & Takashima, T. (2012), 'Heavy-ion radiation characteristics of DDR2 synchronous dynamic random access memory fabricated in 56 nm technology', *Journal of Astronomy and Space Sciences* **29**(3), 315–320.

Sawant, M. (2012), 'Single event effects complicate military avionics system design'.
URL: *http://www.cotsjournalonline.com/articles/view/102279*

Schwank, J., Shaneyfelt, M. & Dodd, P. (2013), 'Radiation hardness assurance testing of microelectronic devices and integrated circuits: Test guideline for proton and heavy ion single-event effects', *IEEE Transactions on Nuclear Science* **60**(3), 2101–2118.

Scripps (2016), 'Bragg peak and the proton difference'.
URL: *https://www.scripps.org/services/cancer-care*$_{proton-therapy/what-is-proton-therapy_{bragg-peak}}$

Sexton, F. (2003), 'Destructive single-event effects in semiconductor devices and ICs', *IEEE Transactions on Nuclear Science* **50**(3), 603–621.

Shougang, D., Suge, Y., Hongxia, L., Long, F. & Hongchao, Z. (2015), 'Predictions for proton and heavy ions induced seus in 65 nm srams', *Journal of Semiconductors* **36**(11), 114010.

Space Weather Prediction Center (2000), 'Coronal mass ejections'.
URL: *http://www.swpc.noaa.gov/phenomena/coronal-mass-ejections*

SPENVIS (2010*a*), 'Background information in SPENVIS - single event upsets'.
URL: *https://www.spenvis.oma.be/help/background/creme/creme.html*

SPENVIS (2010*b*), 'Background information in SPENVIS - trapped radiation models'.
URL: *https://www.spenvis.oma.be/help/background/traprad/traprad.html*

SPENVIS (2011*a*), 'Ionising dose model - SHIELDOSE'.
URL: *https://www.spenvis.oma.be/help/background/shieldose/shieldose.html*

SPENVIS (2011*b*), 'Single event upsets'.
URL: *https://www.spenvis.oma.be/help/background/creme/creme.htmlLET*

Stassinopoulos, E. & Raymond, J. (1988), 'The space radiation environment for electronics', *Proceedings of the IEEE* **76**(11), 1423–1442.

Swift, G. (2014), 'Overview of the XRTC Single-Event Test Results on the Xilinx 7-Series FPGAs', *SEFUW- SpacE FPGA User Workshop* .

Vette, J. (1991), 'The nasa/national space science data center trapped radiation environment model program, 1964-1991'.

Wieszczycka, W. & Scharf, W. (2001), *Proton radiotherapy accelerators*, world scientific.

Wirthlin, M., Johnson, E., Rollins, N., Caffrey, M. & Graham, P. (2003), The reliability of FPGA circuit designs in the presence of radiation induced configuration upsets, *in* 'Field-Programmable Custom Computing Machines, 2003. FCCM 2003. 11th Annual IEEE Symposium on', IEEE, pp. 133–142.

Xapsos, M. A., Barth, J., Stassinopoulos, E., Burke, E. A. & Gee, G. (1999), 'Space environment effects: model for emission of solar protons (esp): cumulative and worst case event fluences'.

Xapsos, M., Summers, G., Barth, J., Stassinopoulos, E. & Burke, E. (1999), 'Probability model for worst case solar proton event fluences', *IEEE Transactions on Nuclear Science* **46**(6), 1481–1485.

Xilinx (2011), 'Field programmable gate array (FPGA)'.
URL: *http://www.xilinx.com/training/fpga/fpga-field-programmable-gate-array.htm*

Zell, H. (2015), 'Radiation belts with satellites'.
URL: *http://www.nasa.gov/mission*$_p$*ages/sunearth/news/gallery/*20130228 − *radiationbelts.html*